From naïve to vigilant:

How Inflammatory and Metabolic Cues Shape Human T Cells

With a focus on Th17 differentiation in chronic inflammation

Xinlai Chen



RADBOUD UNIVERSITY PRESS

From naïve to vigilant:
how inflammatory and metabolic cues shape human T cells
with a focus on Th17 differentiation in chronic inflammation

Xinlai Chen

Xinlai Chen

From naïve to vigilant: how inflammatory and metabolic cues shape human T cells
with a focus on Th17 differentiation in chronic inflammation

Radboud Dissertation Series
ISSN: 2950-2772 (Online); 2950-2780 (Print)

Published by RADBOUD UNIVERSITY PRESS
Postbus 9100, 6500 HA Nijmegen, The Netherlands
www.radbouduniversitypress.nl

Design: ProefschriftOntwerp.nl
Cover image: Xinlai Chen
Printing: ProefschriftMaken/Pumbo

ISBN: 9789465153346
DOI: 10.54195/9789465153346
Free download at: https://doi.org/10.54195/9789465153346

© 2026 Xinlai Chen

RADBOUD UNIVERSITY PRESS

This is an Open Access book published under the terms of Creative Commons Attribution-Noncommercial-NoDerivatives International license (CC BY-NC-ND 4.0). This license allows reusers to copy and distribute the material in any medium or format in unadapted form only, for noncommercial purposes only, and only so long as attribution is given to the creator, see http://creativecommons.org/licenses/by-nc-nd/4.0/.

From naïve to vigilant:
how inflammatory and metabolic cues shape human T cells
with a focus on Th17 differentiation in chronic inflammation

Proefschrift ter verkrijging van de graad van doctor
aan de Radboud Universiteit Nijmegen
op gezag van de rector magnificus prof. dr. J.M. Sanders,
volgens besluit van het college voor promoties
in het openbaar te verdedigen op
dinsdag 24 november 2026
om 10.30 uur precies

door

Xinlai Chen
geboren op 20 augustus 1991
te Sichuan, China

Promotoren:
Prof. dr. P.M. van der Kraan

Copromotoren:
Dr. M.I. Koenders
Dr. A.P.M. van Caam

Manuscriptcommissie:
Prof. dr. A.B. van Spriel
Dr. ir. M.J.W. Adjobo-Hermans
Prof. dr. E. Lubberts (Erasmus Universiteit Rotterdam)

From naïve to vigilant:
how inflammatory and metabolic cues shape human T cells
with a focus on Th17 differentiation in chronic inflammation

Dissertation to obtain the degree of doctor
from Radboud University Nijmegen
on the authority of the Rector Magnificus prof. dr. J.M. Sanders,
according to the decision of the Doctorate Board
to be defended in public on
Tuesday, November 24, 2026
at 10:30 am

by

Xinlai Chen
born on August 20, 1991
in Sichuan, China

Supervisor:
Prof. dr. P.M. van der Kraan

Co-supervisors:
Dr. M.I. Koenders
Dr. A.P.M. van Caam

Manuscript Committee:
Prof. dr. A.B. van Spriel
Dr. ir. M.J.W. Adjobo-Hermans
Prof. dr. E. Lubberts (Erasmus University Rotterdam)

TABLE OF CONTENTS

Chapter 1	General Introduction	9
Chapter 2	TGF-β and hypoxia jointly shape the transcriptional landscape of human Th17 cells	27
Chapter 3	Mitochondrial activity regulates human T helper 17 differentiation and function	63
Chapter 4	Activated but not exhausted: vigilant memory T cells in end-stage osteoarthritis synovium	97
Chapter 5	Summary	117
Chapter 6	General Discussion	123
Appendix		143
	Nederlandse Samenvatting	145
	Research Data Management	147
	Curriculum Vitae	150
	List of publications	151
	Portfolio	152
	Acknowledgements	153



Chapter 1

General Introduction

GENERAL INTRODUCTION

1. Innate and adaptive immunity: distinct but interdependent arms of host defence

The immune system protects the host through two main branches: innate and adaptive immunity[1]. Innate immunity constitutes the first line of defense against invading pathogens and tissue injury. It responds rapidly, often within minutes to hours, and relies on germline-encoded pattern recognition receptors (PRRs) that detect conserved molecular motifs shared across broad classes of microbes[2, 3]. This system is mediated not only by cellular components, including myeloid cells such as macrophages, neutrophils, and dendritic cells, as well as by natural killer (NK) cells, but also by humoral and barrier-associated factors such as the complement system, antimicrobial peptides, and inflammatory cytokines[4]. These soluble mediators are particularly important at epithelial surfaces, where they contribute to immediate antimicrobial protection. Although innate immune responses are traditionally considered nonspecific and lacking classical memory, accumulating evidence indicates that certain innate cells can undergo epigenetic reprogramming, leading to a form of "trained immunity" that alters subsequent responses to pathogens[5].

In contrast, adaptive immunity is characterized by antigen specificity, clonal expansion, and the formation of long-lived immunological memory. Adaptive responses develop more slowly, typically over several days during a primary encounter, but generate highly specific effector mechanisms which are capable of precise pathogen recognition and elimination[6]. This arm of the immune system is mediated primarily by B lymphocytes, which produce antigen-specific antibodies, and T lymphocytes, which orchestrate cellular immune responses through helper, regulatory, and cytotoxic functions[7]. The immense diversity of adaptive immunity arises from somatic recombination of antigen receptor genes, enabling recognition of a vast array of antigens[8].

Despite their distinct features, innate and adaptive immunity do not work in isolation [9]. Together, they form a tightly coordinated system in which innate immune signals shape the magnitude, quality, and fate of adaptive responses through antigen presentation, co-stimulatory signals, cytokine milieus, and tissue-derived cues that critically influence T cell activation, differentiation, and function[10, 11]. Conversely, adaptive immune cells modulate innate responses via cytokine production and feedback regulation, ensuring effective pathogen control while limiting immunopathology[12].

Within this dynamic interplay, T cells function as key integrators of adaptive immune responses. At a broad level, $CD4^+$ helper T cells coordinate immune responses through cytokine production and interaction with other immune and stromal cells, whereas $CD8^+$ cytotoxic T cells primarily eliminate infected or transformed cells. Beyond pathogen clearance, they contribute to tissue

homeostasis, mucosal barrier integrity, and immune tolerance[13, 14], while dysregulated T cell activity can promote chronic inflammation and autoimmune disease[15]. Their capacity to integrate signals from antigen receptors, co-stimulation, cytokines, and the local tissue microenvironment renders T cells highly sensitive to contextual cues, positioning them at the interface between protective immunity and immune-mediated pathology[10].

2. Th17/Treg balance in autoimmune disease pathogenesis

Within adaptive immunity, $CD4^+$ T cells differentiate into functionally distinct subsets that collectively determine the quality and magnitude of immune responses[16, 17]. While these cells are indispensable for host defence, dysregulation of $CD4^+$ T cell differentiation and function is a hallmark of immune-mediated disease[14]. In particular, many autoimmune and inflammatory disorders are associated with an imbalance between regulatory T cells (Treg) and effector T cells, resulting in loss of immune tolerance and sustained tissue inflammation[18, 19].

Treg are important for the maintenance of peripheral tolerance, acting to suppress excessive or inappropriate immune activation[20]. When Treg numbers or suppressive capacity are reduced, effector T cell responses can become unchecked and contribute to autoimmunity[21]. Among effector subsets, T helper 17 (Th17) cells are important drivers of chronic inflammation. Th17 cells produce pro-inflammatory cytokines such as IL-17A, IL-17F, and IL-22, which promote neutrophil recruitment, tissue inflammation and stromal cell activation[22-24].

In various rheumatic diseases, increased frequencies of Th17 cells and elevated IL-17 levels have been detected in inflamed tissues and peripheral blood, while Treg function is often impaired [25]. This imbalance has direct clinical relevance: therapies that interfere with T cell activation or Th17-associated cytokines have demonstrated efficacy in subsets of patients. For example, blockade of T cell co-stimulation with abatacept is widely used in rheumatoid arthritis (RA), whereas IL-17–targeted therapies, such as secukinumab, have demonstrated efficacy in psoriatic arthritis (PsA) and spondylarthritis (SpA)[26, 27]. Despite these advances, the initial mechanisms that disturb the Th17/Treg balance in chronic inflammatory diseases remain incompletely understood. Interestingly, both Treg and Th17 cells arise from a common pool of naïve $CD4^+$ T cell precursors and share overlapping differentiation signals, including transforming growth factor-β (TGF-β)[28, 29]. This shared developmental origin suggests that relatively subtle changes in cytokine availability, metabolic state, or tissue microenvironment can profoundly alter lineage decisions, offering opportunities to restore the Th17/Treg balance. Such changes occur in various pathological settings, including autoimmunity, infection, cancer, and tissue repair.

3. Th17 plasticity

$CD4^+$ T cell differentiation was originally conceptualized as a linear process in which naïve T cells commit to stable and mutually exclusive helper lineages. Over the past two decades, this rigid view has been increasingly challenged, and phenotypic flexibility is now recognized as an intrinsic feature of adaptive immunity[30]. T cell plasticity refers to the capacity of differentiated T cells to acquire features of alternative lineages, either through the emergence of mixed phenotypes or through partial reprogramming of transcriptional and functional states in response to environmental signals[31].

Th17 cells represent one of the most extensively studied examples of such plasticity. Th17 cells are classically defined as a distinct $CD4^+$ T cell subset characterized by expression of the lineage-associated transcription factor RORγt and by production of IL-17 family cytokines, particularly IL-17A and IL-17F[32, 33]. In addition to IL-17A and IL-17F, Th17 cells may produce IL-22 and other effector molecules in a context-dependent manner, highlighting their functional heterogeneity[34]. Initially identified as key mediators of host defence against extracellular bacteria and fungi, Th17 cells have since been implicated in a wide range of inflammatory and autoimmune diseases.

Like other $CD4^+$ effector subsets, including Th1, Th2, and Tregs, Th17 cells arise from naïve $CD4^+$ T cell precursors and their differentiation is shaped by signals encountered during priming. In contrast to the relatively stable lineage identities observed for Th1 and Th2 cells, Th17 cells display pronounced heterogeneity and context-dependent flexibility, as evidenced by their ability to co-produce IFNγ or IL-10 in response to different cytokine milieus and tissue signals [35], highlighting that changes in inflammatory intensity, cytokine availability, and tissue-derived signals can substantially reshape Th17 functional programs, complicating strict lineage classification.

In highly inflammatory environments, Th17 cells can acquire features commonly associated with Th1 cells, including expression of T-bet and production of IFNγ and TNFα[36]. These Th1-like or "pathogenic" Th17 populations have been linked to tissue damage in several autoimmune diseases and chronic inflammatory conditions[37]. Conversely, under conditions characterized by attenuated inflammatory signalling or enhanced regulatory cues, Th17 cells may downregulate inflammatory effector programs and acquire regulatory properties, including expression of FoxP3 or production of IL-10[38, 39]. Rather than representing complete lineage conversion, these states reflect overlapping and adaptable transcriptional programs, underscoring the close developmental relationship between Th17 cells and Tregs[40].

The balance between Th17 and Treg responses is particularly sensitive to microenvironmental signals and is frequently disrupted in chronic inflammatory diseases such as RA and inflammatory

bowel diseases (IBD)[41]. In these settings, skewing toward inflammatory Th17-associated programs, together with impaired regulatory control, contributes to sustained inflammation and tissue pathology. Importantly, disease-associated Th17 pathogenicity is not attributable to IL-17 alone but reflects broader inflammatory transcriptional and metabolic programs that influence interactions with innate immune cells, including NK cells and macrophages[42, 43].

Taken together, Th17 cells are studied not only because of their relevance to immune-mediated disease, but also because their inherent flexibility makes them a powerful model for dissecting how environmental cues shape $CD4^+$ T cell fate decisions. Understanding the signals that govern Th17 differentiation and plasticity is therefore essential for interpreting immune responses across diverse inflammatory contexts and for elucidating mechanisms that regulate the balance between effector and regulatory T cell states.

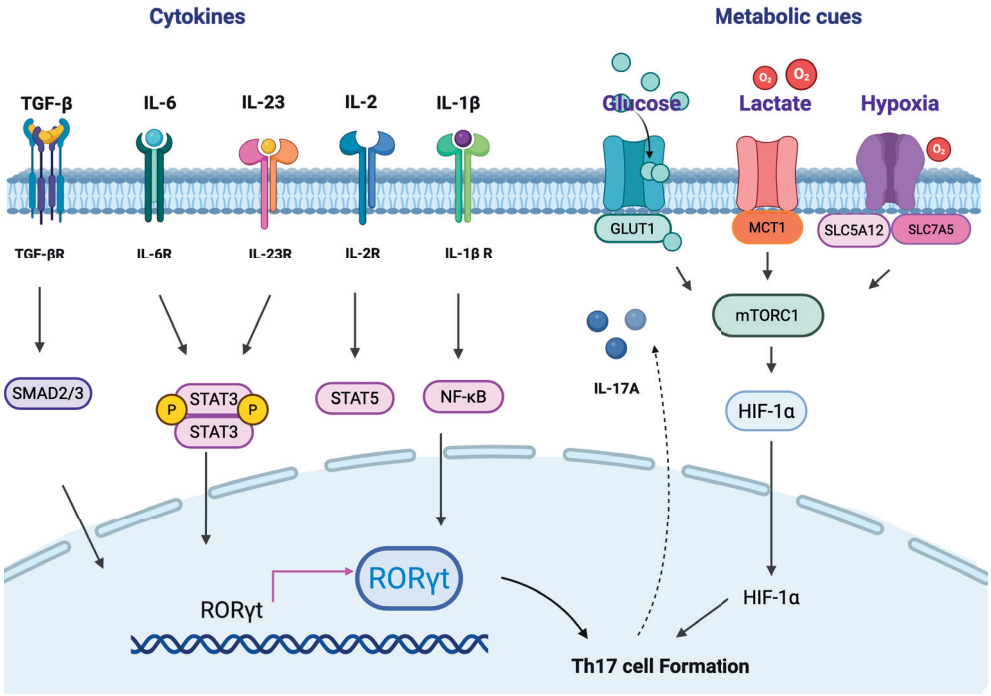

Figure 1: Environmental and metabolic cues regulating Th17 differentiation.
Cytokine signaling (left) and metabolic cues (right) converge to drive Th17 cell formation. Solid arrows indicate signaling that drives Th17 formation; dashed arrows indicate downstream secretion following Th17 differentiation. Figure created with BioRender.com.

4. Environmental cues governing Th17 differentiation

Activation and differentiation of naïve $CD4^+$ T cells require integration of multiple signals delivered by antigen-presenting cells. Initial antigen recognition occurs when the T cell receptor

(TCR) complex, associated with CD3ε, δ, γ and ζ, signalling chains, engages peptide–HLA class II complexes on APCs, providing specificity for the encountered antigen[24, 44]. Effective activation also depends on co-stimulatory signals, most prominently through CD28 engagement by CD80 and CD86 on APCs. This co-stimulation enhances cell survival, proliferation, and cytokine responsiveness, and critically influences downstream differentiation pathways[45, 46].

Upon activation, cytokine signalling plays a particularly prominent role in Th17 differentiation. Whereas IFN-γ promotes Th1 development and IL-4 favours Th2 fate, TGF-β acts as a core instructive signal for both Th17 and Treg differentiation, while IL-6 further guides Th17 formation. TGF-β contributes to induction of the lineage-defining transcription factor RORγt, while IL-6 activates STAT3 signalling to establish the core Th17 transcriptional program[28, 47-49]. Additional cytokines further modulate Th17 differentiation and stability. IL-1β enhances early Th17 commitment and effector function, whereas IL-23 is dispensable for initial differentiation but is critical for transcriptional level promotion, maintenance, expansion, and pathogenicity of differentiated Th17 cells[50-53]. IL-2, classically associated with T cell proliferation and regulatory T cell stability, exerts context-dependent effects on Th17 differentiation, often acting as a limiting factor by restraining excessive Th17 polarization through STAT5 signalling[54]. These cytokines do not operate in isolation but instead form an interconnected signalling network that fine-tunes Th17 fate decisions in response to environmental context[55].

Importantly, many of these cytokines are shared between Th17 and regulatory T cell differentiation pathways, highlighting the close developmental relationship between these lineages. TGF-β occupies a central position in this balance: in the presence of pro-inflammatory cytokines such as IL-6 demonstrated in murine systems, lower concentrations of TGF-β favour induction of RORγt and Th17 differentiation, whereas higher concentrations of TGF-β repress IL-23 receptor expression and promote FoxP3$^+$ regulatory T cell development [29]. This cytokine-dependent modulation of RORγt and FoxP3 expression provides a mechanistic framework for understanding the observed flexibility between Th17 and Treg phenotypes.

Understanding the combinations of environmental signals that model Th17 differentiation, including antigenic stimulation, co-stimulation, and cytokine milieu, is essential for interpreting how inflammatory cues, but also metabolic pressures, influence CD4$^+$ T cell fate decisions.

5. Metabolic cues shaping Th17 differentiation

CD4$^+$ T cell fate is dictated by a complex network of metabolic signals that intersect with cytokine and transcriptional programs. Glucose and amino acids provide both energy and biosynthetic precursors, and their uptake through the glucose transporter GLUT or amino acid transporter ASCT2 feeds into mTORC1 signalling to orchestrate Th17 versus Treg lineage

commitment[56]. Oxygen availability and mitochondrial function constitute a complementary axis: mitochondrial respiration, reactive oxygen species (ROS) production, and HIF1α stabilization integrate with mTORC1 to reinforce glycolysis, drive RORγt expression, and shape chromatin landscapes, ensuring that environmental cues are translated into durable Th17 programs[57]. Integrated with these core pathways, tissue-derived metabolites such as lactate further modulate effector metabolism and Th17 function, coupling local microenvironmental conditions to cytokine production, transcriptional activity, and functional specialization. Together, these interconnected metabolic networks establish a coherent framework in which nutrient availability, oxygen tension, and tissue metabolites converge to control Th17 differentiation and effector function in both homeostatic and inflammatory contexts.

5.1 Glucose and amino acid metabolism in Th17 differentiation

Beyond cytokine signals such as TGF-β and IL-6, the differentiation of Th17 cells is increasingly recognized not to be only driven by those cytokines and transcriptional factors, but also highly dependent on metabolic cues in the microenvironment, such as glucose availability and uptake [57-59], lactate accumulation[60, 61] and oxygen abundance[62-64]. Both glucose availability and hypoxic stress modulate Th17 differentiation through pathways involving mTORC1 and HIF-1α, although they engage this axis through distinct mechanisms.

Th17 differentiation is tightly coupled to enhanced glycolysis. Naïve $CD4^+$ T cells reside in a metabolically quiescent state defined by low biosynthetic demand, limited glycolytic flux, and minimal expression of glucose transporters such as GLUT1. This basal programme is sufficient to maintain energy homeostasis and long-term survival, but it is rapidly reconfigured upon activation to support the glycolysis-dependent clonal expansion and effector functions characteristic of T(h17) differentiation[65]. Upon antigen recognition, TCR and co-stimulatory signals trigger a pronounced glycolytic switch accompanied by sharply increased expression of GLUT1 and GLUT3 compared to naïve T cells[59, 66]. This enhanced glucose uptake sustains the high adenosine triphosphate (ATP) demand of proliferating Th17 precursors and supplies glycolytic intermediates required for nucleotide, amino-acid, and lipid biosynthesis, all of which are essential for proliferating Th17 precursors[67].

While early studies suggested a simple metabolic dichotomy in which Th17 cells depend on glycolysis and Tregs on oxidative phosphorylation (OXPHOS), more recent work demonstrates a more nuanced landscape. Th17 differentiation is influenced not only by glycolytic flux but also by fatty-acid synthesis (FAS) and mitochondrial metabolism, whereas Tregs exhibit metabolic plasticity that allows adaptation to glycolytic or oxidative environments[68]. Thus, simply blocking glycolysis may not be sufficient to shift the Th17/Treg balance[69], whereas modulating fatty-acid metabolism, such as inhibiting FAS or promoting fatty acid oxidation (FAO), appears to more consistently favour Treg differentiation, reflecting the complexity of

metabolic regulation in $CD4^+$ T cell fate[70, 71]. Consistently, Treg cells exhibit limited GLUT1 expression and relatively low levels of GLUT3, although *in vivo* activated Tregs are still capable of engaging GLUT1-dependent glucose uptake for expansion[66]. Whereas enhanced GLUT3 expression allows Th17 cells to meet their high metabolic requirements, Tregs retain the flexibility to adapt to varying nutrient conditions[59]. Differential nutrient utilization helps shape helper T cell lineage outcomes according to local metabolic cues, with high glucose availability not only supporting Th17 metabolic activation but also limiting FoxP3 stability[72], further shifting the balance away from Treg differentiation. Microenvironments with abundant glucose, such as barrier tissues or inflamed sites, may preferentially sustain Th17 responses, providing a metabolic basis for their enrichment in these contexts and may exacerbate the Th17-mediated autoimmunity[58].

Besides glucose, amino acids are also highly involved in shaping Th17 formation, serving dual functions as metabolic fuels and as precursors for protein and nucleic acid biosynthesis. Among these amino acids, glutamine plays a particularly central role in shaping Th cell fate. In addition to providing nitrogen for nucleotide synthesis, glutamine feeds carbon into the tricarboxylic acid (TCA) cycle via anaplerosis, supporting biosynthesis even during glycolytic flux. This metabolic input is especially important for proliferating Th17 cells, which depend on continuous replenishment of TCA intermediates to maintain effector differentiation. Consistent with this, metabolic tracing studies show that glutamine restriction markedly reduces IL-17 production and disrupts core Th17 transcriptional programs, underscoring the tight link between glutamine availability and Th17 lineage stability[73].

The uptake of glutamine is largely mediated by the amino acid transporter ASCT2 (SLC1A5), whose expression is rapidly induced following T cell receptor activation. ASCT2 acts as a gatekeeper that couples extracellular nutrient availability to intracellular signalling pathways. Genetic deletion or pharmacological inhibition of ASCT2 reduces glutamine import, impairs Th17 differentiation, suppresses RORγt, and blunts IL-17 production[74]. Strikingly, ASCT2-deficient cells preferentially adopt a $FoxP3^+$ regulatory T cell phenotype, illustrating that amino acid access is not merely permissive but actively instructive in determining inflammatory versus regulatory fates. These observations extend earlier findings showing that T cell activation depends on coordinated activity of multiple amino acid transporters, including System L transporters such as SLC7A5, which regulate the uptake of large neutral amino acids and these are required for full activation of the metabolic program that underlies Th17 polarization.

A key regulator of Th17 metabolic programming is mTORC1, a nutrient- and growth-factor–sensing kinase complex that integrates signals from glucose metabolism, glutaminolysis, and extracellular cues to influence $CD4^+$ T cell fate. Effective mTORC1 activation requires glycolytic intermediates and ATP, as well as glutamine-derived α-ketoglutarate, which supports chromatin

remodelling and STAT3 phosphorylation while partially suppressing STAT3's inhibitor SOCS3. Activated mTORC1 promotes RORγt expression and IL-17 production, driving Th17 differentiation, whereas its inhibition favours FoxP3$^+$ regulatory T cell development[75]. Beyond transcriptional regulation, mTORC1 reprograms cellular metabolism by inducing HIF1α-mediated glycolysis and supporting anabolic pathways, including nucleotide and lipid synthesis, which underpin effector proliferation and cytokine production[76].

Glucose and glutamine availability converge with transporter-mediated nutrient uptake, particularly via GLUT1/GLUT3 and ASCT2, to define this metabolic checkpoint. Collectively, the glucose–glutamine–mTORC1 axis operates as an integrated network linking nutrient availability[77], intracellular signalling, and transcriptional programs, thereby translating environmental and metabolic cues into Th17 versus Treg lineage commitment[78].

5.2 Oxygen, mitochondria, and HIF-1α in Th17 differentiation

Oxygen tension and mitochondrial metabolism define a second major regulatory axis in CD4$^+$ T cell differentiation, complementing nutrient-sensing pathways. In inflamed tissues such as arthritic synovium, hypoxia intersects with cytokine-driven signals to shape lineage choice[79]. Mitochondria integrate these cues through both anterograde inputs (nuclear control of biogenesis and respiratory capacity) and retrograde signals that report mitochondrial fitness back to the nucleus[80]. These retrograde pathways allow T cells to assess whether their mitochondrial state is compatible with high-demand effector programs such as Th17 differentiation.

Mitochondria shape Th17 differentiation through several interconnected mechanisms (involving energy production, metabolite availability, and redox signalling). First, OXPHOS supports ATP production and biosynthetic flux in the context of sustaining TCA cycle activity[81]. TCA intermediates such as α-ketoglutarate serve as anaplerotic substrates and essential cofactors for dioxygenases that regulate histone and DNA demethylation, providing a direct link between mitochondrial function and chromatin accessibility[82]. Second, mitochondrial dynamics modulate the balance between effector and regulatory states: fusion enhances respiratory capacity and favors regulatory or memory programs, whereas fission and selective mitophagy reduce OXPHOS efficiency and reshape redox signalling to support effector specialization[83, 84].

A central consequence of altered mitochondrial activity is the controlled production of ROS. Moderate ROS stabilize HIF-1α by inhibiting prolyl hydroxylases, promoting a transcriptional program that cooperates with RORγt and enhances glycolytic flux— both hallmarks of Th17 differentiation[85]. Excessive ROS, however, induces mitochondrial stress responses or cell death, emphasizing the requirement for tight redox control. Hypoxia reinforces this axis by

directly stabilizing HIF-1α, thereby amplifying glycolytic gene expression and promoting FoxP3 degradation, tilting the balance toward Th17 rather than Treg differentiation[57, 81, 86].

Emerging evidence indicates that mitochondrial metabolism imprints epigenetic states that influence $CD4^+$ T cell lineage choices[87]. TCA-derived metabolites act as cofactors for dioxygenases that regulate histone and DNA demethylation. Altering mitochondrial production or availability of these metabolites shifts the balance between Th17 and induced Treg differentiation by modifying chromatin accessibility at key loci such as Foxp3 and Il17a. Mitochondrial activity itself governs how much of these metabolites are available: OXPHOS and TCA cycle flux scale with mitochondrial membrane potential ($\Delta\Psi$), so highly polarized mitochondria generate more TCA-derived metabolites while damaged mitochondria produce less. Beyond this point, mitochondrial stress acts as a checkpoint that halts further effector differentiation. In line with this metabolic licensing model, Liver kinase B1 (LKB1) deficiency has been reported to skew $CD4^+$ T cells toward pathogenic Th17 differentiation via reduced AMPK activation and increased mTORC1 signaling[88]. This is reminiscent of other contexts where mitochondrial stress checkpoint failure produces a similar pathogenic Th17 bias, underscoring a common mechanistic outcome[89]. This provides a mechanistic explanation for how mitochondrial activity, rather than transient metabolic flux, enforces long-term transcriptional programs relevant to inflammatory disease[90].

Together, oxygen tension, mitochondrial output, ROS-dependent HIF-1α stabilization, and TCA-derived epigenetic signals form a coherent metabolic signalling circuit that directs Th17 differentiation. Under hypoxic or mitochondrially stressed conditions, this circuit favours effector commitment over regulatory programs by reinforcing HIF-1α activity, glycolytic gene expression, and Th17-associated chromatin states. Understanding this axis clarifies how mitochondrial fitness and oxygen availability shape T cell behaviour within inflamed tissues and reveals specific metabolic nodes that may be targeted to modulate pathogenic Th17 responses in chronic inflammatory disease.

5.3 Lactate metabolism and Th17 differentiation

Increased lactate levels in the tissue microenvironment are a well-known feature of chronic inflammation in inflamed or hypoxic tissues. Whereas the role of lactate as a fuel source has been well-appreciated in the field of physiology, the role of lactate as a metabolic feedback regulator and distinct signalling molecule is emerging to be a cue that shapes $CD4^+$ T cell differentiation and effector function[60, 61]. Unlike naïve or regulatory T cells, which rely primarily on OXPHOS and FAO to maintain their quiescence and suppressive capacity, Th17 cells exploit environmental metabolites such as lactate to reinforce their lineage commitment. In inflamed tissues, high glycolytic activity from resident cells generates local lactate accumulation, which promotes Th17 differentiation alongside local glucose and oxygen availability[91].

$CD4^+$ T cells import extracellular lactate predominantly through SLC5A12. Once internalized, lactate contributes to cellular metabolism and acts as a signalling molecule. Metabolically, lactate is converted to pyruvate, feeding cellular energy metabolism, and separately supports the phosphorylation of pyruvate kinase M2 (PKM2)[92]. Phosphorylated PKM2 translocates to the nucleus, where it interacts with STAT3, a transcription factor essential for Th17 differentiation. This interaction enhances IL-17A expression and stabilizes Th17 effector identity, linking microenvironmental metabolite availability directly to transcriptional programming[93].

Lactate-dependent Th17 enhancement is closely intertwined with glucose metabolism. Glucose uptake fuels glycolysis, providing ATP for cellular processes, while lactate metabolism sustains the intracellular NAD^+/NADH balance required for optimal STAT3 phosphorylation. This metabolic cooperation enables Th17 cells to persist and function effectively in nutrient-restricted, hypoxic microenvironments. Furthermore, lactate uptake intersects with the mTOR–HIF-1α axis, which consolidates Th17 differentiation while suppressing regulatory T cell (Treg) programs [57, 79].

Beyond its metabolic and transcriptional roles, lactate exerts epigenetic influence. Recent evidence indicates that lactate can serve as a substrate for histone lactylation, altering chromatin accessibility at the Foxp3 locus[60]. This epigenetic modification can shift Th17 cells toward a Treg-like phenotype, reducing IL-17A production. This suggests lactate does not act through a single, fixed pathway: it can reinforce Th17 identity via PKM2/STAT3 signalling, or oppose it via lactylation-driven epigenetic remodelling.

The functional relevance of lactate-driven Th17 differentiation has been demonstrated in autoimmune and inflammatory models. Elevated lactate in synovial fluid or inflamed tissues correlates with increased IL-17 production and persistent Th17 responses, highlighting that microenvironmental metabolites act as endogenous regulators of T cell fate. Consequently, Th17 identity is not determined solely by cytokine cues and lineage-specific transcription factors but is strongly modulated by the metabolic context, with lactate serving as a critical integrator of nutrient availability, oxygen tension, and redox state.

In summary, lactate functions as both a substrate and a signal that reinforces Th17 differentiation through transporter-mediated uptake, PKM2-dependent STAT3 activation, and interplay with glucose metabolism and the mTOR–HIF-1α axis. By coupling environmental conditions to transcriptional and epigenetic programs, lactate stabilizes Th17 effector identity and provides a mechanistic link between tissue metabolic states and pathogenic T cell responses. Understanding these pathways highlights potential metabolic targets for modulating Th17 activity and promoting regulatory programs in autoimmune disease.

5.4 T cell exhaustion during Th17 differentiation and fate commitment

Persistent antigenic stimulation, such as that encountered during chronic inflammation, drives T cells into a distinct state of functional decline known as T cell exhaustion. This state is characterized by sustained expression of inhibitory receptors including PD-1, TIM-3, LAG-3, and TIGIT, along with reduced cytokine production and proliferative capacity[94] [95]. Although originally described in chronic viral infection and cancer, exhaustion-like transcriptional programs also emerge in autoimmune and inflammatory contexts, including within the Th17 lineage[96]. Th17 cells, owing to their high glycolytic flux and biosynthetic activity, are particularly susceptible to metabolic and oxidative stress that precipitate exhaustion[97]. In hypoxic and lactate-rich inflamed tissues, persistent activation of HIF-1α and mTOR pathways sustains effector function but simultaneously imposes energetic strain, activating inhibitory feedback circuits that preserve viability under stress[98, 99].

During Th17 differentiation, a delicate balance exists between activation, effector function, and exhaustion. The metabolic reprogramming that supports robust cytokine secretion, particularly IL-17A, IL-22, and GM-CSF, depends on continuous nutrient uptake via GLUT1 and amino acid transporters. However, chronic exposure to antigen and pro-inflammatory cytokines such as IL-6, IL-1β, and IL-23 enforces sustained STAT3 and NF-κB activation, leading to epigenetic remodelling reminiscent of early exhaustion programs [100]. Transcription factors including TOX and BATF, which are essential for Th17 effector differentiation, progressively establish repressive chromatin landscapes that restrict proliferative renewal and favour exhaustion[101]. Concurrently, hypoxia-induced stabilization of HIF-1α enhances both RORγt and PD-1 expression[102], further linking metabolic demand with inhibitory receptor upregulation. Thus, within the same Th17 compartment, metabolic vigour and functional decline coexist, forming a dynamic continuum rather than mutually exclusive states.

As Th17 cells transit toward long-lived memory or tissue-resident phenotypes, partial exhaustion may represent a protective adaptation. By attenuating excessive effector activity under nutrient deprivation, these cells enhance their persistence while maintaining readiness for recall responses. Single-cell transcriptomic studies have identified Th17-like subsets co-expressing intermediate exhaustion markers yet retaining effector potential—analogous to “pre-exhausted” or “vigilant” states described in chronic infection[103, 104] . These subsets exhibit restrained glycolysis and preserved mitochondrial integrity, features favouring long-term survival over terminal differentiation. Therefore, the interplay among activation, metabolism, and exhaustion ultimately determines whether Th17 cells perpetuate inflammation, undergo dysfunction, or persist as memory-like progenitors. Understanding this balance is crucial for elucidating Th17 plasticity in chronic disease and for designing metabolic interventions or immune checkpoint receptor modulation that restore immune equilibrium without compromising host protection.

This framework highlights how metabolic reprogramming underlies immune cell identity and provides a mechanistic basis for understanding the influence of tissue microenvironments on T cell responses in both homeostasis and inflammation.

6.T cells in osteoarthritis

These observations are highly relevant in disease settings where the pathogenic role of Th17 cells is well established in autoimmune and inflammatory diseases such as rheumatoid arthritis, psoriasis, and inflammatory bowel disease. In osteoarthritis (OA), however, the contribution of T cell mediated inflammation is less clearly defined. This makes OA an important context in which to examine whether T cell are involved in inflammation and contribute to disease progression.

6.1 Osteoarthritis as a heterogeneous inflammatory joint disease

Osteoarthritis (OA) is the most prevalent degenerative joint disease and a leading cause of chronic pain and disability worldwide affecting an estimated 595 million people globally, 7.6% of the world's population, with projections indicating a further 60–100% increase by 2050[105, 106]. Long regarded as a consequence of mechanical “wear and tear” affecting articular cartilage, OA is now understood as a complex, heterogeneous joint disease involving the coordinated failure of multiple joint tissues, including cartilage, subchondral bone, synovium, and peri-articular structures[107]. Established risk factors such as ageing, obesity, joint trauma, genetic predisposition, and sex contribute to disease susceptibility and progression, yet do not fully explain the marked inter-individual variability in clinical presentation and outcome[108]. This heterogeneity has led to the recognition of OA as a syndrome rather than a single disease entity, representing a final common pathway of joint failure driven by distinct biological processes.

6.2 Synovial inflammation as a driver of OA progression

Synovitis (synovial membrane inflammation) is observed in approximately half of OA patients and correlates with both structural joint damage and pain severity[109-111]. Although the initiating events remain incompletely defined, synovial inflammation is thought to be triggered by endogenous danger signals released from damaged joint tissues, including cartilage matrix fragments and other damage-associated molecular patterns (DAMPs). These signals activate resident synovial cells, leading to the production of pro-inflammatory cytokines, chemokines, and matrix-degrading enzymes that exacerbate cartilage breakdown. The resulting feed-forward loop between tissue damage and inflammation establishes a state of low-grade, chronic joint inflammation that contributes to disease progression.

6.3 Innate immune activation and the role of synovial macrophages

Early immunological models of osteoarthritis primarily focused on the innate immune compartment. Among innate immune cells, synovial macrophages are now recognized as the

most important regulators of inflammatory processes within the osteoarthritic joint[112, 113]. Importantly, alterations in macrophage activation states and polarization profiles have been associated with disease severity and structural progression in OA, highlighting their functional relevance beyond passive inflammation[114]. In addition to their direct effects on tissue remodelling, synovial macrophages actively shape the local immune microenvironment through cytokine and chemokine secretion[115]. These signals are likely to influence the recruitment, activation, and functional differentiation of adaptive immune cells within the synovium, providing a mechanistic link between innate and adaptive immunity in osteoarthritis.

6.4 Adaptive immunity in OA: an emerging frontier

While the contribution of innate immunity to osteoarthritis is well established, the role of adaptive immune responses remains less clearly defined. T lymphocytes are consistently detected in OA synovial tissue and synovial fluid[116], often appearing in focal aggregates or clustered distributions, with substantial inter-patient heterogeneity in both abundance and localization. Early studies reported the presence of $CD4^+$ and $CD8^+$ T cells and provided evidence for clonal T cell receptor expansion within OA synovium, suggesting that T cell accumulation is not entirely stochastic[117]. However, whether synovial T cells in OA are merely recruited as a consequence of chronic tissue inflammation or represent antigen-experienced, functionally specialized populations actively contributing to disease processes remains unresolved. Moreover, the activation state, differentiation status, and regulatory capacity of synovial T cells, have not been systematically characterized, though some studies report an increased Th17/Treg ratio and IL-17 activity in OA, suggesting that Th17-related inflammation may contribute to synovial pathology and cartilage catabolism, but human evidence remains limited and heterogeneous[118].

6.5 Rationale for focusing on synovial T cells in end-stage OA

Addressing these gaps requires a detailed phenotypic analysis of synovial T cells within the OA joint environment. In this thesis, we focus on end-stage OA synovial tissue to establish whether T cells are consistently present, to define their subset composition and functional phenotype, and to examine their relationship to the local inflammatory milieu. End-stage synovial tissue is particularly suitable for this purpose because it is accessible in sufficient quantity and quality for detailed *ex vivo* analysis. Although earlier disease stages may be even more informative for understanding initial immune alterations, access to such samples is substantially more limited, constraining systematic analysis.

Although interactions between macrophages and T cells are known to shape synovial inflammation in highly inflammatory joint diseases such as rheumatoid arthritis, whether similar immune crosstalk operates in the low-grade, heterogeneous inflammatory context of OA remains unclear. By characterizing synovial T cells in situ, this work provides a descriptive, hypothesis-generating framework that may inform future studies aimed at identifying immune-

driven endotypes and their relevance to disease progression and therapeutic stratification in osteoarthritis patients.

Aims and Outline of the Thesis

T cells are fundamental mediators of adaptive immunity. Their activation, differentiation, exhaustion, and memory formation are shaped by the dynamic interplay between external inflammatory cues and internal metabolic states. These fate decisions not only determine immune protection and tolerance but also contribute to chronic inflammation and autoimmune pathology. A central question in human immunology is how specific microenvironments, defined by cytokines, nutrients, and metabolic stress, can guide these T cell trajectories over time.

Among $CD4^+$ T cell subsets, T helper 17 (Th17) cells exemplify this complexity: They are essential for mucosal defence but are also implicated in multiple autoimmune diseases. Their differentiation is highly responsive to cytokine context and metabolic signals, and they exhibit notable plasticity between effector, exhausted, and memory states. Yet in human systems, particularly under physiologically relevant conditions, the connections between early differentiation, metabolic pressure, and long-term functional outcomes remain incompletely defined.

This thesis explores how inflammatory and metabolic environments shape human T cell fate, using Th17 cells as a model for studying differentiation and exhaustion, and extending these principles to tissue-resident memory populations. **Chapter 2** establishes an *in vitro* system to model human Th17 differentiation from naive precursors. By manipulating cytokines (IL-6, TGF-β), glucose availability, lactate and oxygen tension, we dissect how the microenvironment influences Th17 polarization, with a focus on the hypoxia and TGF-beta interaction for Th17 differentiation. This chapter also demonstrates that under inflammatory conditions, Th17 and Treg display substantial plasticity and can coexist within the same microenvironment.

Chapter 3 investigates mitochondrial membrane potential as a regulator of T cell fate. We show that cells with elevated mitochondrial polarization exhibit higher activation and exhaustion marker expression, suggesting that strong metabolic pressure accelerates effector differentiation and functional burnout. This chapter connects metabolic checkpoints with Th17 plasticity and offers insight into how some activated cells might escape exhaustion and persist as effector memory T cells—potential contributors to autoimmune pathology.

Chapter 4 moves to an *ex vivo* human context, characterizing synovial T cell populations in end-stage osteoarthritis. Unlike autoimmune diseases, OA involves chronic low-grade inflammation and lacks a clear Th17 signature. Consistent with this, we observed minimal exhaustion and

Th17 presence, and a dominant population of central memory T cells. This suggests that in low-inflammatory environments, T cells retain vigilance without progressing to exhaustion or pathogenic effector memory states.

Together, these chapters propose a concept in which inflammatory and metabolic pressure dictate T cell differentiation outcomes. By integrating *in vitro* modelling with *ex vivo* tissue analysis, this work highlights potential mechanisms by which T cells transition between effector, exhausted, and memory states in human health and disease.

Finally, **Chapter 5** provides a summary of the studies presented in this thesis, **Chapter 6** discusses their findings and drawbacks in the context of current literature, and offers perspectives for future research directions.



Chapter 2

TGF-β and hypoxia jointly shape the transcriptional landscape of human Th17 cells

Xinlai Chen[1], Anne H.G. van Essen[1], Quynh Anh Le[1], Lorena Wunderink[1], Martijn A. Huijnen[2], Peter M. van der Kraan[1], Arjan P. M. van Caam[1], Marije I. Koenders[1]

[1]Department of Rheumatology, Radboudumc, Nijmegen, the Netherlands.

[2]Department of Medical BioSciences, Radboudumc, Nijmegen, the Netherlands.

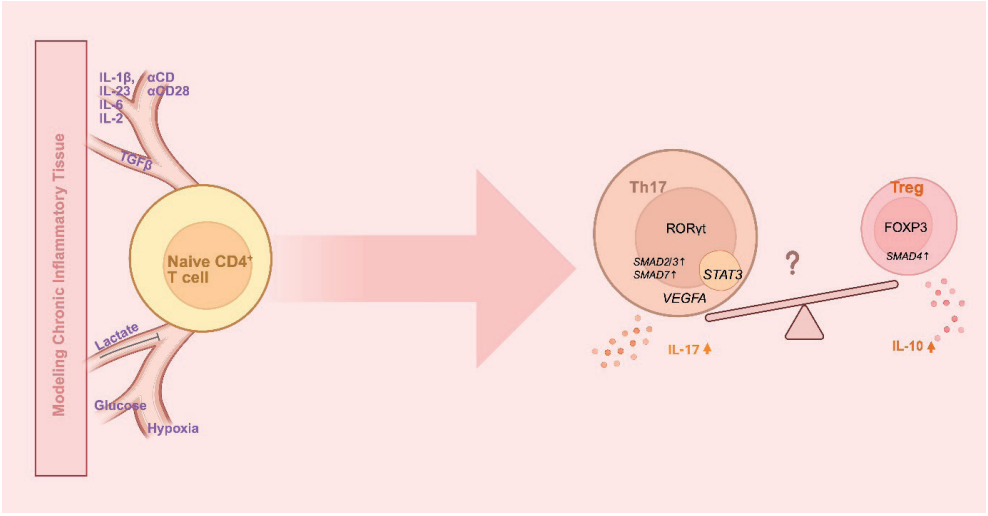

Created with BioRender.com

ABSTRACT

The Th17/Treg balance shapes inflammatory outcome in autoimmunity and cancer. These Th17 and regulatory T (Treg) cells share a naïve $CD4^+$ T cell origin and both require TGF-β, yet diverge according to the surrounding cytokine context. How TGF-β concentration and the local tissue microenvironment shape human Th17 transcriptional identity remains poorly defined. We established a serum-free human *in vitro* Th17 differentiation model from healthy donors' naive $CD4^+$ T cells and profiled the transcriptional response to different doses of TGF-β, glucose, lactate, and oxygen tension, including single-cell RNA sequencing.

TGF-β acted as a dose-dependent regulator rather than a binary on-off switch: low-dose TGF-β (1 ng/mL) supported the highest Th17 formation, while high-dose (10 ng/mL) suppressed it and induced SMAD-pathway feedback genes. Extracellular lactate reduced Th17 formation without affecting proliferation and increased expression of metabolic and JAK-STAT signaling genes, including STAT3. Hypoxia stabilized HIF-1α and induced a glycolytic program without altering Th17 formation. Hypoxia induced VEGFA expression, an effect that reached significance in the presence of TGF-β . Notably, STAT3 was induced both by lactate and by combined TGF-β and hypoxia, placing it at the intersection of cytokine, metabolic, and oxygen-sensing inputs.

Single-cell profiling resolved two transcriptionally distinct clusters within the same Th17 differentiation cultures, Th17-enriched and Treg-like, with different SMAD configurations under the same culture conditions: elevated SMAD2/3 with SMAD7 feedback in Th17 cells, and elevated SMAD4 in Treg-like cells. At the protein level, both populations secreted IL-17A and IL-10. These findings identify a point of convergence for cytokine, metabolic, and oxygen-sensing inputs in human Th17 cells, with potential relevance to chronically inflamed and tumor-associated tissues, which are characterized by elevated lactate, hypoxia, and TGF-β, where STAT3 sustains pathogenic Th17 activity.

INTRODUCTION

CD4⁺ T helper 17 (Th17) cells are an effector lineage defined by RORγt expression and IL-17A and IL-17F production[22]. They mediate mucosal host defense and drive autoimmune pathology in diseases such as rheumatoid arthritis, inflammatory bowel disease, and multiple sclerosis[119]. In contrast to Th17 cells, Treg characterized by FOXP3 are anti-inflammatory and suppress auto-immunity. Interestingly, Th17 and regulatory T cells (Treg) share TGF-β as a common differentiation signal but adopt opposing functions depending on the cytokine milieu[28]. The Th17/Treg balance shapes inflammatory outcome: Th17 expansion drives inflammation and tissue damage in autoimmunity, while Treg dominance suppresses protective T cell responses in cancer[79, 120].

In mice, Th17 differentiation from naive CD4⁺ T cells requires TGF-β plus IL-6 to induce RORγt and repress FOXP3, blocking Treg development[121]. IL-21, produced by Th17 cells themselves, sustains an autocrine loop that amplifies the Th17 population[122]. A key signaling mediator in this process is STAT3, which is activated downstream of IL-6, IL-21, and IL-23, binds the RORC locus, and is required for Th17 differentiation[123, 124]. In humans, TGF-β -induced FOXP3 directly antagonizes RORγt, and the balance between the two transcription factors determines Th17 versus Treg fate[29]. Early studies using peripheral blood naive T cells reported that human Th17 cells developed in IL-1β, IL-6, and IL-23 without exogenous TGF-β [125, 126]. A subsequent study using naive CD4⁺ T cells showed that TGF-β was required for RORγt induction and IL-17A production[127]; the discrepancy was attributed to TGF-β in the fetal bovine serum used in those protocols, so cultures without added TGF-β were not TGF-β -free. Serum-free conditions are required to study defined TGF-β doses. With pro-inflammatory cytokines such as IL-6, low TGF-β favors RORγt induction and Th17 differentiation, whereas high TGF-β represses IL-23 receptor expression and drives FOXP3⁺ Treg development[33]. However, how TGF-β doses shape the human Th17 transcriptional response has not yet been examined at single-cell resolution.

Beyond cytokines, metabolic and oxygen-sensing inputs from the tissue microenvironment can also shape T cell function. Chronically inflamed and tumor-associated tissues are hypoxic, owing to disorganized and poorly perfused vasculature despite increased vessel density [128]. Hypoxia stabilizes HIF-1α, which transactivates glycolytic enzymes and the lactate exporter MCT4 and shifts cells toward glycolysis, contributing to extracellular lactate accumulation [129-131]; lactate is further generated by glycolytic stromal and immune cells [92]. In murine CD4⁺ T cells, HIF-1α directly transactivates RORγt and the IL17 locus and targets FOXP3 for proteasomal degradation, skewing the Th17/Treg balance toward Th17. VEGFA, a canonical HIF-1α target produced by activated CD4⁺ T cells, drives neovascularization that amplifies leukocyte infiltration into inflamed tissue[132, 133]. Hypoxia and lactate both modify T cell

behavior, but their effects on human Th17 differentiation, and their interaction with TGF-β signaling, have not been directly tested. In rheumatoid arthritis synovium and inflammatory bowel disease mucosa, TGF-β combined with IL-1β, IL-6, and IL-23 drives Th17 expansion in tissue rich in lactate and hypoxia. By contrast, the tumor microenvironment is rich in TGF-β, produced by tumor cells, cancer-associated fibroblasts, and regulatory immune populations, and Treg accumulate while Th17 responses are typically restrained[134, 135]. These contrasting outcomes raise the possibility that TGF-β dose, together with hypoxia, determines whether human $CD4^+$ T cells adopt a Th17 or Treg fate.

To test this hypothesis, here we established a human *in vitro* Th17 differentiation model from healthy donors' naïve $CD4^+$ T cells in defined, serum-free, xeno-free medium. We optimized polarizing conditions, including TCR stimulation strength, CD28 co-stimulation, TGF-β dose, IL-6, glucose, and lactate, and then applied single-cell RNA sequencing across graded TGF-β concentrations under normoxia and hypoxia to resolve how TGF-β dose and oxygen tension jointly shape human Th17 transcriptional identity, and whether they interact during Th17 differentiation.

RESULTS

Establishment and optimization of human *in vitro* Th17 differentiation

To establish a human *in vitro* Th17 differentiation model, naïve $CD4^+$ T cells isolated from PBMCs were cultured under Th17-polarizing conditions. Th17 cells were defined as live $CD4^+ROR\gamma t^+IL\text{-}17A^+$ cells **(Fig. 1A)** .Differentiation efficiency varied substantially across donors and conditions, ranging from 1 to 15% **(Fig. 1A)**.

We first compared two anti-CD3 doses (1 versus 5 μg/mL). Th17 frequency was similar between conditions, while supernatant IL-17A was on average 4 times higher with 5 μg/mL anti-CD3 (n = 6; **Fig. 1B**), indicating that stronger CD3 stimulation increases IL-17A secretion without (consistently) changing Th17 frequency. We next titrated anti-CD28 across both anti-CD3 doses (**Fig. 1C**). Th17 frequency showed a biphasic response to CD28, peaking at low and high CD28 concentrations with a trough at intermediate doses. Across the titration, 5 μg/mL anti-CD3 supported higher Th17 frequencies than 1 μg/mL. IL-17A secretion decreased as anti-CD28 increased under both CD3 conditions, indicating that CD28 dose differentially affects Th17 readouts depending on whether frequency or IL-17A secretion is assessed.

We then assessed the contribution of TGF-β. Addition of TGF-β increased Th17 differentiation across CD28 concentrations (n = 4; **Fig. 1D**). Under fixed activation conditions (5 μg/mL anti-CD3 and 0.25 μg/mL anti-CD28), titration of TGF-β produced a bell-shaped response,

with 1 ng/mL yielding the highest Th17 frequency compared with 0 or 10 ng/mL (n = 5; **Fig. 1E**). Higher TGF-β also reduced the frequency of RORγt$^+$IFN-γ$^+$ cells (**Fig. 1E**). Under these optimized conditions, IL-6 increased both Th17 frequency and IL-17A secretion (n = 11; **Fig. 1F**), without significantly altering GM-CSF, IFN-γ, or TNF-α production (**Fig. 1F**), suggesting a selective effect on the Th17/IL-17A axis. Based on these data, 5 μg/mL anti-CD3, 0.25 μg/mL anti-CD28, 1 ng/mL TGF-β, and 30 ng/ml IL-6 were selected as the standard Th17-polarizing conditions for subsequent experiments.

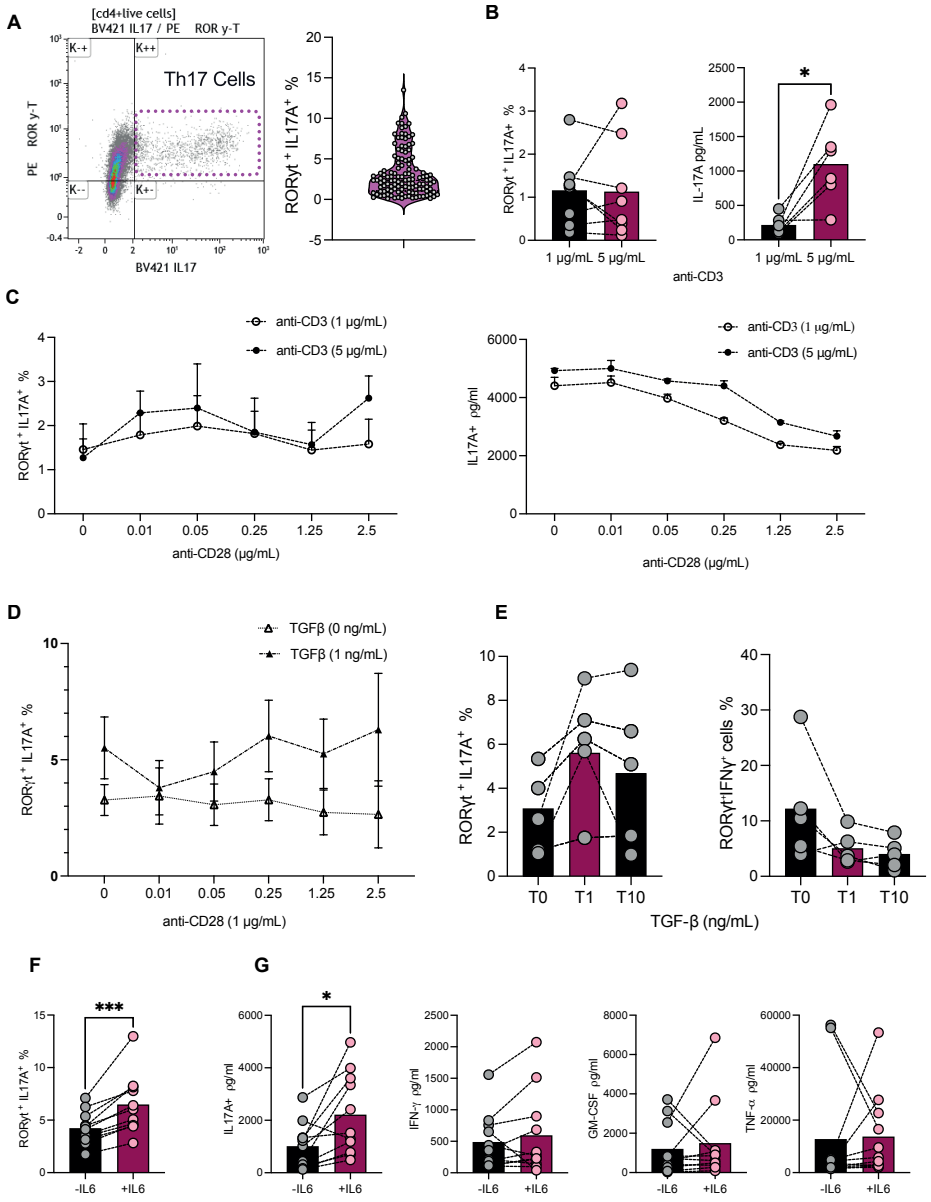

Figure 1: Establishment and optimization of human *in vitro* Th17 differentiation model.

(A) Representative flow cytometry plot showing the gating strategy for human Th17 cells, defined as live CD4⁺RORγt⁺IL-17A⁺ cells following *in vitro* polarization conditions. **(B)** Naïve CD4⁺ T cells were stimulated under Th17-polarizing conditions with 1 or 5 µg/mL anti-CD3. Th17 frequency and IL-17A production were assessed (n = 6). **(C)** Naïve CD4⁺ T cells were stimulated under Th17-polarizing conditions with 1 or 5 µg/mL anti-CD3 in combination with graded concentrations of anti-CD28. Th17 frequency and IL-17A production were assessed (Th17 frequency n = 5; IL-17A production n = 3). **(D)**

Effect of TGFβ on Th17 differentiation across anti-CD28 conditions (n = 4). **(E)** Titration of TGFβ under fixed activation conditions (5 μg/mL anti-CD3 and 0.25 μg/mL anti-CD28). Frequencies of Th17 cells and RORγt$^+$IFN-γ$^+$ cells were assessed (n = 5). **(F)** Effect of 30 ng/mL IL-6 on Th17 differentiation under optimized activation conditions in the presence of 1 ng/mL TGFβ (n = 11). **(G)** Cytokine concentrations (IL-17A, IFN-γ, GM-CSF, TNF-α) in supernatants under ± 30 ng/mL IL-6 conditions (n = 11). Each data point represents an independent donor.
*Data are presented as mean ± SEM unless otherwise indicated. Statistical analyses were performed using two-tailed paired Student's t-test. *P < 0.05, **P < 0.01, ***P < 0.001. Only statistically significant differences are indicated.*

Lactate, but not glucose, alters human Th17 differentiation and associated gene expression

To determine whether glucose availability affects Th17 differentiation, naive CD4$^+$ T cells were polarized under standard Th17 conditions across a range of glucose concentrations. Th17 frequency appeared comparable from 3.9 to 55 mM (n = 2; **Fig. 2A**). At physiological and moderately elevated glucose (5.5 mM and 11 mM), neither Th17 frequency nor proliferation (Ki-67 expression) differed significantly (n = 4; **Fig. 2B**).

Lactate, by contrast, modulated Th17 differentiation. Increasing lactate to 10 mM significantly reduced Th17 frequency under both 5.5 mM and 11 mM glucose, compared with 0 mM and 2 mM (n = 4; **Fig. 2C–D**), while Ki-67 expression was not detectably altered across lactate concentrations (**Fig. 2C–D**).

qPCR on selected metabolic and immune-regulatory genes showed that 10 mM lactate induced metabolic transporters and enzymes (*SLC2A1, MCT1, LDHA, LDHB, CD36*), JAK-STAT signaling components (*STAT3, STAT5, SOCS3*), and the transcription factor *BATF*. (n = 4; **Fig. 2E**).

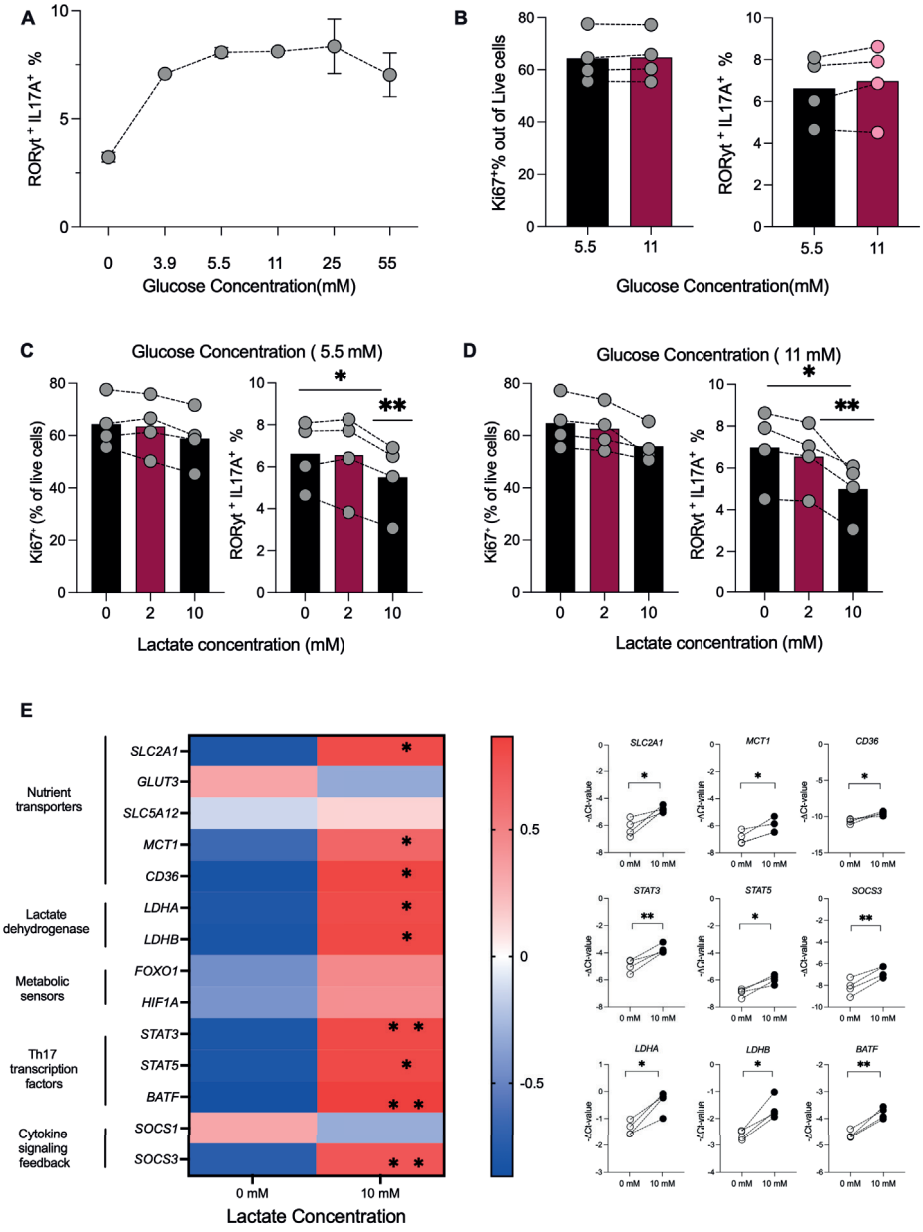

Figure 2: Effect of glucose and lactate on human Th17 differentiation *in vitro*.

(A) Naïve CD4⁺ T cells were differentiated under Th17-polarizing conditions in glucose-free RPMI 1640 supplemented with glucose to final concentrations of 0, 3.9, 5.5, 11, 25, or 55 mM. Th17 frequency was assessed by flow cytometry (n = 2). **(B)** Naïve CD4⁺ T cells were differentiated under Th17-polarizing conditions in medium containing 5.5 mM or 11 mM glucose. T-cell proliferation (Ki-67⁺ cells among live CD4⁺ T cells) and Th17 frequency were assessed (n = 4). **(C–D)** Cells were cultured under 5.5 mM (C) or 11 mM (D) glucose in the presence of 0, 2, or10 mM sodium L-lactate. Th17 frequency and T-cell

proliferation (Ki-67 expression) were assessed. Lactate at 10 mM significantly reduced Th17 frequency compared with 0 mM and 2 mM under both glucose conditions; proliferation was not significantly affected. Each data point represents an independent donor (n = 4). **(E)** Relative mRNA expression of metabolic and lactate-associated genes in cells cultured with 0 or 10 mM lactate. Heatmap shows row-wise z-scores of −ΔCt values for comparison across genes. Genes with significant differential expression between conditions are indicated (n = 4). Each data point represents an independent donor.
*Data are presented as mean ± SEM unless otherwise indicated. Statistical analysis was performed using repeated-measures one-way ANOVA with Tukey's multiple-comparisons test (C, D) or two-tailed paired Student's t-test (A, B, E). For panel E, the test was applied to −ΔCt values. *P < 0.05, **P < 0.01. Only statistically significant differences are indicated.*

HIF-1α accumulates under hypoxia without Th17 frequency alteration across TGF-β doses

To assess how oxygen availability affects Th17 differentiation, naïve $CD4^+$ T cells were activated under standard Th17-polarizing conditions and transferred to hypoxia (approximately 1% O_2) at day 2 for an additional two days **(Fig. 3A)**. Hypoxia increased HIF-1α protein expression compared with normoxia (**Fig. 3B**). Viability remained above 80% under both conditions. Th17 frequency was not significantly different between oxygen conditions in cultures differentiated with 1 ng/mL TGF-β (**Fig. 3B**).

We next examined whether hypoxia altered transcriptional responses associated with TGF-β signaling. Using ΔΔCt normalized to 0 ng/mL TGF-β, we measured *SMAD7, IFNG, VEGFA, JUNB,* and *TGFB1* under normoxia and hypoxia in the presence of 1 ng/mL TGF-β (n = 3; **Fig**. **3C**). No statistically significant differences were detected between normoxia and hypoxia, although variability was observed for *SMAD7, VEGFA,* and *JUNB*. We focused on VEGFA. Hypoxia increased VEGFA expression in the presence of 1 ng/mL TGF-β ($p < 0.01$, n = 3; Fig. 3D). A similar increase was observed without TGF-β, but did not reach statistical significance at this sample size **(Fig. 3D)**.

To test whether oxygen tension influences the TGF-β dose response, TGF-β was titrated (0, 1, and 10 ng/mL) under normoxia and hypoxia. Th17 frequency was not significantly different between oxygen conditions across all TGF-β concentrations (n = 6; **Fig. 3E**). Hypoxia stabilized HIF-1α and altered VEGFA expression in a TGF-β -dependent manner, but did not measurably change Th17 frequency.

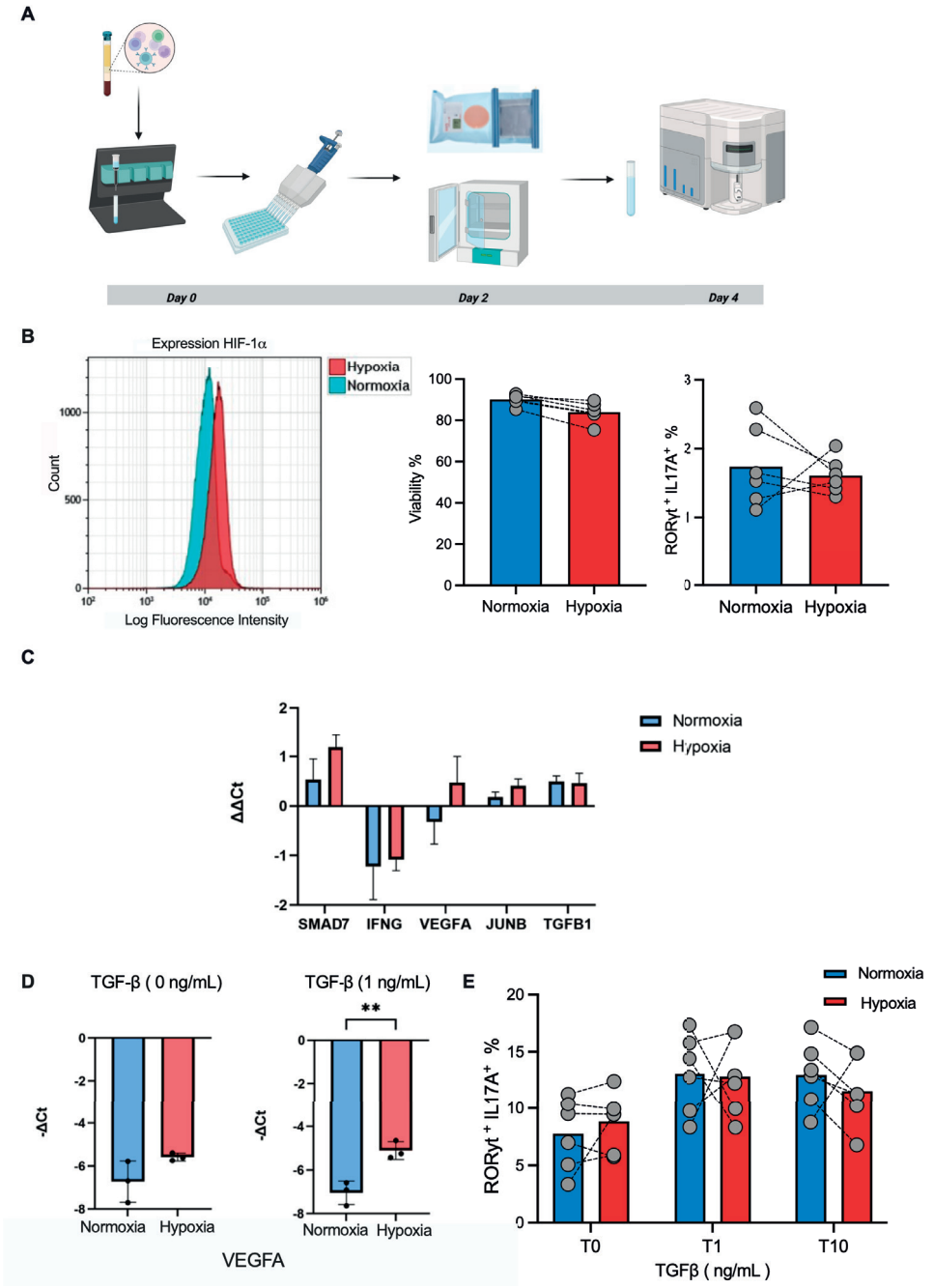

Figure 3: Effect of hypoxia on human Th17 differentiation and TGFβ-associated transcriptional responses. **(A)** Schematic overview of the *in vitro* Th17 differentiation protocol under hypoxic conditions. Cells were activated under normoxia (21% O_2) for 48 hours, then transferred to hypoxia (approximately 1% O_2) for

a further 48 hours. **(B)** Representative flow cytometry histogram of HIF-1α expression under normoxic and hypoxic conditions. Cell viability and Th17 frequency were assessed in cultures differentiated with 1 ng/mL TGFβ (n=6). Each data point represents an independent donor. **(C)** Relative mRNA expression of *SMAD7, IFNG, VEGFA, JUNB*, and *TGFB1* in cells differentiated with 1 ng/mL TGFβ under normoxic or hypoxic conditions (ΔΔCt relative to 0 ng/mL TGFβ; n = 3). Each data point represents an independent donor. **(D)** *VEGFA* expression in cells differentiated in the absence (0 ng/mL) or presence (1 ng/mL) of TGFβ under normoxic and hypoxic conditions (n = 3). Each data point represents an independent donor. **(E)** TGFβ titration (0, 1, and 10 ng/mL) under normoxic and hypoxic conditions during Th17 differentiation (n = 6). Each data point represents an independent donor.

*Data are presented as mean ± SEM unless otherwise indicated. Statistical analyses were performed using two-tailed paired Student's t-test. *P < 0.05, **P < 0.01, ***P < 0.001. Only statistically significant differences are indicated.*

Single-cell profiling identifies Th17- and Treg-enriched clusters across TGF-β conditions

To define the effects of TGF-β in our Th17 model at single-cell resolution, naïve $CD4^+$ T cells from three donors were cultured under Th17-polarizing conditions with 0, 1, or 10 ng/mL TGF-β under normoxic or hypoxic conditions and we performed single cell sequencing. Cells were harvested on day 2 and day 4 and profiled using the 10x Genomics platform (**Fig. 4A**). After quality-control filtering, datasets were integrated and subjected to graph-based clustering, yielding seven transcriptionally distinct clusters (**Fig. 4B**). We focused on the two lineage-defined clusters relevant to Th17/Treg differentiation.

Cluster identities were assigned based on canonical lineage-associated transcripts. One cluster enriched for *IL17A, IL17F, RORC, RORA, IL23R*, and *CCR6* was designated as the Th17-enriched cluster. A separate cluster with high expression of *FOXP3, CTLA4, IL2RA*, and *IKZF2* was designated as the Treg-like cluster (**Fig. 4B–C**). Lineage-associated transcripts were not restricted to single clusters, and partial overlap between Th17 and Treg-associated gene expression was observed (**Fig. 4C**).

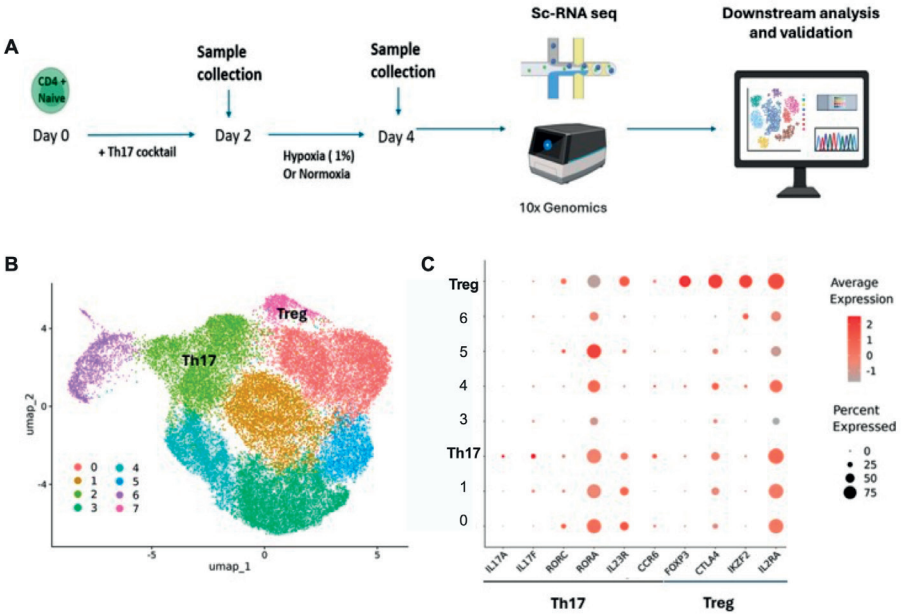

Figure 4: Single-cell transcriptomic profiling of *in vitro* Th17 differentiated of human naïve CD4 T cells across TGFβ conditions.

(A) Schematic overview of the experimental design and timeline for Single-cell transcriptomic profiling of *in vitro*–differentiated human naïve $CD4^+$ T cells across TGFβ conditions (0ng/ml-10ng/ml) in normoxic and hypoxic conditions. Cells were harvested on day 2 and day 4 for transcriptomic analysis. **(B)** Uniform Manifold Approximation and Projection (UMAP) visualization of integrated single-cell RNA sequencing data from cultures exposed to different TGFβ concentrations. Clusters were annotated based on canonical lineage-associated gene expression profiles. **(C)** Dot plot showing expression of ten selected lineage-associated genes across Th17 and Treg clusters. Color intensity represents scaled average normalized gene expression, and dot size indicates the percentage of cells expressing the respective gene.

TGF-β dose induces graded SMAD-pathway transcriptional responses within Th17 cells

To examine how TGF-β dose shapes transcriptional responses within the Th17-enriched cluster, we assessed the expression of TGF-β /SMAD pathway components and associated transcriptional regulators across 0, 1, and 10 ng/mL TGF-β conditions. *TGFBR1, TGFBR2, SMAD2,* and *SMAD4* showed dose-associated expression patterns at day 2; *SMAD2* and *SMAD4* maintained this pattern at day 4 (**Fig. 5A**). *RUNX* family members and *SMARCA2* also showed dose-associated expression.

Differential expression analysis comparing 0 and 1 ng/mL TGF-β at day 4 (adjusted $P < 0.05$; $|\log_2$ fold change$| > 1$) identified increased expression of *AHR, SKIL,* and *PMEPA1,* with reduced expression of *CSF2, DPP4,* and *TNFSF10* (**Fig. 5B**). Selected targets were validated using an independent short-term assay (16 h) followed by quantitative PCR. Consistent with the single-cell data, *AHR* and *PMEPA1* were significantly increased in the presence of 1 ng/mL TGF-β (n = 3; **Fig. 5C–D**), and *SKIL* showed a similar trend that did not reach statistical significance. Reductions in *CSF2, DPP4,* and *TNFSF10* were modest at this early 16-hour time point and did not reach the magnitude observed in the day-4 single-cell data (**Fig. 5C**).

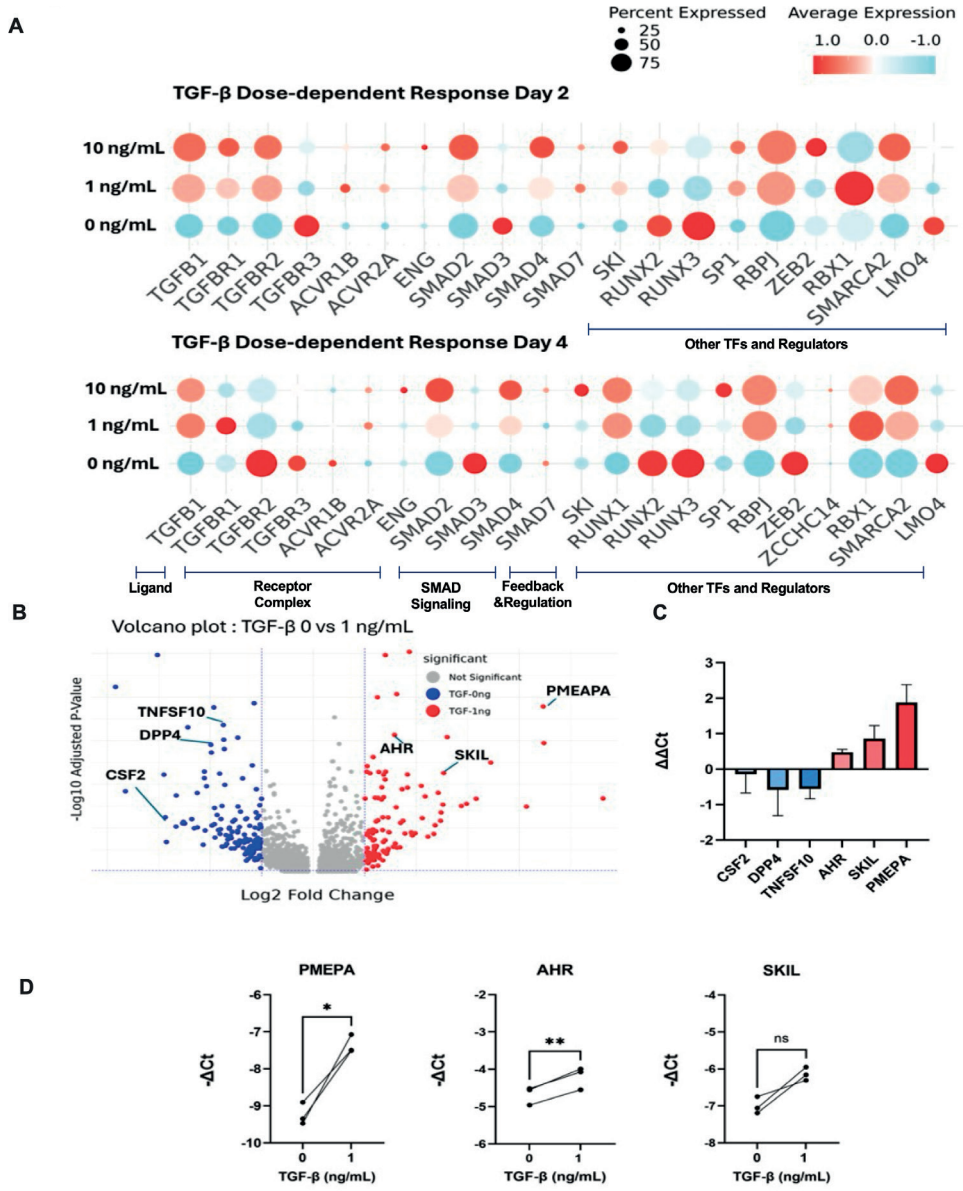

Figure 5: Effect of TGFβ dose on transcriptional programming within the Th17-enriched cluster.

(A) Dot plot showing expression of TGFβ/SMAD signaling pathway components and associated transcriptional regulators across 0, 1, and 10 ng/mL TGFβ conditions within the Th17-enriched cluster at day 2 (top) and day 4 (bottom). Color intensity represents scaled average normalized gene expression; dot size indicates the percentage of cells expressing each gene. **(B)** Volcano plot of differentially expressed genes comparing 0 and 1 ng/mL TGFβ conditions within the Th17-enriched cluster at day 4. Genes with adjusted $P < 0.05$ and $|\log^2 \text{fold change}| > 1$ are highlighted. Genes upregulated in the 1 ng/mL TGFβ condition are shown in red; downregulated genes in blue. **(C)** Quantitative PCR validation of selected

differentially expressed genes following 16 hours of stimulation under 0 or 1 ng/mL TGFβ. Relative mRNA expression was calculated using the ΔΔCt method normalized to GAPDH and RPS27A (n = 3). Each data point represents an independent donor. **(D)** Relative mRNA expression of PMEPA1, AHR, and SKIL under 0 and 1 ng/mL TGFβ conditions, normalized to GAPDH and RPS27A. PMEPA1 and AHR were significantly upregulated; SKIL showed a similar trend that did not reach statistical significance (ns). Each data point represents an independent donor.
*Data are presented as mean ± SEM unless otherwise indicated. Statistical analysis was performed using paired two-tailed Student's t-test. *P < 0.05, **P < 0.01. Only statistically significant differences are indicated.*

Hypoxia induces a HIF-linked transcriptional signature in Th17 cells and enriches glycolytic and cytokine-associated pathways

To examine how hypoxia alters the Th17 cell transcriptome at the dose where the combined TGF-β and hypoxia effect on VEGFA was observed, we compared single-cell gene expression within the Th17-enriched cluster at day 4 under normoxic and hypoxic conditions. Differential expression analysis identified a clear hypoxia-associated transcriptional signature. Genes upregulated under hypoxia included BNIP3L, BNIP3, HILPDA, PFKFB4, MIR210HG, and AK4 **(Fig. 6A)**. STAT3 expression was also elevated under hypoxia **(Fig. 6A)**, consistent with the upregulation observed under lactate exposure **(Fig. 2E).** Comparison of TGF-β pathway transcripts between hypoxia 10 ng/mL and normoxia 10 ng/mL showed that a greater proportion of cells expressed SMAD2 and SMAD4 under hypoxia, while expression intensity per cell and the patterns of SMAD3, SMAD7, TGFBR1/2, PMEPA1, and SKIL were largely unchanged **(Fig. 6C)**. This indicates that hypoxia broadens engagement of canonical SMAD components across the Th17 population rather than altering transcript abundance per cell. Gene set enrichment analysis showed enrichment of HIF-1 signaling and glycolysis/gluconeogenesis under hypoxia, alongside immune signaling pathways including cytokine-cytokine receptor interaction, JAK–STAT signaling, Th17 cell differentiation, and TNF signaling **(Fig. 6B).** Normoxic cells were enriched for oxidative phosphorylation, ribosome-associated, and RNA-processing gene sets **(Fig. 6B).**

To examine whether hypoxia influenced TGF-β -associated transcripts, expression of TGF-β pathway genes was compared across day 4 Th17 cells cultured under normoxia or hypoxia with 0 or 10 ng/mL TGF-β (**Fig. 6C**). Multiple pathway components, including *TGFBR1, TGFBR2, TGFBR3, SMAD2, SMAD3, SMAD4, SMAD7,* and *SKIL,* were detectable across all conditions. TGF-β -responsive genes including *PMEPA1, DIXDC1, BCAR3,* and *RGS16* showed higher expression in the presence of TGF-β (Fig. 6C). Hypoxia-associated transcripts *BNIP3L, HILPDA,* and *AK4* remained elevated under hypoxia irrespective of TGF-β dose (Fig. 6C). The TGF-β responsive genes were preserved under hypoxia, and the hypoxia-associated transcripts were preserved across TGF-β doses, indicating that the two transcriptional programs are engaged in parallel in Th17 cells, without evidence that hypoxia suppresses the TGF-β -driven response.

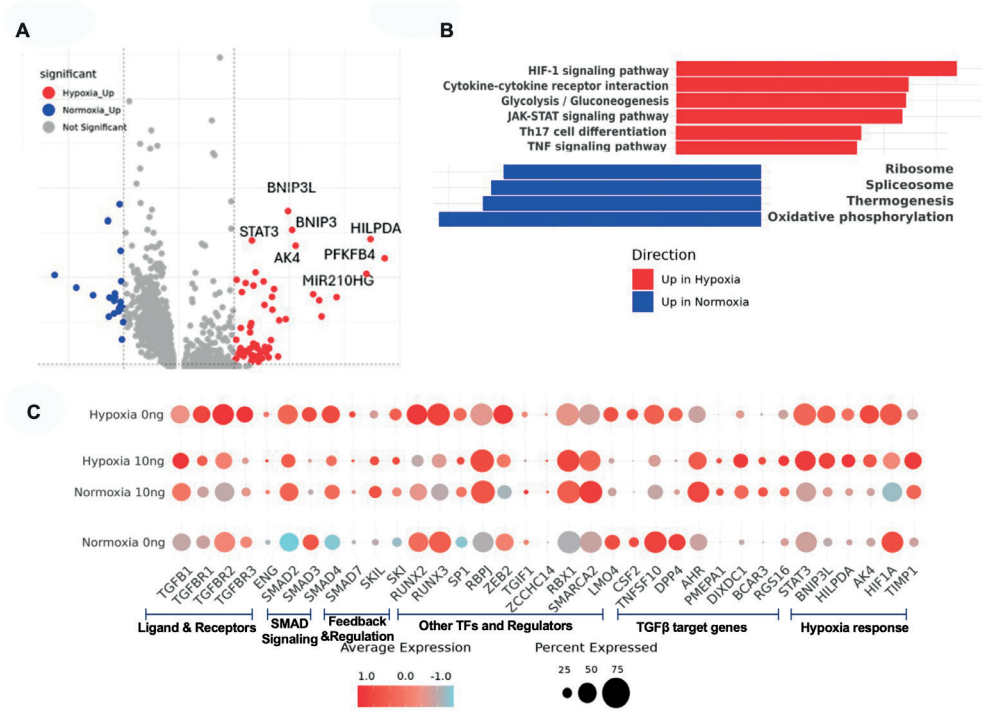

Figure 6: Single-cell transcriptional profiling of Th17 cells under normoxic versus hypoxic conditions.

(A) Volcano plot of differentially expressed genes comparing hypoxic and normoxic conditions in cells cultured with 10 ng/mL TGFβ at day 4. Genes upregulated under hypoxia are shown in red; genes upregulated under normoxia in blue. BNIP3L, the gene with the highest fold change and most significant adjusted P value under hypoxia, is indicated. **(B)** Gene set enrichment analysis (GSEA) of differentially expressed genes comparing hypoxic and normoxic conditions. Pathways enriched under hypoxia (red) and normoxia (blue) are shown, ranked by normalized enrichment score. Adjusted $P < 0.05$ was considered significant. **(C)** Dot plot showing expression of TGFβ signaling pathway genes and associated targets in single Th17 cells cultured under normoxic or hypoxic conditions with 0 or 10 ng/mL TGFβ at day 4. Dot color represents scaled average expression; dot size indicates the percentage of cells expressing the respective gene.

Th17- and Treg-enriched clusters show distinct cytokine and TGF-β-related transcriptional profiles

Differential expression analysis between the Th17-enriched and Treg-like clusters, using merged day 4 data across all TGF-β doses, first confirmed that the canonical markers used to annotate the clusters showed the expected pattern: *IL17A*, *IL17F*, *RORC*, *RORA*, *IL23R*, and *CCR6* were elevated in the Th17-enriched cluster, and *FOXP3*, *CTLA4*, *IL2RA*, and *IKZF2* were elevated in the Treg-like cluster (**Fig. 7A**). Beyond these markers, additional genes distinguished the two populations: the Th17-enriched cluster showed elevated *IL26* and *RUNX2*, while the Treg-like cluster showed elevated *BATF* (**Fig. 7A**). Gene set enrichment analysis of differentially expressed genes showed that genes elevated in the Th17-enriched cluster were associated with cytokine–cytokine receptor interaction, IL-17 signaling, chemokine signaling, JAK–STAT signaling, and inflammatory disease-associated gene sets (**Fig. 7B**). Beyond the IL-17 cytokines used for cluster annotation, the Th17-enriched cluster also expressed higher levels of *CSF2*, and *TNF* was co-expressed with IL-17 in this cluster (**Fig. 7C**).

We next examined expression of TGF-β pathway-associated genes across the two clusters. Both subsets expressed multiple components of the TGF-β receptor/SMAD axis, including ligands, receptors, SMAD-associated components, and transcriptional regulators (**Fig. 7D**). Expression patterns differed between clusters: *SMAD2, SMAD3,* and *SMAD7* were higher in the Th17-enriched cluster, while *SMAD4* was higher in the Treg-like cluster. The elevation of *SMAD7* alongside SMAD2/3 in Th17 cells reflects induction of canonical negative feedback under active TGF-β signaling.

To relate these transcriptional profiles to cytokine output, cytokines were measured in culture supernatants under standard Th17-polarizing conditions with 1 ng/mL TGF-β (Fig. 7E). Both IL-17A and IL-10 were detected across donors (n = 6), reflecting the mixed Th17/Treg profile within this *in vitro* model.

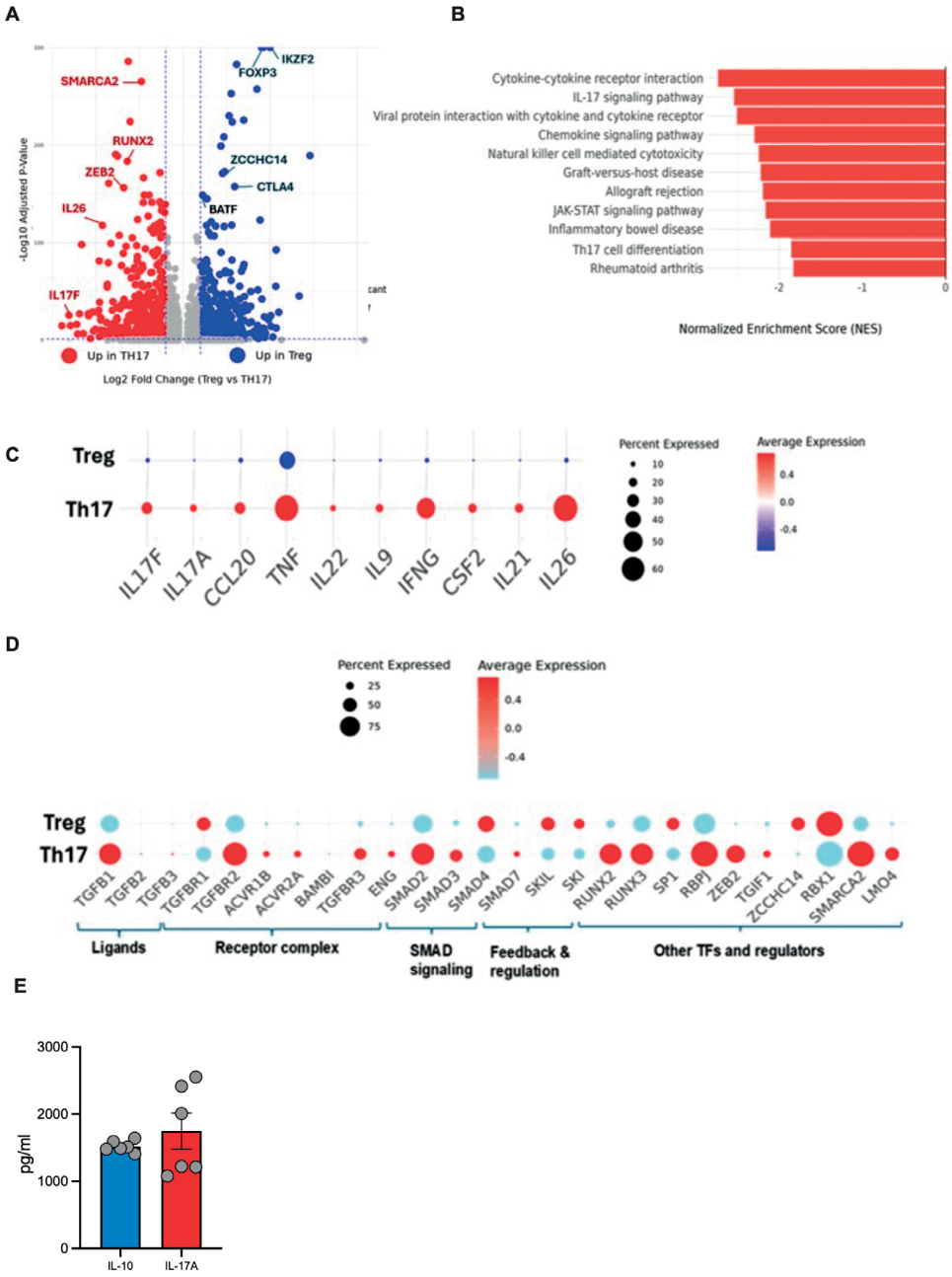

Figure 7: Differential transcriptional and cytokine profiles between Th17-enriched and Treg-like clusters.

Analysis was performed on merged single-cell RNA sequencing data across all TGFβ doses at day 4. **(A)** Volcano plot of differentially expressed genes between the Th17-enriched and Treg-like clusters. Genes with adjusted $P < 0.05$ and average $\log^2$ fold change > 1 were considered significant. Selected significant genes are

highlighted. **(B)** Gene set enrichment analysis (GSEA) of differentially expressed genes between the Th17-enriched and Treg-like clusters. Pathways shown are enriched in the Th17-enriched cluster relative to the Treg-like cluster, ranked by normalized enrichment score. Adjusted $P < 0.05$ was considered significant. **(C)** Dot plot showing expression of selected IL-17 signaling and JAK–STAT pathway genes across the Th17-enriched and Treg-like clusters. Colour intensity represents scaled average expression; dot size indicates the percentage of cells expressing the respective gene. **(D)** Dot plot showing expression of TGFβ signaling pathway components and associated regulators across the Th17-enriched and Treg-like clusters, grouped by functional category (ligands, receptor complex, SMAD signaling, feedback and regulation, other transcription factors and regulators). Colour intensity represents scaled average expression; dot size indicates the percentage of cells expressing the respective gene. **(E)** Cytokine concentrations in culture supernatants following *in vitro* Th17 differentiation under 1 ng/mL TGFβ (n = 6). IL-10 and IL-17A were quantified by multiplex immunoassay. Each data point represents an independent donor. Both IL-10 and IL-17A were detected across donors.

DISCUSSION

This study demonstrates the complexity of human Th17 differentiation, being shaped by the local microenvironment. Using an *in vitro* differentiation model combined with single-cell transcriptomics, we found that TGF-β acts as a dose-dependent regulator with intrinsic SMAD negative feedback rather than a binary switch. Cytokine, metabolic, and oxygen-sensing inputs all converge on *STAT3*, and Th17 and Treg-like populations co-emerge within our Th17-polarizing culture with distinct SMAD configurations at the single-cell level. Extracellular lactate reduced Th17 frequency, and hypoxia induced *VEGFA* gene expression only in the presence of TGF-β . Differentiation efficiency varied substantially across donors, consistent with the heterogeneity of human immune responses not captured by murine models[22, 34].

Th17 frequency and secreted IL-17A did not change in parallel across our activation conditions. Stronger TCR stimulation increased IL-17A secretion without expanding the Th17 population, showing that frequency and cytokine output report different aspects of the response and are not interchangeable readouts. Intracellular cytokine staining after PMA/ionomycin restimulation reports maximum cytokine-producing potential, whereas supernatant IL-17A reflects cumulative secretion under polarizing conditions. CD28 co-stimulation gave a different pattern: Th17 frequency was biphasic across the anti-CD28 titration, while IL-17A secretion dropped with increasing anti-CD28. The biphasic frequency response is unusual and may reflect the dose-dependence of CD28-driven PI3K/AKT/mTOR signaling, where both insufficient and excessive activation can disturb the Th17 program[136]. The progressive decline in IL-17A at higher anti-CD28 doses likely reflects CD28-driven IL-2 production: IL-2/STAT5 signaling represses RORγt-dependent IL-17A transcription in T helper cells[54]. This may explain why the highest anti-CD28 doses gave the lowest IL-17A output despite high Th17 frequencies.

Unlike CD28, IL-6 increased both Th17 frequency and IL-17A secretion without significantly changing IFN-γ, GM-CSF, or TNF-α. This selectivity reflects the IL-6 → STAT3 → RORγt axis that drives IL-17A transcription[137], without engaging the transcriptional programs that direct IFN-γ, GM-CSF, or TNF-α in T helper cells. Together with TGF-β, IL-6 suppresses FOXP3 induction and prevents naïve $CD4^+$ T cells from adopting a Treg fate[28, 127].

TGF-β acts as a dose-dependent regulator of the human Th17 response rather than a simple on/off switch. Low-dose TGF-β (1 ng/mL) supported the highest Th17 frequency, while high-dose (10 ng/mL) suppressed Th17 formation and reduced the IFN-γ^+ population, indicating a shift away from a pro-inflammatory Th17/IFN-γ-producing phenotype. TGF-β -induced FOXP3 directly antagonizes RORγt, and the balance between these two transcription factors determines Th17 versus Treg fate[29]. Endogenous TGFB1 transcript was detectable in the Th17-enriched cluster even in the absence of exogenous TGF-β at day 2, consistent with autocrine TGF-β1 production by activated T cells[138], which may sustain TGF-β signaling under low exogenous-ligand conditions if locally activated from its latent form.

Single-cell analysis revealed dose-associated expression of TGFBR1, TGFBR2, SMAD2, SMAD4, and SMAD7 within the Th17-enriched cluster, alongside dose-dependent induction of canonical TGF-β target genes, indicating that pathway activity scales with ligand concentration. AHR was among the most significantly upregulated genes at 1 ng/mL TGF-β . AHR cooperates with RORγt to drive IL-17A and IL-22 transcription, and its TGF-β -driven induction shifts Th17 cells toward an IL-22-co-producing phenotype[139]. PMEPA1 sequesters phosphorylated R-SMADs in the cytoplasm and prevents their nuclear translocation[140], while SKIL recruits transcriptional co-repressors to SMAD target promoters[141]. Their coordinated induction at higher TGF-β doses creates intrinsic negative feedback that restrains pathway output as ligand concentration rises; together with TGF-β -driven FOXP3 induction, this feedback may contribute to the bell-shaped Th17 dose-response. In parallel, CSF2 (encoding GM-CSF), TNFSF10, and DPP4 were reduced at 1 ng/mL TGF-β . GM-CSF is an effector cytokine of inflammatory Th17 cells in autoimmunity[142, 143], and its reduction at low TGF-β doses indicates that the response shifts away from a GM-CSF-producing Th17 phenotype. Dose-dependent TGF-β signaling therefore does more than scale Th17 differentiation: it shifts cells toward an IL-22-co-producing, GM-CSF-low phenotype while engaging intrinsic negative feedback that limits SMAD-driven output.

Beyond cytokine signaling, the metabolic microenvironment shapes T cell differentiation. Glucose and lactate are both metabolic cues in inflamed tissues but have markedly different effects in our system. Glucose availability had little effect on Th17 differentiation across a wide concentration range, from 3.9 mM to supraphysiological 55 mM. Glycolysis is required for Th17 effector function[144], and the simplest interpretation is that all glucose concentrations

tested were sufficient to sustain glycolytic flux during the 4-day differentiation, since activated T cells upregulate the glucose transporter *GLUT1* to maintain glucose uptake across a range of extracellular concentrations[66]. Th17 cells may additionally draw on glutamine oxidation and fatty acid metabolism, with $CD4^+$ T cells flexibly switching substrate preferences depending on nutrient availability and activation state[145].

By contrast, extracellular lactate had a clear effect on Th17 differentiation. At 10 mM, lactate reduced Th17 frequency under both physiological (5.5 mM) and elevated (11 mM) glucose conditions while T cell proliferation remained intact. Lactate constrains T cell proliferation through NAD^+/NADH redox imbalance[146], but in our system proliferation was preserved despite reduced Th17 differentiation, suggesting that the primary effect of lactate at this concentration is on differentiation rather than cell cycle progression. Lactate also induces metabolic and epigenetic reprogramming of $CD4^+$ T cells, reducing IL-17A production and biasing toward Treg-like states[92]. *MCT1* upregulation in our qPCR panel indicates active lactate import[147]; once internalized, lactate shifts the NAD^+/NADH ratio toward a more reduced state and constrains glycolytic flux. Elevated *LDHA* and *LDHB* both reflect active lactate metabolism in response to the extracellular load.

STAT3 and *STAT5* transcripts were also upregulated under lactate exposure. STAT3 is the canonical driver of Th17 differentiation downstream of IL-6, so its upregulation alongside reduced Th17 frequency is paradoxical at first reading. The resolution comes from distinguishing *STAT3* transcript abundance from STAT3 signaling activity, and from the multiple mechanisms by which lactate engages the STAT3 axis. *SOCS3*, a direct STAT3 transcriptional target and potent JAK-STAT inhibitor[148], was also upregulated. SOCS3 restrains IL-6/STAT3-driven Th17 development, generating a negative feedback loop in which elevated STAT3 transcript is offset by SOCS3-mediated suppression of upstream JAK-STAT signaling. PKM2 has been implicated in modulating STAT3 activity in Th17 cells, with nuclear *PKM2* acting as a co-regulator of STAT3-dependent transcription[93]. In addition, lactate serves as a substrate for histone lactylation, an epigenetic modification that links metabolic state to chromatin accessibility[60]. These mechanisms operate on different timescales and may explain why STAT3 transcript upregulation in our system does not translate into increased IL-17A output: SOCS3-mediated suppression dominates at the signaling level while lactate-driven epigenetic changes accumulate independently. Lactate therefore acts as an active environmental cue rather than a passive metabolite[149].

Beyond nutrient availability, oxygen tension is a distinct environmental variable that shapes T cell metabolic and transcriptional state. Hypoxia stabilized HIF-1α and induced a canonical glycolytic gene signature in our Th17 cells, including *BNIP3L, HILPDA, PFKFB4*, and *AK4*, while normoxic cells maintained oxidative phosphorylation. This response is consistent with

HIF-1α-driven metabolic reprogramming in activated T cells and confirms that hypoxia was effectively imposed in our system [128, 150]. Despite this clear metabolic reprogramming, hypoxia did not alter Th17 frequency at any TGF-β concentration tested. This contrasts with murine studies in which HIF-1α directly promotes Th17 differentiation by binding the RORγt promoter and targeting FOXP3 for degradation [79], and with human work supporting HIF-1α as a positive regulator of Th17 responses under hypoxia. The discrepancy in our system likely reflects the delayed introduction of hypoxia after initial activation of the naïve $CD4^+$ T cells, missing the early HIF-1α-dependent lineage decisions. A technical caveat may further contribute: cells were exposed to abrupt re-oxygenation and strong PMA/ionomycin activation signals prior to flow cytometric measurement, which may have masked hypoxia-driven differences in cytokine output.

Although hypoxia did not alter Th17 frequency, the question remained whether hypoxia reshapes key signaling pathways through integration with other environmental cues. *STAT3* transcript was elevated under hypoxia in the presence of TGF-β, and was also elevated under lactate exposure alongside *SOCS3* upregulation. Lactate and the combined hypoxic/TGF-β condition therefore both raised *STAT3* transcript levels in our system; together with the canonical IL-6/STAT3 axis driving Th17 differentiation, these observations point to STAT3 as a convergence node for multiple environmental signals.

This convergence is biologically meaningful because these signals co-occur in disease tissues. Elevated lactate, persistent hypoxia, and abundant TGF-β are defining features of the rheumatoid arthritis synovium, inflammatory bowel disease mucosa, and the tumor microenvironment [150]. The cellular outcomes differ between contexts: Th17 cells dominate in autoimmunity, while Tregs dominate in most solid tumors. Yet the underlying microenvironmental signal combination is shared, raising the question of why the same signals produce opposite cellular landscapes. Persistent *STAT3* activation is a consistent molecular feature of chronic inflammation and sustains Th17 responses in inflamed tissue[151, 152]. Our data raise the possibility that *STAT3* expression in these settings is not driven by IL-6 alone but is reinforced by lactate and by combined hypoxia and TGF-β, contributing to the dysregulated immune outcomes seen in chronically inflamed and tumor-associated tissues.

The simultaneous upregulation of *VEGFA* under combined TGF-β and hypoxia supports this convergence in our model. *VEGFA* transcription is regulated by HIF-1α at hypoxia-response elements[132] and by SMAD3 cooperating with HIF-1α under combined stimulation[153]. In our model, hypoxia-driven VEGFA induction reached statistical significance in the presence of TGF-β, consistent with cooperative regulation by HIF-1α and SMAD3 at the VEGFA locus. In the combined TGF-β + hypoxia environment of inflamed and tumor tissues, Th17-derived VEGFA may exert autocrine or paracrine effects on T cell differentiation and tissue remodeling.

VEGFR2 blockade in human Th17 cultures under combined TGF-β and hypoxia would clarify whether the VEGFA induction observed here has autocrine consequences on Treg-like cluster expansion[154].

Single-cell profiling identified Th17-enriched and Treg-like clusters co-existing within our Th17-polarizing environment, partly explaining the variable differentiation efficiency observed across donors. Both clusters expressed multiple components of the TGF-β /SMAD pathway, but in distinct configurations. *SMAD2* and *SMAD3*, the canonical R-SMADs activated by TGF-β receptor signaling, were higher in Th17 cells, consistent with the dose-associated signaling described above. *SMAD7*, an inhibitory SMAD and direct TGF-β -induced feedback target, was also higher in Th17 cells, indicating that active R-SMAD signaling in Th17 cells is accompanied by engagement of canonical negative feedback. *SMAD4*, the co-SMAD that partners with phosphorylated R-SMADs to enter the nucleus, was higher in the Treg-like cluster. This pattern indicates that the two lineages engage the TGF-β /SMAD pathway in distinct configurations: Th17 cells with active R-SMAD signaling and induced negative feedback, and Treg-like cells with elevated co-SMAD availability that may support engagement with broader TGF-β family ligands. *SMARCA2*, a component of the SWI/SNF chromatin remodeling complex, was higher in Th17 cells than in Treg-like cells, suggesting that TGF-β responses in Th17 cells may involve chromatin-level regulation alongside SMAD transcription factor binding. *TGFB1* itself was preferentially expressed in the Th17-enriched cluster, supporting the autocrine TGF-β1 production discussed above as a feature of differentiating Th17 cells. *BATF*, although essential for Th17 differentiation, is also required for the generation and function of effector regulatory T cells[155]; its higher expression in the Treg-like cluster is therefore consistent with this shared role rather than at odds with its Th17 function. Functional output reflected this transcriptional heterogeneity: both IL-17A and IL-10 were detected in culture supernatants, confirming that both populations are present and functionally active. Whether these cytokines arise from the same or distinct cells will require single-cell cytokine release analysis in future work. These distinct SMAD configurations within a single culture provide a transcriptional framework for the persistent co-existence of Th17 and Treg-like populations widely observed in human Th17 differentiation systems [156] and may underlie Th17 plasticity in response to changing microenvironmental cues [157, 158].

This work has limitations: The scRNA-seq dataset was generated from donor-pooled libraries, so donor-resolved sequencing in larger cohorts will be needed to confirm reproducibility, and key mechanistic claims rest on transcript-level evidence that requires protein-level confirmation, particularly through pSTAT3 and pSMAD3 as proximal readouts of pathway activation. STAT3 is already targeted in inflammatory disease through IL-6/IL-6R blockade and JAK inhibitors with only partial benefit[159]; our finding that STAT3 expression is shaped by multiple

microenvironmental inputs suggests that combination strategies targeting STAT3 alongside metabolic and oxygen-sensing pathways may be more effective than IL-6/JAK blockade alone.

METHODS

Human samples

Cryopreserved peripheral blood mononuclear cells (PBMCs) were obtained from anonymous healthy blood donors via Sanquin Blood Bank (Nijmegen, the Netherlands). All samples were handled in accordance with Sanquin guidelines. Informed consent was obtained from all donors as part of the blood donation procedure. PBMCs were thawed in RPMI 1640 (Lonza) supplemented with 10% heat-inactivated fetal calf serum (FCS; Sigma-Aldrich, F7524) and 1% penicillin-streptomycin (Lonza, 09-757F), washed twice, and used immediately for naïve $CD4^+$ T-cell isolation.

Naïve $CD4^+$ T-cell isolation

Naïve $CD4^+$ T cells were isolated from PBMCs by negative magnetic selection using the Human Naïve $CD4^+$ T Cell Isolation Kit (Miltenyi Biotec, 130-097-093) in MACS buffer containing 0.5% BSA (Sigma-Aldrich, A8806) and 2 mM EDTA (Gibco, 15400054). Cell viability and numbers were determined using the automated cell counter LUNA (Logos Biosystems). Only preparations with viability exceeding 80% were used.

In vitro Th17 differentiation

For standard Th17 differentiation, naïve $CD4^+$ T cells were seeded at 1×10^5 cells per well in 96-well round-bottom plates pre-coated with anti-CD3 antibody (clone OKT3, BioLegend, 317326) in X-VIVO 15 serum-free medium (Lonza, 04-418Q) supplemented with 5% Cell-Vive T-NK Xeno-Free Serum Substitute (BioLegend, 420502) and 1% sodium pyruvate (Invitrogen, 11360088). Unless otherwise indicated, plates were pre-coated with 5 µg/mL anti-CD3 for standard differentiation experiments. Cells were cultured for five days at 37°C, 5% CO_2, 21% O_2 unless otherwise stated.

Th17 polarization was induced by addition of soluble anti-CD28 (0.25 µg/mL, clone CD28.2, BioLegend, 302934), IL-1β (10 ng/mL, R&D Systems, 201-LB), IL-2 (10 IU/mL, BioLegend, 589104), IL-6 (30 ng/mL, BioLegend, 570804), IL-23 (10 ng/mL, BioLegend, 574102), anti- IFNγ (10 µg/mL, clone B27, BioLegend, 506533), and anti-IL-4 (10 µg/mL, clone MP4-25D2, BioLegend, 500839). TGF-β1 (PeproTech, 100-21C) was added at 0, 1, or 10 ng/mL as indicated.

Glucose and lactate experiments

For glucose titration, cells were cultured in glucose-free RPMI 1640 (ThermoFisher, 11879020) supplemented with 10% FCS and 1% penicillin-streptomycin, with glucose (Gibco) added to final concentrations of 3.9, 5.5, 11, or 55 mM. For lactate experiments, sodium L-lactate (Sigma-Aldrich) was added at 0, 2, or 10 mM under either 5.5 mM or 11 mM glucose conditions. All other conditions were identical to the standard differentiation protocol.

Hypoxic culture conditions

Cells were activated under standard normoxic conditions (21% O_2) for 48 hours, then transferred to hypoxia (approximately 1% O_2) using the nBIONIX Hypoxic Cell Culture Kit (Bulldog Bio) at 37°C, 5% CO_2 for a further 48 hours. HIF-1α stabilization under hypoxic conditions was confirmed by intracellular flow cytometry (Supplementary Figure 1). Normoxic control cultures were maintained at 21% O_2 throughout.

Flow cytometry

Prior to flow cytometric analysis, cells were restimulated for 3.5 hours with PMA (50 ng/mL, Sigma-Aldrich), ionomycin (1 µg/mL, Sigma-Aldrich, I0634), and GolgiPlug (1 µL per 10^6 cells, BD Biosciences, 51-2301KZ). Cells were stained with ViaKrome 808 viability dye (Beckman Coulter) for 20 minutes at 4°C, then fixed and permeabilized using the Foxp3/Transcription Factor Staining Buffer Set (eBioscience, 00-5521-00). Intracellular and surface staining antibodies are listed in Table 1. A minimum of 100,000 events were acquired on a CytoFlex LX flow cytometer (Beckman Coulter). Data were analyzed using Kaluza Analysis Software (v2.2.0). Th17 cells were defined as $CD4^+ROR\gamma t^+IL\text{-}17A^+$ among live $CD4^+$ T cells.

Cytokine measurement

Culture supernatants were collected after five days and stored at −80°C. Cytokine concentrations were quantified using the Bio-Plex Pro Human Cytokine Group I 27-plex assay (Bio-Rad, M500KCAF0Y) according to the manufacturer's instructions. Data were acquired on a Bio-Plex 200 system and analyzed using Bio-Plex Manager software.

RNA isolation and cDNA synthesis

Cells were harvested at indicated time points, washed in ice-cold PBS, and lysed in 500 µL TRIzol reagent (Sigma-Aldrich) per the manufacturer's instructions. Total RNA was extracted by chloroform phase separation, precipitated with isopropanol, washed in 75% ethanol, and resuspended in RNase-free water. RNA concentration and purity were assessed by NanoDrop (ThermoFisher). Residual genomic DNA was removed by DNase I treatment. Up to 1 µg of total RNA was reverse-transcribed using oligo-dT primer and 200 U M-MLV Reverse Transcriptase (Life Technologies) in a thermal cycler at 37°C, per the manufacturer's instructions.

Quantitative real-time PCR

cDNA was diluted 1:20 in RNase-free water. Each qPCR reaction contained 5 µL Power SYBR Green PCR Master Mix (Applied Biosystems, 4368708), 2 µL gene-specific primer mix, and 3 µL diluted cDNA in a total volume of 10 µL. Reactions were run on an Applied Biosystems QuantStudio 1 with the following cycling conditions: 95°C for 10 minutes, then 40 cycles of 95°C for 15 seconds and 60°C for 1 minute. A dissociation curve was generated after each run to confirm specificity. Relative gene expression was calculated using the −ΔCt method, normalized to TBP, RPLP0, and RPS27A for standard differentiation experiments, and to GAPDH and RPS27A for the 16-hour validation experiments. Reference genes were selected based on expression stability across the relevant experimental conditions.

Single-cell RNA sequencing

Naïve $CD4^+$ T cells from three healthy donors were pooled at equal proportions before activation; donor identity was therefore not tracked in the scRNA-seq data. Pooled cells were cultured under Th17-polarizing conditions with 0, 1, or 10 ng/mL TGF-β under normoxia or hypoxia, harvested on day 2 and day 4, washed twice in ice-cold PBS containing 0.04% BSA, and resuspended at 1×10^6 cells/mL. Cell viability exceeded 80% in all samples prior to loading. Approximately 100,000 cells per sample were loaded onto the 10x Genomics Chromium Controller using the Chromium Single Cell 3′ Reagent Kit v3.1. Libraries were prepared and sequenced on the Illumina platform according to the manufacturer's recommendations for 10x Genomics Single Cell 3′ chemistry.

Raw sequencing data were processed using Cell Ranger (v9.0.0) with the GRCh38-2024-A reference genome. UMI count matrices were imported into Seurat (v5.0) for downstream analysis. Cells with fewer than 250 or more than 9,000 detected genes, cells with greater than 9% mitochondrial reads, and genes detected in fewer than three cells were excluded. Datasets from all TGF-β concentrations and oxygen conditions at each time point were combined using the Seurat merge () function without batch correction. Gene expression was normalized using LogNormalize with a scale factor of 10,000. The top 2,000 variable genes were identified using FindVariableFeatures and scaled using ScaleData. Principal component analysis was performed on scaled data, and significant principal components were selected by elbow plot. KNN graph construction and Louvain clustering were performed using FindNeighbors and FindClusters; clustering resolution was selected using clustree (Zappia and Oshlack 2018, PMID: 30010766). Clusters were visualized by UMAP. Cluster identities were assigned based on canonical marker expression: IL17A, IL17F, RORC, RORA, IL23R, and CCR6 for the Th17-enriched cluster; FOXP3, CTLA4, IL2RA, and IKZF2 for the Treg-like cluster, and validated using AddModuleScore. Differential expression analysis was performed using FindMarkers with the Wilcoxon rank-sum test (thresholds: adjusted $P < 0.05$; $|\log_2 \text{fold change}| > 1$). Gene set

enrichment analysis was performed against KEGG pathway annotations on genes ranked by $\log_2$ fold change between conditions.

Statistical analysis

All statistical analyses and graphical presentations were performed using GraphPad Prism (v10.0). Data are presented as mean ± SEM unless otherwise stated, with individual data points representing independent donors. Paired comparisons between two conditions were analyzed by two-tailed paired Student's t-test on −ΔCt or log-transformed values. For single-factor experiments with more than two conditions, repeated-measures one-way ANOVA with Tukey's multiple comparisons test was applied. For two-factor experiments, repeated-measures two-way ANOVA with Šídák's multiple comparisons test was applied. The specific test is indicated in each figure legend. $P < 0.05$ was considered statistically significant; $^{*}P < 0.05$, $^{**}P < 0.01$, $^{***}P < 0.001$. Only statistically significant differences are indicated in figures.

ACKNOWLEDGMENTS

We thank Monique M. Helsen for performing the Luminex measurements, and Laura Wingens and Klaas Mulder for performing and processing the single-cell RNA sequencing samples. We thank Annet Sloetjes for training and supervising Lorena Wunderink in RNA isolation and qPCR analysis. We thank Elly L. Vitters, Birgitte Walgreen for performing the majority of PBMC isolations from buffy coats, and assistance with experiments. We thank Theodoros Ioannis Papadimitriou and the RTC / flow cytometry facility for advice on FACS gating and panel design.

Declaration of Generative AI and AI-Assisted Technologies in the Writing Process

AI-assisted technologies (e.g., grammar and language editing tools) were used to correct grammar and spelling errors in the manuscript. No AI tools were used to generate scientific content, perform data interpretation, or draw conclusions.

SUPPLEMENTARY FIGURES

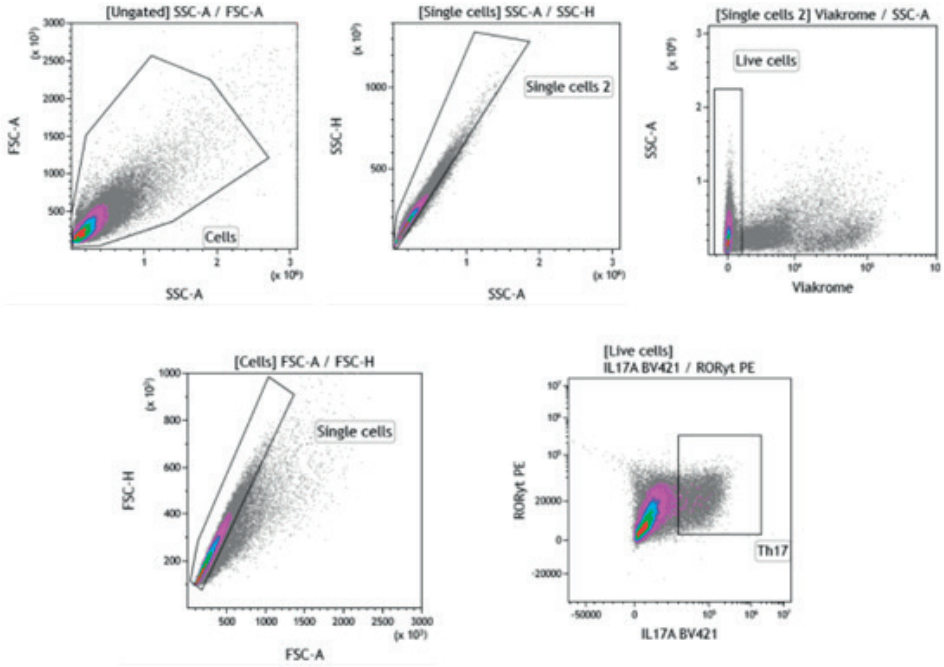

Supplementary Figure 1: Flow Cytometry Gating Strategy for Th17 cells (RORyt$^+$IL17A$^+$).

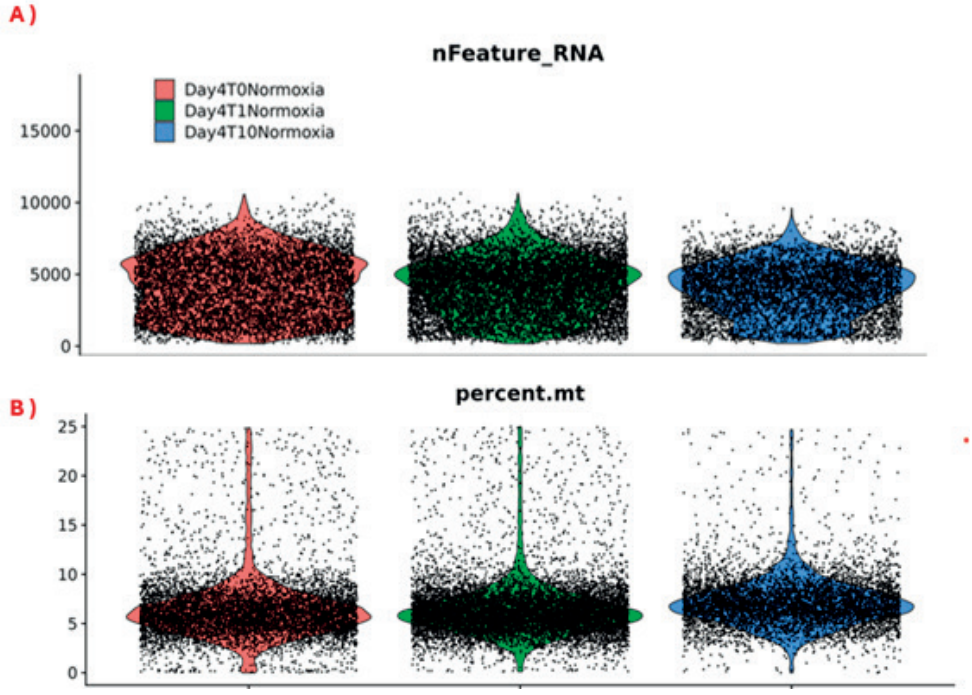

Supplementary Figure 2: Quality control metrics from samples stimulated with TGF-β at 0, 1 or 10 ng/mL on day 4.

A) Violin plots showing distribution of the number of genes detected per cell across 3 conditions, with each dot representing a cell. **B)** Violin plots showing the distribution of percentage of mitochondrial genes in each cells across 3 conditions, with each dot representing a cell. Based on these results, we selected cells that expressed more than 250 but less than 9000 genes. In addition, we omitted cells with percentage of mitochondrial genes higher than 9 %.

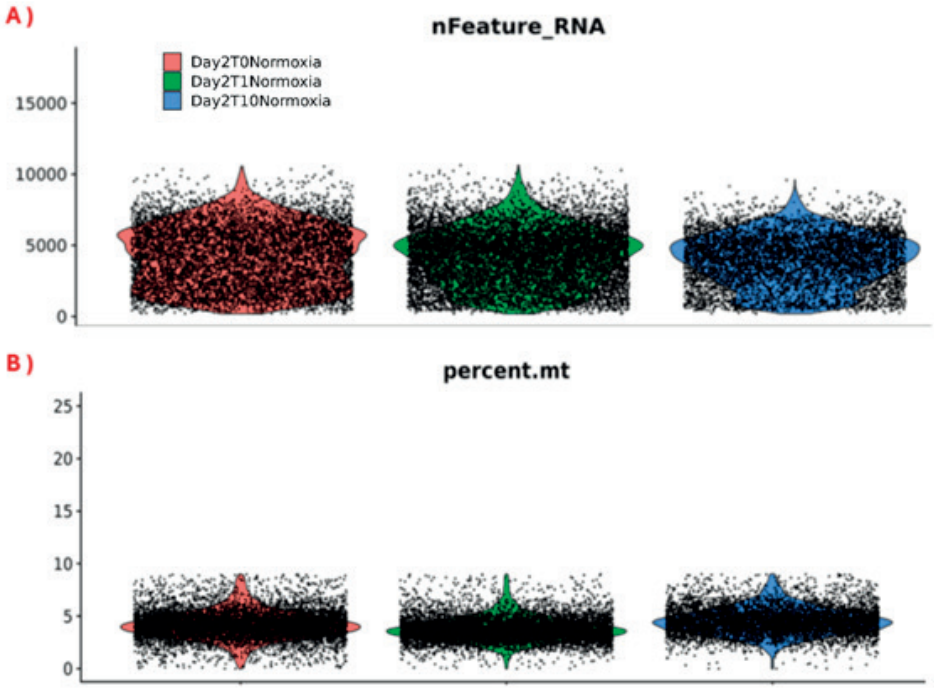

Supplementary Figure 3: Quality control metrics from samples stimulated with TGF-β at 0, 1 or 10 ng/mL on day 2.

A) Violin plots showing distribution of the number of genes detected per cell across 3 conditions, with each dot representing a cell. **B)** Violin plots showing the distribution of percentage of mitochondrial genes in each cells across 3 conditions, with each dot representing a cell. Based on these results, we selected cells that expressed more than 250 but less than 9000 genes. In addition, we omitted cells with percentage of mitochondrial genes higher than 9 %.

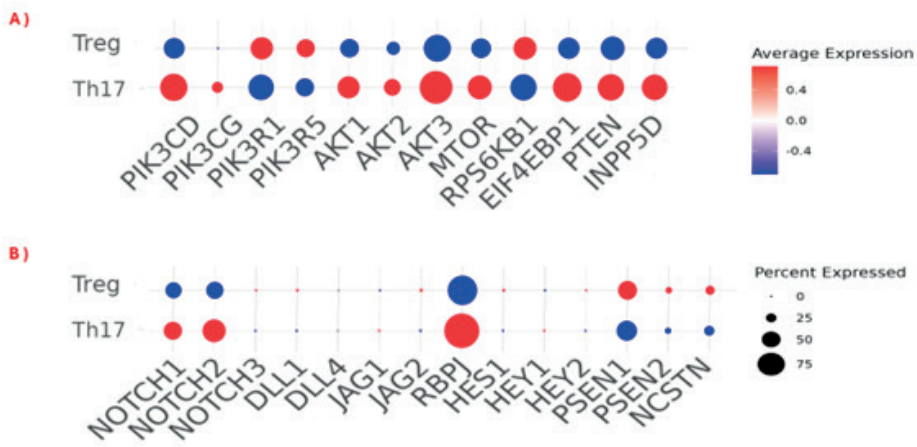

Supplementary Figure 4: Dot plot comparing the expression levels of genes involved in non-canonical and crosstalk signaling pathways.

A) Comparison of key genes from the PI3K/Akt pathway, which is a non-canonical branch of TGF-β signaling. **B)** Comparison of selected genes from the Notch signaling pathway, which interacts with TGF-β through crosstalk mechanisms.

Color intensity indicates average expression level, while dot size represents percentage of cells that express the gene.

SUPPLEMENTARY TABLES

Supplementary Table 1: qPCR primer list.

Gene	Forward (5′→3′)	Reverse (5′→3′)
SLC2A1	TGGCATCAACGCTGTCTTCT	AGCCAATGGTGGCATACACA
HIF1A	TATGAGCCAGAAGAACTTTTAGGC	CACCTCTTTTGGCAAGCATCCTG
SLC5A12	TCCTCTTCACCCGCAAAAACCC	CCACGCCATTATTCTCCTCCAC
SLC16A1	GTCATGTATGGTGGAGGTCCTATC	TGACAAGCAGCCACCAACAA
FOXO1	GGCGGGCTGGAAGAATTCAA	TTGCCACCCTCTGGATTGAG
STAT3	AACGACCTGCAGCAATACCA	TGTCAAAGGTGAGGGACTCAAA
STAT5A	ACTCCTGTGCTGGCTAAAGC	CCAGCATCTGCAGATGCATTC
CD36	CTTTGGCTTAATGAGACTGGGAC	GCAACAAACATCACCACACCA
LDHA	AGTTTCCACCATGATTAAGGGTCTT	AACGGGCCTCTTCCTCAGAA
LDHB	ATCAGCATTCTGGGAAAGTCTCT	CTCCCATGCTGCAGATCCAT
BATF	CCCTGGCAAACAGGACTCAT	TCTGGGCGGCAATACGATTT
SOCS1	TTCGCCCTTAGCGTGAAGATGG	TAGTGCTCCAGCAGCTCGAAGA
SOCS3	CATCTCTGTCGGAAGACCGTCA	GCATCGTACTGGTCCAGGAACT
SLC2A3	TGCCTTTGGCACTCTCAACCAG	GCCATAGCTCTTCAGACCCAAG
GAPDH	ATCTTCTTTTGCGTCGCCAG	TTCCCCATGGTGTCTGAGC
RPS27A	TGGCTGTCCTGAAATATTATAAGGT	CCCCAGCACCACATTCATCA

All primers used for quantitative PCR, with gene symbol, gene name, and forward and reverse sequences (5′→3′). GAPDH and RPS27A were used as reference genes.

Supplementary Table 2: List of genes used in the analysis and their primer sequences.

Gene	Forward (5′→3′)	Reverse (5′→3′)
AHR	AACGGAGGCCAGGATAACTG	ACAAAGCCATTCAGAGCCTGTA
CSF2	ACACTGCTGCTGAGATGAATGA	GGCTCCTGGAGGTCAAACAT
DPP4	GAATGTCCAGATGCCCTCCAA	CATGGGCCTGCATACACATCT
JUNB	AACAGCCCTTCTACCACGAC	CAGGCTCGGTTTCAGGAGTT
PMEPA1	AGAAGATGCCCTGTCCTCAGAAG	CGAGGCGGGGCGTAGA
RPLP0	CCATTCTATCATCAACGGGTACAA	TCAGCAAGTGGGAAGGTGTAAT
RPS27A	TGGCTGTCCTGAAATATTATAAGGT	CCCCAGCACCACATTCATCA
TBP	GCTTCGGAGAGTTCTGGGATTG	GCAGCAAACCGCTTGGGATTA
TGFB1	GAGGTCACCCGCGTGCTA	TGCTTGAACTTGTCATAGATTTCGTT
TNFSF10	TCCGTCAGCTCGTTAGAAAGATGA	TCCTCTGGTCCCAGTTATGTGA
SMAD7	CCTTAGCCGACTCTGCGAACT	CCAGATAATTCGTTCCCCCTGTA
VEGFA	CAGGGAAGAGGAGGAGATGAGA	GCTGGGTTTGTCGGTGTTC

Forward and reverse primer sequences (5′→3′) for each gene.

Supplementary Table 3: Cell recovery summary across samples.

Sample	Cell Ranger estimate	After QC filtering
Day 2 T0 Normoxia	8772	8216
Day 2 T1 Normoxia	8157	7824
Day 2 T10 Normoxia	6835	6541
Day 4 T0 Normoxia	7662	7618
Day 4 T1 Normoxia	10513	10492
Day 4 T10 Normoxia	6804	6789
Day 4 T0 Hypoxia	6597	6585
Day 4 T10 Hypoxia	8577	8566

For each sample, the number of cells estimated by the Cell Ranger pipeline and the number of high-quality cells retained after standard quality-control filtering. Genes expressed in fewer than 3 cells and cells expressing fewer than 250 genes were excluded.

Supplementary Table 4: List of antibodies used for Flow Cytometry staining.

Antigen	Clone	Fluorochrome	Supplier	Catalogue no.
RORγt	AFKJS-9	PE	Invitrogen	12-6988-82
IL-17A	BL168	BV421	BioLegend	512322
IFN-γ	4S.B3	BV510	BioLegend	502544
HIF1a	546-16	Alexa Fluor 647	BioLegend	359706
IL-10	JES3-9D7	PE/Cy7	BioLegend	501419
Foxp3	PCH101	APC	Invitrogen	17-4776-42



Chapter 3

Mitochondrial activity regulates human T helper 17 differentiation and function

Xinlai Chen[1], Theodoros Ioannis Papadimitriou[1, 2], Anne H.G. van Essen[1], Britt van Brunschot[1], Monique M. Helsen[1], Annet Sloetjes[1], Elly L. Vitters[1], Werner J.H. Koopman[3,4,5], Peter M. van der Kraan[1], Arjan P.M. van Caam[1], Marije I. Koenders[1]

Immunology. 2026;177(1):185-198.

1. Department of Rheumatology and Laboratory of Experimental Rheumatology, Radboudumc, Nijmegen, the Netherlands
2. Department of Laboratory Medicine – Medical Immunology, Radboudumc, Nijmegen, the Netherlands
3. Department of Pediatrics, Amalia Children's Hospital, Radboudumc, Nijmegen, the Netherlands
4. Radboud Center for Mitochondrial Medicine, Radboudumc, Nijmegen, the Netherlands
5. Human and Animal Physiology, Wageningen University, Wageningen, the Netherlands

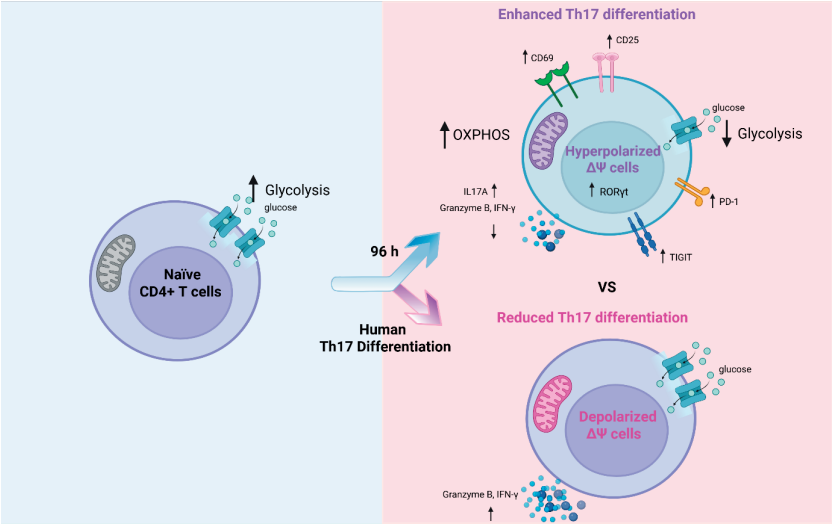

Created with BioRender.com

ABSTRACT

Introduction: Immunometabolism plays a pivotal role in T cell fate decisions, yet its specific contribution to human Th17 differentiation remains incompletely understood. Th17 cells, a subset of $CD4^+$ T cells, are central to autoimmune pathogenesis through their secretion of pro-inflammatory cytokines. Elucidating the metabolic drivers of Th17 differentiation may reveal novel therapeutic targets.

Methods: We investigated the role of mitochondrial activity in Th17 differentiation using an *in vitro* model with naïve human $CD4^+$ T cells. Single-cell metabolic profiling and functional assays were used to characterize metabolic changes during differentiation.

Results: Th17 cells exhibited a hyperpolarized mitochondrial membrane potential ($\Delta\Psi$) compared to non-Th17 cells. Hyperpolarized $\Delta\Psi$ cells displayed increased metabolic activity and enhanced differentiation capacity. Metabolic profiling at 48 hours revealed an early reliance on glycolysis, followed by a shift towards increased dependence on oxidative phosphorylation (OXPHOS) by 96 hours. Gene expression analysis indicated early upregulation of *TEFM*, a mitochondrial transcription regulator, at 48 hours. By 96 hours, $\Delta\Psi$ hyperpolarized cells exhibited a downregulation of *DRP1* and *MFN2*, genes responsible for mitochondrial fission and fusion. Functionally, $\Delta\Psi$ hyperpolarized cells expressed elevated activation markers (CD69, CD25) but also showed increased exhaustion markers (TIGIT, PD-1), indicating a link between high metabolic activity and exhaustion. Additionally, these cells triggered weaker NF-κB and AP-1 signaling and secreted lower levels of effector molecules (IFN-γ, Granzyme B) than $\Delta\Psi$ depolarized cells.

Conclusion: Mitochondrial activity critically shapes Th17 differentiation. Although hyperpolarized $\Delta\Psi$ cells exhibit greater activation, they are more prone to exhaustion and reduced effector function. These findings offer insights into Th17 metabolic regulation and its therapeutic potential in autoimmune diseases.

1. INTRODUCTION

T helper 17 (Th17) cells play a pivotal role in host defence against extracellular pathogens, including bacteria and fungi [160, 161]. These cells originate from naive $CD4^+$ T cell precursors [162, 163] and are characterized by the expression of the transcription factor RAR-related orphan receptor C (RORC) and the production of interleukin (IL)-17A [32]. Beyond their protective function, Th17 cells are critically involved in the pathogenesis of various autoimmune diseases, such as inflammatory bowel disease [164, 165], spondyloarthritis [166], psoriatic arthritis [167] and rheumatoid arthritis (RA) [168]. Targeting IL-17A has demonstrated significant therapeutic efficacy in reducing disease activity and improving clinical outcomes in these conditions [169, 170].

Understanding the mechanisms governing Th17 cell differentiation is essential for devising strategies to prevent the emergence and expansion of pathogenic Th17 cells during the early stages of autoimmune disease. Early intervention is considered critical in achieving disease remission. However, the differentiation of Th17 cells —particularly in humans —remains incompletely understood. Further insights into these mechanisms could help restore immunological homeostasis by preventing the formation of pathogenic Th17 cells [22].

In addition to the three classical signals that drive $CD4^+$ T cell differentiation—T cell receptor activation, co-stimulation, and the cytokine milieu—recent studies emphasize the crucial role of cell metabolism in determining T cell fate and function [65, 171]. Metabolic reprogramming, particularly the interplay between glycolysis, fatty acid oxidation (FAO), and mitochondrial oxidative phosphorylation (OXPHOS), is essential for the differentiation of naïve T cells into the Th17 phenotype. For instance, in murine models of central nervous system autoimmunity, the metabolic switch between glycolysis and FAO directly guides Th17 cells toward a more pathogenic state, characterized by the production of IFN-γ [172]. Disrupting OXPHOS in these polyfunctional Th17 cells alters their gene expression, causing them to adopt a profile more akin to non-pathogenic Th17 cells [173]. Furthermore, OXPHOS has been shown to enhance the resistance of effector Th17 cells to apoptosis, which may contribute to their prolonged persistence *in vivo* and the potential to acquire memory-like properties [174].

However, the extent to which these metabolic programs regulate Th17 differentiation in human cells remains unclear. Given that differentiating human Th17 cells from naive T cells *in vitro* remains a significant challenge, current knowledge on the metabolic factors regulating Th17 development is largely dependent on murine studies. Thus, whether mitochondrial metabolism similarly shapes the differentiation and function of human Th17 cells remains an open question.

In this study, we directly addressed this gap by investigating how mitochondrial activity influences the differentiation of human naive CD4⁺ T cells into effector Th17 cells. By developing an *in vitro* human Th17 differentiation model and utilizing single-cell metabolic profiling techniques, we explored the role of mitochondrial function in shaping Th17 formation. Our findings provide new insights into the energy metabolic regulation of human Th17 cells and highlight potential therapeutic opportunities for targeting mitochondrial function in autoimmune disease.

2. RESULTS

2.1 Th17 cells exhibit hyperpolarized mitochondrial membrane potential compared to non-Th17 cells

Naive CD4⁺ T cells were differentiated into Th17 cells over a 96-hour *in vitro* culture under Th17-polarizing conditions (Figure 1A). Th17 cells, identified by flow cytometry as RORγt⁺IL-17A⁺ populations (Figure 1B; gating strategy shown in Supplementary Figure 1), were distinguished from non-Th17 cells lacking these markers. Mitochondrial membrane potential (ΔΨ), an indicator of mitochondrial bioenergetic status, was assessed using MitoTracker Deep Red (MDR) staining and quantified as geometric mean of cellular fluorescence intensity (gMFI). Higher MDR accumulation, consistent with a hyperpolarized ΔΨ, was observed in Th17 cells compared to non-Th17 cells (Figure 1C).

To validate the reproducibility of this observation, we compared three Th17 polarization protocols (cocktail 1, cocktail 2, and our optimized cocktail 3; Supplementary Table 1), reflecting common variations used for *in vitro* human Th17 differentiation [175, 176]. Although the field employs multiple differentiation protocols, we sought to determine whether the mitochondrial phenotype—specifically increased MDR accumulation—was consistent across different conditions. All three cocktails successfully induced Th17 differentiation, with our optimized cocktail achieving the highest yield of IL-17A⁺ Th17 cells (Figure 1D). Across all conditions (n = 6), Th17 cells consistently exhibited higher MDR staining intensity than non-Th17 cells (Figures 1E and F), supporting a robust association between mitochondrial hyperpolarization and Th17 identity.

Early transcriptional analysis revealed upregulation of RORC and IL17A mRNA as early as 24 hours, (Figure 1G), although IL-17A protein expression was not detected until 48–72 hours (Figure 1H). Initiation of Th17 polarization was detectable at 24 hours but became more robust from 48 hours onward (Figure 1I). Based on these kinetics, subsequent analyses of mitochondrial activity focused on 48-hour and 96-hour time points to capture early and late phases of Th17 development.

To further assess the specificity of Th17 differentiation across cocktails, we evaluated the expression of the effector cytokine IFN-γ alongside IL-17A by intracellular flow cytometry. Our optimized cocktail (cocktail 3) produced the highest proportion of IL-17A$^+$ cells with reduced IFN-γ production, whereas cocktails 1 and 2 predominantly induced IFN-γ$^+$ cells (Figure 1J). All conditions were analyzed using equal numbers of input cells, confirming that observed differences reflected true differences in Th17 yield and cytokine profile.

To characterize T helper subset heterogeneity, we further analyzed the intracellular protein expression of lineage-defining transcription factors, including T-bet, FOXP3, and GATA3, alongside their signature cytokines (IL-4, IFN-γ, and IL-10), by multicolor flow cytometry. Our optimized cocktail generated the lowest frequency of non-Th17 T helper subsets, as reflected by reduced frequency of non-Th17 markers (Supplementary Figure 2).

Given these findings, we next sought to determine whether the observed differences in mitochondrial membrane potential merely correlate with Th17 differentiation or actively influence Th17 fate. To address this, we sorted cells based on MDR staining intensity at defined time points and performed functional analyses to investigate the impact of mitochondrial activity on Th17 commitment and metabolic reprogramming.

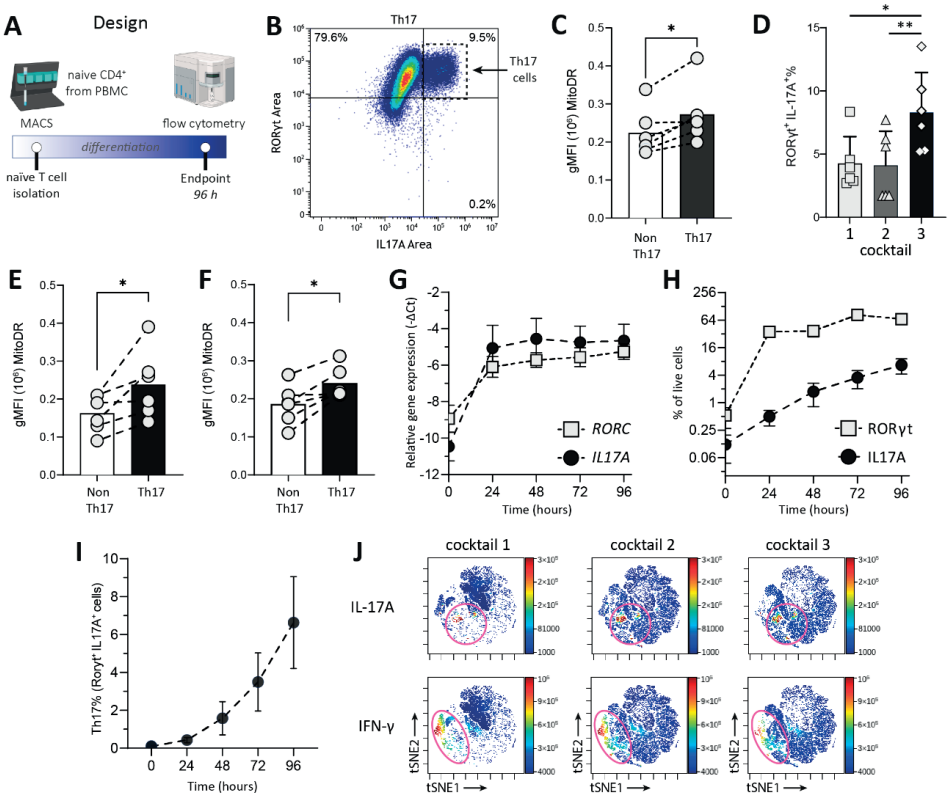

Figure 1: Th17 cells exhibit higher mitochondrial activity than non-Th17 cells.

(A) Schematic representation of the *in vitro* Th17 differentiation process. **(B)** Representative flow cytometry shows Th17 cells (RORγt⁺ IL-17A⁺) generated after 96 hours under optimized conditions. **(C)** Mitochondrial membrane potential (ΔΨ), assessed via MitoTracker Deep Red (MDR) geometric mean fluorescence intensity (gMFI), is significantly higher in Th17 cells compared to non-Th17 counterparts (n = 6, P = 0.0117). **(D)** Th17 cell frequency is significantly increased under the optimized polarization cocktail (cocktail 3) compared to cocktails 1 and 2 (n = 6; cocktail 1 vs. 3, P = 0.0312; cocktail 2 vs. 3, P = 0.0079). **(E–F)** MDR gMFI is also elevated in Th17 cells versus non-Th17 cells under cocktail 1 (P = 0.0363) and cocktail 2 (P = 0.0129), respectively. **(G)** Mean RORC and IL17 mRNA expression over time during *in vitro* Th17 differentiation (n = 6). **(H)** Mean RORγt and IL-17A protein production over time during *in vitro* Th17 differentiation (n = 6). **(I)** Kinetics of Th17 cell differentiation over time as determined by flow cytometry (n = 6). **(J)** tSNE analysis of Th17 polarization, comparing cytokine production across three Th17 polarization cocktails with equal event counts. The optimized cocktail yields the highest IL-17A production with reduced IFN-γ levels. Data for panels G, H, and I are presented as mean ± SD. Error bars represent standard deviation.

2.2 Hyperpolarized ΔΨ cells exhibit increased metabolic activity and enhanced Th17 differentiation

To directly assess the relationship between mitochondrial activity and human Th17 differentiation, we sorted hyperpolarized and depolarized ΔΨ $CD4^+$ T cells at 48 and 96 hours and evaluated their metabolic profiles and differentiation capacity (Figure 2A). ΔΨ was determined by MitoTracker Deep Red (MDR) staining. To assess metabolic activity, we measured NADH conversion rates over a 2-hour period using the XTT assay, with readings taken every 15 minutes. Hyperpolarized ΔΨ cells consistently exhibited higher NADH conversion compared to depolarized ΔΨ cells at both 48 and 96 hours (Figure 2B, C), indicating greater metabolic activity. These results were consistent across three independent experiments, each involving two donors.

Total ATP content was then assessed using the CellTiter-Glo (CTG) assay, which quantifies total cellular ATP levels based on luminescence. Hyperpolarized ΔΨ cells displayed significantly higher ATP content than depolarized ΔΨ cells at both time points (Figure 2D). All measurements were performed on highly viable cells, and viability was comparable across groups.

Based on these metabolic differences, we re-sorted hyperpolarized and depolarized ΔΨ cells at 48 hours and re-seeded them into Th17-polarizing conditions for an additional 48 hours. Following extended culture, hyperpolarized ΔΨ cells exhibited significantly enhanced Th17 differentiation compared to depolarized ΔΨ cells (Figure 2E). These findings suggest that elevated metabolic activity is associated with an increased capacity for Th17 lineage commitment.

Given the importance of mitochondrial morphology and structure in T cell function, we next assessed the expression of genes involved in mitochondrial fusion (OPA1, MFN1, MFN2), fission (DRP1, FIS1), transcription (TEFM, POLRMT, TFB2M, NRF1), and metabolism (GOT1, which has been linked to Th17 differentiation [177]) at 48 and 96 hours (Figure 2F). Gene expression was normalized to housekeeping genes using the $-\Delta Ct$ method. At 48 hours, TEFM was significantly upregulated in hyperpolarized ΔΨ cells compared to depolarized cells (Figure 2G), suggesting enhanced mitochondrial transcriptional activity during early Th17 differentiation. By 96 hours, hyperpolarized ΔΨ cells exhibited downregulation of DRP1 and MFN2 (Figure 2G), suggesting dynamic regulation of mitochondrial morphology as differentiation progressed.

To further investigate the functional role of mitochondrial activity, we used the mitochondrial uncoupler carbonyl cyanide-p-trifluoromethoxy phenylhydrazone (FCCP) to disrupt ΔΨ. FCCP was applied at a final concentration of approximately 500 nM. As expected, FCCP treatment reduced MDR fluorescence intensity (data not shown). When FCCP was added at the beginning of culture (0 hours), Th17 differentiation was significantly impaired; however, when FCCP was added at 48 hours, no clear inhibition was observed (Figure 2H). These results suggest that mitochondrial activity is particularly critical during the early stages of Th17 polarization.

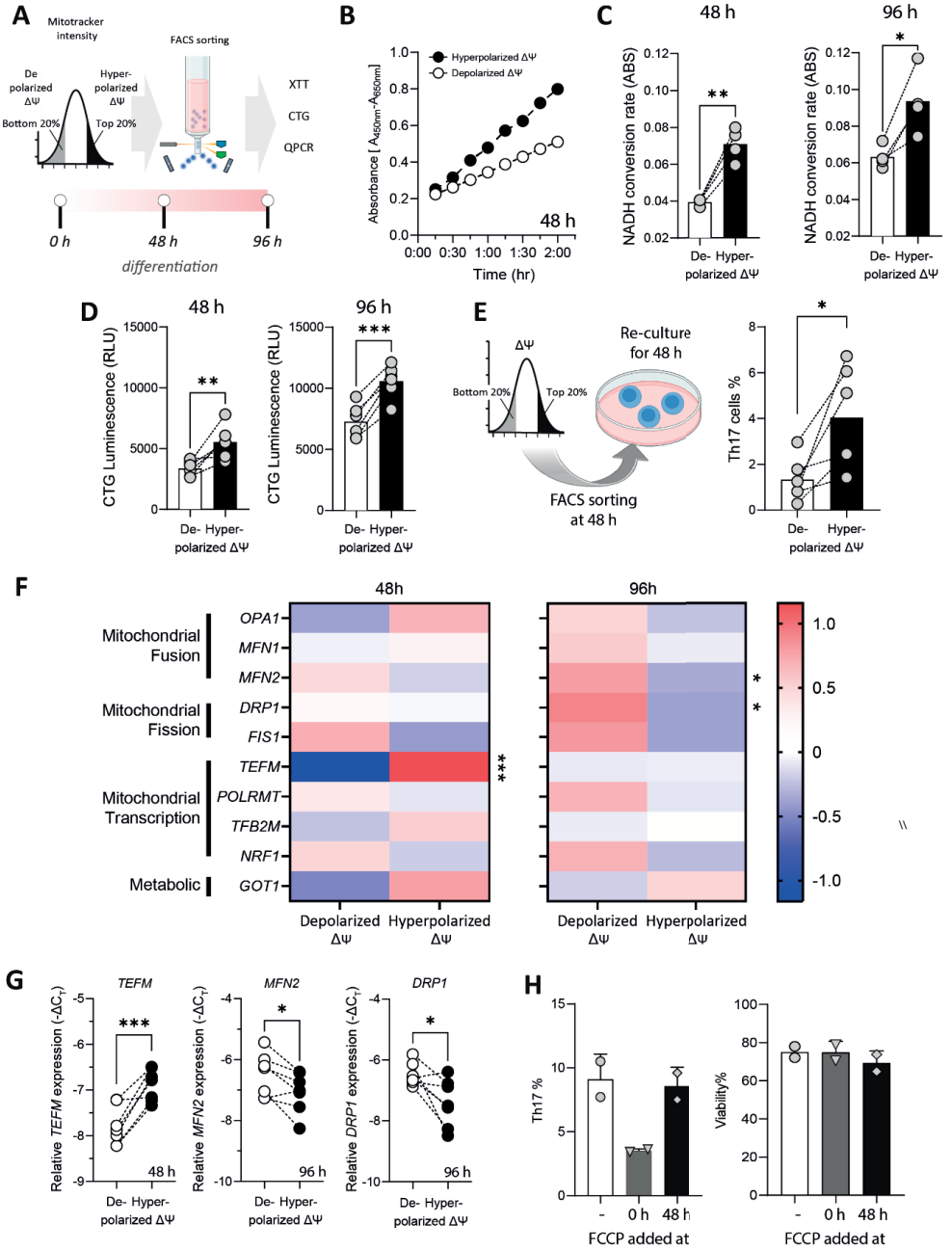

Figure 2: Hyperpolarized ΔΨ cells exhibit increased metabolic activity and enhanced Th17 differentiation.

(A) A schematic illustrates the sorting strategy of hyperpolarized ΔΨ cells and depolarized ΔΨ cells $CD4^+$ T cells at 48 and 96 hours of Th17 differentiation for further analysis. (B) Representative XTT absorbance

data, indicating NADH conversion hyperpolarized ΔΨ cells and depolarized ΔΨ cells sorted by FACS at 48 hours. Absorbance was measured every 15 minutes over a 2-hour period using a colorimetric assay. (C) XTT analysis (n = 6) revealed a significant difference in NADH conversion rates between hyperpolarized ΔΨ cells and depolarized ΔΨ cells at both 48 hours (n = 6 unique donors, P = 0.0017) and 96 hours (n = 6 unique donors, P = 0.0107). (D) Total ATP content, measured by CellTiter-Glo (CTG), in hyperpolarized ΔΨ cells and depolarized ΔΨ cells at both 48 hours (n = 6 unique donors, P = 0.0060) and 96 hours (n = 6 unique donors, P = 0.0017). Luminescence (RLU) was used as a proxy for metabolic activity.(E) Th17 differentiation was assessed at day 4 after re-seeding sorted hyperpolarized ΔΨ cells and depolarized ΔΨ cells into the Th17 polarization cocktail at 48 hours (n = 6 unique donors, P = 0.0219). (F) Gene expression analysis of mitochondrial dynamics-related genes in hyperpolarized ΔΨ cells and depolarized ΔΨ cells at 48 and 96 hours, visualized in a heatmap. Gene expression values were normalized using Z-scores for better comparison across samples.(G) TEFM mRNA expression in hyperpolarized ΔΨ cells and depolarized ΔΨ cells at 48 hours (P = 0.0071); MFN2 and DRP1 expression in ΔΨm high and ΔΨm low cells at 96 hours (n = 6 unique donors; DRP1 P = 0.0461; MFN2 P = 0.0391).(H) FCCP (500 nM) was added at 0 or 48 hours during a 96-hour culture period. Th17 yield and cell viability were measured by flow cytometry. Data represent mean ± SD from two donors. Statistical significance was determined using paired t-tests or Wilcoxon tests where appropriate.

2.3 ΔΨ high T cells favour glucose uptake and glycolysis over FAO and AAO cap and OXPHOS during Th17 differentiation

To further characterize the metabolic differences between hyperpolarized ΔΨ and depolarized ΔΨ cells during Th17 differentiation, we employed the SCENITH technique [178] at 48 and 96 hours. SCENITH quantifies protein synthesis under specific metabolic inhibition conditions, allowing inference of pathway utilization and metabolic dependencies (Figure 3A). This method measures puromycin incorporation into nascent proteins as a direct proxy for available ATP, following treatment with specific inhibitors: 2-deoxy-D-glucose (2-DG) to block glycolysis, oligomycin (O) to inhibit oxidative phosphorylation (OXPHOS), and their combination (DGO). Harringtonine, a general inhibitor of translation, served as a positive control. These conditions allow assessment of glycolytic, mitochondrial, fatty acid oxidation (FAO), and amino acid oxidation (AAO) capacities.

At 48 hours, hyperpolarized ΔΨ cells exhibited significantly higher geometric mean fluorescence intensity (gMFI) of puromycin incorporation compared to depolarized ΔΨ cells across all SCENITH conditions (control, 2-DG, oligomycin, and DGO) (Figure 3B). Of note, only a subset of hyperpolarized ΔΨ cells corresponds to Th17 cells, as sorting directly based on Th17 markers was technically challenging under live-cell conditions. By 96 hours, hyperpolarized ΔΨ cells maintained higher gMFI values under control, 2-DG, oligomycin, and DGO treatments (Figure 3D), indicating sustained overall metabolic activity reflected by elevated protein synthesis.

Further analysis of metabolic pathway contributions revealed distinct metabolic dependencies between hyperpolarized and depolarized ΔΨ cells during Th17 polarization. At 48 hours, hyperpolarized ΔΨ cells displayed significantly greater glucose dependence and glycolytic capacity compared to depolarized ΔΨ cells. Conversely, they exhibited lower reliance on FAO and AAO capacities, as well as reduced mitochondrial dependency, suggesting a preferential engagement of glycolysis for energy generation at this stage (Figure 3C).

By 96 hours, these metabolic distinctions persisted in terms of glucose dependence and reduced FAO and AAO capacities, with hyperpolarized ΔΨ cells continuing to favor glucose metabolism. However, no significant differences were observed in glycolytic capacity or mitochondrial dependence between the two groups at this later time point (Figure 3E). This may suggest that, over time, hyperpolarized ΔΨ cells begin to adjust their metabolic reliance, although direct evidence of a functional metabolic shift would require additional validation, such as lactate production assays. Together, these findings suggest that hyperpolarized ΔΨ T cells primarily rely on glycolysis over FAO, AAO, and OXPHOS during early Th17 polarization, although whether these metabolic distinctions translate into functional differences remains to be fully determined.

Figure 3: Metabolic profiles of hyperpolarized ΔΨ cells and depolarized ΔΨ cells during Th17 differentiation.

(A) Representative example of puromycin incorporation (gMFI) in hyperpolarized ΔΨ cells and depolarized ΔΨ cells, analysed using the SCENITH workflow, illustrating metabolic dependencies during Th17 differentiation. **(B)** Puromycin incorporation (MFI) at 48 hours in hyperpolarized ΔΨ cells and depolarized ΔΨ cells under control, 2-DG, oligomycin, and DGO conditions, showing significantly higher incorporation in hyperpolarized ΔΨ cells (n = 11 unique donors; control $P < 0.0001$, 2-DG $P = 0.001$, oligomycin $P = 0.0001$, DGO $P = 0.001$). **(C)** Comparative metabolic profiles of hyperpolarized ΔΨ cells and depolarized ΔΨ cells at 48 and 96 hours reveal significant differences in glucose dependence ($P = 0.0029$), fatty acid and amino acid oxidation (FAAO) capacity ($P = 0.0029$), mitochondrial dependence ($P = 0.0473$), and glycolytic capacity ($P = 0.0473$) across 11 unique donors. **(D)** Puromycin incorporation at 96 hours shows consistent differences between hyperpolarized ΔΨ cells and depolarized ΔΨ cells (n = 11; control $P < 0.0001$, 2-DG $P < 0.0001$, oligomycin $P = 0.0001$, DGO $P < 0.0001$). **(E)** Metabolic profiles at 96 hours demonstrate significant differences in glucose dependence ($P = 0.001$) and FAAO capacity ($P = 0.001$). Statistical comparisons were performed using paired t-tests or Wilcoxon matched-pairs tests, as appropriate.

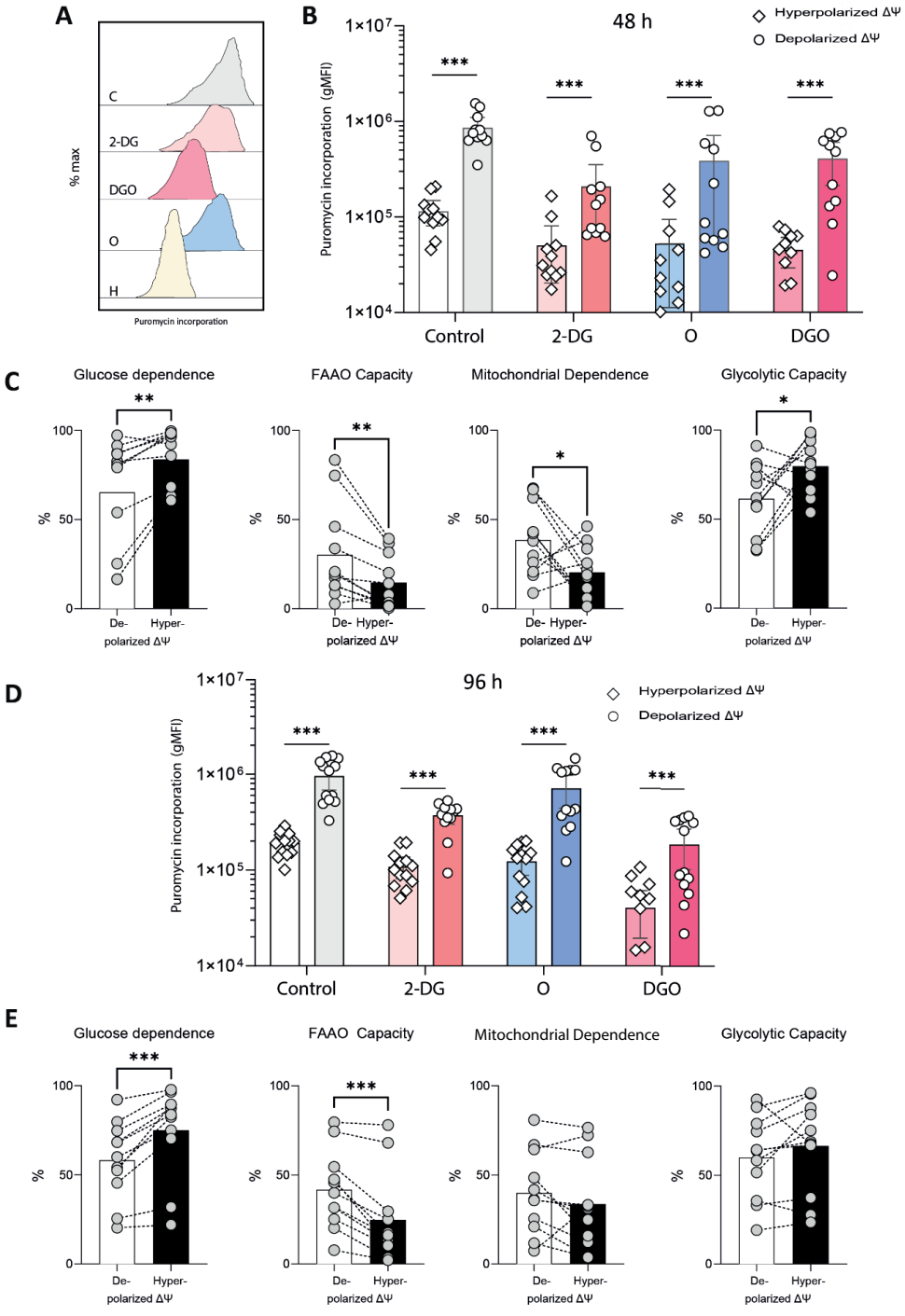
A
% max
C
2-DG
DGO
O
H
Puromycin incorporation
B
48 h
Hyperpolarized ΔΨ
Depolarized ΔΨ
Puromycin incorporation (gMFI)
1×10^7
1×10^6
1×10^5
1×10^4
***
Control
2-DG
O
DGO
C
Glucose dependence
FAAO Capacity
Mitochondrial Dependence
Glycolytic Capacity
**
*
%
100
50
0
De-
Hyper-
polarized ΔΨ
D
96 h
Hyperpolarized ΔΨ
Depolarized ΔΨ
Puromycin incorporation (gMFI)
Control
2-DG
O
DGO
E
Glucose dependence
FAAO Capacity
Mitochondrial Dependence
Glycolytic Capacity

2.4 Mitochondrial activity defines activation, signaling, and functional heterogeneity of Th17 cells

To determine whether mitochondrial activity influences Th17 cell function, we examined activation status, signaling potential, and cytokine production capacity in hyperpolarized and depolarized ΔΨ T cells. Cells were sorted at 48 hours using FACS and cultured for an additional 48 hours in our optimized Th17 polarization cocktail (cocktail 3). By 96 hours, hyperpolarized ΔΨ cells exhibited a significantly higher Th17 yield (Figure 2E) and increased expression of the activation markers CD25 and CD69, compared to depolarized ΔΨ cells (Figure 4A), indicating a heightened activation state.

Given that T cell activation can influence downstream signaling, we examined how hyperpolarized and depolarized ΔΨ cells engaged key pathways. We co-cultured them with pathway-specific reporter fibroblast lines at a 1:1 ratio for 24 hours. These fibroblasts were engineered to report activation of NF-κB, MAPK (AP-1), and JAK-STAT signaling pathways. Notably, depolarized ΔΨ cells induced significantly higher activation of NF-κB and AP-1 compared to hyperpolarized ΔΨ cells (Figure 4B), suggesting that cells with lower mitochondrial membrane potential may more effectively trigger inflammatory signaling. No significant differences were observed for STAT-mediated (SIE) reporter activity between the two groups, highlighting the specificity of the differences observed.

To further investigate functional consequences linked to mitochondrial activity, we assessed intracellular cytokine production. At 48 hours, both populations exhibited minimal cytokine expression. However, after an additional 48 hours of culture (96 hours total), hyperpolarized ΔΨ cells displayed significantly higher expression MFI levels of IL-4, IL-6, IL-10, IL-17A, IFN-γ, IL-21, and granzyme B (GZMB) compared to depolarized ΔΨ cells (Figure 4C). These findings indicate that hyperpolarized ΔΨ cells are primed for effector cytokine production following Th17 differentiation. Notably, cytokine expression was measured after 4 hours of PMA/ionomycin stimulation in the presence of a Golgi transport inhibitor to reflect production capacity rather than basal secretion.

To complement these findings, we assessed cytokine secretion by performing a Luminex assay on culture supernatants collected at 96 hours (Figure 4D). Depolarized ΔΨ cells secreted significantly higher levels of IFN-γ and GZMB compared to hyperpolarized ΔΨ cells, whereas secretion of IL-17A, IL-10, and TNF-α showed no significant differences. This discrepancy between intracellular cytokine expression and secreted cytokine levels suggests functional suppression in hyperpolarized ΔΨ cells. We hypothesized that this suppression might be linked to exhaustion. Consistent with this, hyperpolarized ΔΨ cells exhibited significantly higher expression of the exhaustion markers PD-1 and TIGIT at 96 hours compared to depolarized ΔΨ cells (Figure 4E).

Together, these findings suggest that mitochondrial activity influences not only Th17 differentiation but also functional heterogeneity. Hyperpolarized ΔΨ cells exhibit enhanced differentiation and cytokine production potential, but reduced actual cytokine secretion, likely due to exhaustion-related functional impairment, whereas depolarized ΔΨ cells are more effective in triggering inflammatory signaling and cytokine release.

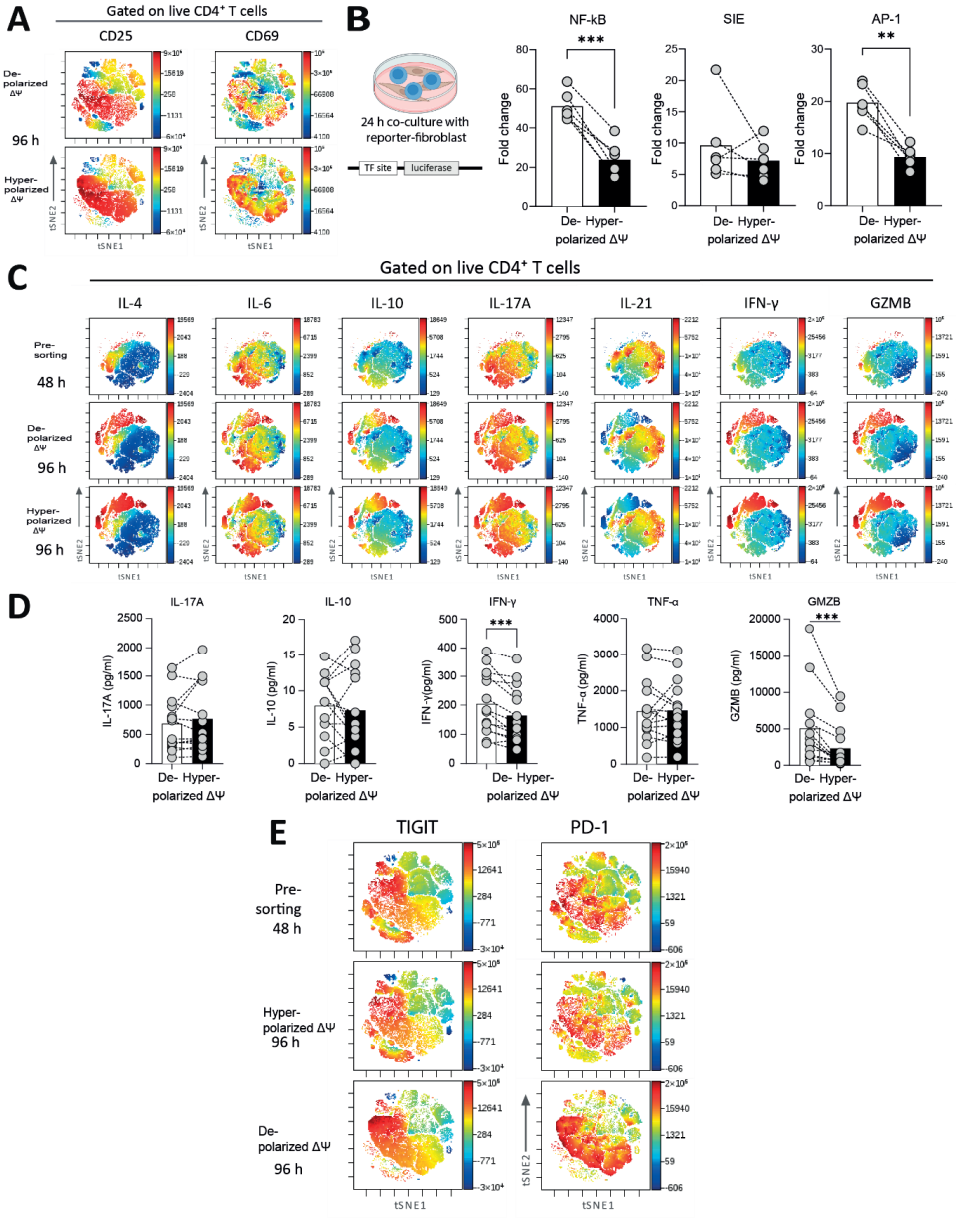

Figure 4: Hyperpolarized ΔΨ cells exhibit enhanced activation but reduced cytokine secretion, weaker signaling activation, and elevated exhaustion.

(A) Assessment of CD25 and CD69 expression in hyperpolarized ΔΨ cells and depolarized ΔΨ cells at 96 hours (n = 6 unique donors). **(B)** Activation of NF-κB (P = 0.0003), SIE, and AP-1 (P = 0.0004) signaling pathways in sorted hyperpolarized ΔΨ cells and depolarized ΔΨ cells. Reporter activity for NF-κB, JAK-STAT, and AP-1 pathways was normalized to the activity observed in negative control conditions. Data

represent normalized fold changes relative to the negative control (n = 6 unique donors). **(C)** Cytokine production potential was measured after a 4-hour PMA/ionomycin stimulation with Golgi inhibition to assess intracellular cytokine levels (n = 6 unique donors). **(D)** Secreted cytokine levels were quantified from culture supernatants using Luminex. Cytokine secretion of IFN-γ (P = 0.0007) and GZMB (P = 0.0009) was significantly lower in hyperpolarized ΔΨ cells. No significant differences were observed in IL-17A, IL-10, or TNF-α secretion. **(E)** Exhaustion markers (e.g., TIGIT, PD-1) were evaluated on day 4 in sorted cells (n = 6 unique donors). Data for panels A, C, and E were processed and analysed using vi-SNE (Cellular Interaction Tuning by Recursive Sampling) in Cytobank for further interpretation of activation, exhaustion signatures, and cytokine production.

3. DISCUSSION

Mitochondrial metabolism plays a crucial role in T cell activation, differentiation, and function [179], and exhibits distinct patterns in effector versus memory T cells [180]. In this study, we investigated how mitochondrial activity influences Th17 differentiation from naïve $CD4^+$ T cells. Using an *in vitro* human Th17 differentiation model, we found that Th17 polarization is accompanied by a metabolic shift—characterized by a reduced reliance on glycolysis and increased dependence on mitochondrial oxidative phosphorylation (OXPHOS). This metabolic reprogramming occurs early during differentiation, linking mitochondrial activity to Th17 commitment. We observed that hyperpolarized ΔΨ cells exhibited enhanced differentiation capacity and increased Th17 formation. However, this was also accompanied by elevated expression of exhaustion markers PD-1 and TIGIT, suggesting that heightened mitochondrial activity simultaneously supports both Th17 differentiation and functional constraints, such as exhaustion.

Our first key observation was that Th17 cells exhibit significantly higher ΔΨ compared to non-Th17 $CD4^+$ T cells, indicating increased mitochondrial activity. This finding was further validated by XTT and CTG assays, which showed a metabolic distinction between hyperpolarized and depolarized ΔΨ cells. Importantly, while hyperpolarized ΔΨ cells are not exclusively Th17 cells, these cells exhibited enhanced differentiation capacity and a greater potential to form Th17 cells, supporting the notion that mitochondrial activity plays a pivotal role in Th17 differentiation.

Mitochondrial fission, fusion, and mitophagy are critical for supporting T cell activation, differentiation, and survival [68, 181]. While much is known about their roles in T cell biology, the specific contribution of mitochondrial dynamics during Th17 differentiation remains incompletely understood. Recent studies indicate that OXPHOS promotes early Th17 development by driving expression of the pioneer transcription factor BATF, which is essential for Th17 lineage commitment, and by facilitating TCR and mTOR signaling [84]. In our study, we observed that mitochondrial dynamics undergo distinct changes over time during

Th17 differentiation. At the early stage (48 hours), hyperpolarized ΔΨ cells exhibited increased expression of *TEFM***,** a key regulator of mitochondrial transcription elongation[182], suggesting enhanced mitochondrial gene expression at this time point**.** By 96 hours, however, Th17 cells exhibited downregulation of *DRP1* (a mediator of mitochondrial fission) and *MFN2* (a regulator of mitochondrial fusion) [183, 184], indicating a shift in mitochondrial dynamics that corresponds with the later stages of differentiation. These findings suggest that mitochondrial-related genes are differentially regulated at distinct stages of Th17 differentiation, with early upregulation of mitochondrial activity associated with differentiation commitment, and later changes in mitochondrial dynamics possibly reflecting functional specialization**.**

To further explore the metabolic profiles beyond mitochondrial activity, we employed the SCENITH assay to analyze the metabolic programs of hyperpolarized ΔΨ and depolarized ΔΨ subsets. Our findings support the well-established concept of metabolic flexibility in T cell differentiation [180], in which early activation relies on glycolysis, followed by a shift toward OXPHOS and FAO and AAO capacities in later stages to sustain effector functions.

Our data build upon this concept by demonstrating that hyperpolarized ΔΨ cells exhibit a stronger reliance on glycolysis early in differentiation, potentially contributing to their enhanced Th17 differentiation. This glycolytic preference highlights the metabolic adaptability of T cells during activation, ensuring efficient energy production in inflammatory environments that characterize Th17-driven autoimmune diseases and Th17 cell differentiation within the tumor microenvironment [57, 185]. In both autoimmunity and cancer, changes in the balance between Th17 and Treg cells play a key role in disease progression — with heightened Th17 activity driving autoimmune inflammation, and expanded Treg populations often seen in cancers like CLL, where they may suppress anti-tumor immunity [120]. In healthy immunity, Th17 cells protect against extracellular bacteria and fungi, yet our healthy donor–derived Th17 model allows controlled analysis of differentiation and metabolic changes. Notably, Th17 cells play a dual role in the tumor microenvironment, promoting tumor progression via immunosuppressive and pro-angiogenic pathways, yet also mediating anti-tumor effects through Th1-like conversion and IFN-γ production [119, 186]. Considering that tumor sites impose distinct chemokine (e.g., CCL22, CCL28) and nutrient constraints compared with inflamed autoimmune tissues, integrating these contexts could broaden the translational relevance of our model to both malignancy progression and autoimmune disease.

Furthermore, our SCENITH data reveal a dynamic shift in mitochondrial activity during Th17 polarization. At 48 hours, hyperpolarized ΔΨ cells predominantly rely on glycolysis, likely to support the rapid energy production and biosynthesis required for differentiation. By 96 hours, mitochondrial activity increases, indicating a transition toward OXPHOS, which supports Th17 formation, though the cells exhibit limited effector function due to increased exhaustion

markers. This shift likely explains why hyperpolarized ΔΨ cells generate more Th17 cells compared to depolarized ΔΨ cells. OXPHOS has been implicated in long-term T cell survival by preventing apoptosis, suggesting that metabolic adaptation contributes to the durability of Th17 responses [174].

In contrast, our FCCP data highlight that early mitochondrial activity is indispensable for Th17 differentiation. Adding FCCP at the onset of differentiation (0 hours) significantly reduces Th17 yield, highlighting the critical role of mitochondrial function in initiating differentiation. However, when FCCP is added at 48 hours, its inhibitory effect is less pronounced, suggesting that by this stage, differentiation is more robust and can tolerate mitochondrial disruption. These findings demonstrate the role of mitochondrial metabolism in regulating Th17 differentiation and function, with early mitochondrial activity being essential for initiation and later stages relying on metabolic flexibility to sustain differentiation and effector function.

To investigate how metabolic heterogeneity translates into functional differences, we assessed the activation states and signaling capacities of hyperpolarized ΔΨ and depolarized ΔΨ cells. While hyperpolarized ΔΨ cells exhibited increased expression of activation markers such as CD25 and CD69, their ability to trigger inflammatory signaling, measured by NF-κB and AP-1 activation in luciferase reporter fibroblasts, was surprisingly weaker compared to depolarized ΔΨ cells**.** These findings suggest that elevated activation marker expression in hyperpolarized ΔΨ cells does not necessarily correlate with stronger inflammatory signaling. Instead, our data imply that metabolic state influences not only the degree of T cell activation but also the capacity to drive inflammatory responses in the immune microenvironment. This highlights the complexity of metabolic programming in regulating intercellular communication, with hyperpolarized ΔΨ cells potentially driving more activation but exhibiting less efficient inflammatory signaling compared to depolarized ΔΨ cells**.**

Paradoxically, although hyperpolarized ΔΨ cells display elevated activation markers and higher intracellular cytokine production, their reduced actual cytokine secretion (e.g., IFN-γ and GZMB) suggests the presence of intrinsic regulatory mechanisms that temper effector output. This paradox becomes more apparent when considering the link between heightened activation and cellular exhaustion**.** Hyperpolarized ΔΨ cells express elevated levels of exhaustion markers, including PD-1 and TIGIT, which are associated with chronic activation and immune regulation [187]. Exhaustion, resulting from prolonged activation, impairs cellular function and serves as a protective mechanism to prevent excessive immune responses and maintain immune homeostasis [188]. The concurrent upregulation of PD-1 and TIGIT is consistent with findings from chronic infection and cancer models, where sustained antigen exposure drives functional exhaustion. Importantly, studies in $CD8^+$ T cells have shown that PD-1 blockade can transiently restore effector function but often fails to reprogram exhausted cells into durable

memory populations when antigen levels remain high, due to stable epigenetic constraints [189]. This raises the question of whether targeting PD-1 pathways or mitochondrial function could produce lasting restoration of Th17 activity.

Addressing this will require *in vivo* validation in established autoimmune models such as EAE or collagen-induced arthritis, enabling direct assessment of how checkpoint or metabolic modulation impacts Th17 persistence, functional polarization, and disease progression. Specifically, reduced IL-17A secretion can impair pathogen clearance or tissue repair, promoting persistent inflammation and tissue damage. This loss of functional Th17 cells results in an imbalance between immune activation and regulation, contributing to persistent inflammation, tissue damage, and disease progression. Recent studies suggest that targeting exhaustion markers like PD-1 and TIGIT could restore Th17 function, enhance immune responses, and mitigate disease progression in these disorders [188, 190]. While our study does not directly assess therapeutic modulation of exhaustion, our findings suggest a potential link between mitochondrial activity and Th17 dysfunction. Future studies will be needed to determine whether targeting mitochondrial function or exhaustion pathways could restore Th17 effector capacity and influence autoimmune and cancer outcomes. In cancer immunotherapy, metabolic reprogramming, such as targeting mitochondrial dysfunction and PD-1 pathways, has successfully restored the activity of exhausted T cells and improved their persistence and function [191, 192].

Our findings suggest that heightened mitochondrial activity in hyperpolarized $\Delta\Psi$ cells may drive both increased activation and the development of exhaustion, ultimately impairing their ability to secrete cytokines effectively, despite their enhanced differentiation potential. This highlights a critical gap in our understanding of Th17 cell biology, specifically in how mitochondrial activity contributes to the induction of exhaustion during chronic inflammation. While targeting exhaustion markers like PD-1 and TIGIT could be a promising therapeutic approach, our findings emphasize the need for further investigation into how mitochondrial function in Th17 cells can be modulated to restore immune responses and prevent pathogenic dysfunction. Given the growing evidence linking mitochondrial function to T cell exhaustion [99], future research into mitochondrial dynamics in Th17 cells during autoimmune diseases may uncover novel therapeutic targets for modulating immune responses and mitigating disease progression.

In summary, our findings highlight the critical role of early mitochondrial activity in shaping Th17 differentiation. Cells with heightened mitochondrial activity gradually decrease their reliance on glycolysis while increasing OXPHOS contribution over time, supporting both Th17 activation and differentiation. However, despite maintaining cytokine production potential, their actual cytokine secretion is impaired due to exhaustion. These results emphasize

the importance of mitochondrial activity in balancing Th17 differentiation and functional persistence. We acknowledge the limitation of isolating pure RORγt⁺IL-17A⁺ Th17 cells due to their low frequency and the effects of stimulation on mitochondrial measurements. Additionally, our study focused on the 48 and 96 hour timepoints, which were chosen to represent early activation and later functional stages of Th17 cells. Including earlier timepoints, such as 24 hours to capture initial gene activation during differentiation, as well as intermediate points like 72 hours, could offer an overview picture of how mitochondrial regulation and exhaustion develop over time. Due to practical constraints, we limited our analysis to these two key stages but recognize that examining additional timepoints would be valuable for future research. Future studies should also employ improved sorting techniques and relevant *in vivo* models to better understand how mitochondrial activity regulates Th17 function and pathogenicity. Importantly, mitochondrial metabolism represents a promising target to modulate Th17-driven immune responses, potentially leading to novel metabolic interventions for autoimmune diseases.

4. METHODS

4.1 PBMC Isolation

Human peripheral blood mononuclear cells (PBMCs) (obtained from Sanquin, The Netherlands, project number: NVT 0397-02) were isolated from buffy coats of healthy donors' peripheral blood by Ficoll Pacque PLUS density centrifugation according to manufacturer's guidelines. After isolation, PBMCs were cryopreserved in 10% HPS (Gibco-Invitrogen, Cat No.16000-044), 10% DMSO (MP Biomedicals, Cat No.196055) in RPMI 1640 medium (Gibco-Invitrogen Cat No. 11875093) and stored in liquid nitrogen until further use.

4.2 Naïve CD4+ T cell Isolation and Th17 differentiation

To isolate naïve CD4+ T cells, cryopreserved PBMCs were thawed and washed twice using RPMI 1640 medium supplemented with 10% heat-inactivated FCS + 100 U/ml penicillin, 100 mg/ml streptomycin. CD4+ naïve T cells were negatively selected using the Naive CD4+ T Cell Isolation Kit II, human (Miltenyi Biotec, 130-094-131) according to manufacturer's protocol. After isolation, enriched naïve CD4+ T cell exhibited more than 95% purity and viability in the majority of the donors for experiments, as evaluated by flow cytometry staining for CD4, CD45RA and viability marker 7-AAD(FigureS3). The isolated naïve CD4+ T cells were cultured with XVIVO™ 15 medium (Lonza, cat02-53Q) supplemented with 5% Cell-Vive™ T-NK Xeno-Free Serum Substitute (BioLegend, 420502), 100 U/ml penicillin, 100 mg/ml streptomycin and 100 mg/L pyruvate, at a density of 100,000 cells/well in 96-well round-bottom plates (Greiner). Cells were activated with precoated anti-CD3 (clone OKT-3, BioLegend) 5 µg/ml overnight at 4 °C and anti-CD28 0.25 µg/ml (clone 28.2, BioLegend) and with a cocktail containing a final concentration with anti-human IFN-γ 10 µg/ml (BioLegend,

506533), anti-human IL-4 10 μg/ml (Biolegend,500839), IL-2 10 IU/ml (BioLegend, 589102), TGF-β1 1 ng/ml (ThermoFisher, 100-21-10UG), IL-6 30 ng/ml (Biolegend,570802), IL-23 10 ng/ml (BioLegend, 574102), IL-1β 10ng/ml (R&D system, 201-LB) in complete XVIVO™ 15 medium to differentiate them into Th17 cells.

4.3 Antibody Staining and Flow Cytometry Analysis

Approximately 1 × 10^6 cells per condition/sample were washed twice with PBS and labelled with ViaKrome 808 fixable viability dye (Beckman Coulter) at a dilution of 1.5:1000 in PBS for 30 minutes at 4°C in the dark. After washing, cells were optionally stained with antibodies targeting extracellular markers, fluorescently labelled, for 25 minutes at room temperature, protected from light, in 100 μL staining buffer (PBS + 1% BSA). BSA (bovine serum albumin) is used to block nonspecific binding sites on cells.

For intracellular staining, cells were fixed with 50 μL Foxp3 Transcription Factor Staining Buffer (ThermoFisher, 00-5523-00) for 25 minutes at room temperature, following the manufacturer's instructions. After fixation, cells were washed and stained with antibodies targeting intracellular markers for 20 minutes at room temperature in the dark.

To detect intracellular cytokines, cells were pre-stimulated with 50 ng/mL phorbol 12-myristate 13-acetate (PMA, Merck, P1585-1MG), 1 μg/mL ionomycin (Merck, I0634-1MG), and 1 μg/mL Golgi Plug (BD Biosciences, 555029) for 4 hours prior to staining. Samples were acquired immediately after staining using a Beckman Coulter CytoFLEX LX 21-color flow cytometer. Flow cytometry data were analyzed with Kaluza software version 2.1.3 (Beckman Coulter). Details of all antibodies used for extracellular and intracellular staining are provided *in Supplementary Tables 2 and 3.*

4.4 Fluorescence-Activated Cell Sorting (FACS)

To generate cells with relatively high and low metabolic activity, naïve $CD4^+$ T cells were cultured with a Th17 polarization cocktail and stained with MitoTracker dye (ThermoFisher, M22426) at a dilution of 1:6000 in staining buffer (PBS + 1% BSA) for 30 minutes at 37°C. Cells were also stained with 7-AAD (ThermoFisher, A1310) at a concentration of 1:1000 at approximately 48 and 96 hours. After staining, cells were resuspended in staining buffer at a concentration of ~50 × 10^6 cells/mL and sorted using a Cytek® Aurora cytometer under high pressure (70 psi) with a 70 μm nozzle at a maximum flow rate setting of 6/11, maintained at 4°C.

For sorting, the top and bottom 20% of cells with hyperpolarized ΔΨ and depolarized ΔΨ based on MFI were collected into polypropylene tubes containing 2 mL of XVIVO™ 15 medium, supplemented with 5% Cell-Vive™ T-NK Xeno-Free Serum Substitute, 100 mg/L pyruvate,

and 1% Penicillin-Streptomycin. Post-sort, both hyperpolarized ΔΨ cells and depolarized ΔΨ cells populations were assessed for viability (approximately 96%) and purity. Acquisition was performed using the same instrument layout. An overview of the gating strategy is provided in *Supplementary Figure 4.*

4.5 XTT Assay

To evaluate NADH-dependent metabolic activity in sorted cells, the XTT Cell Viability Kit (Cell Signaling, #9095) was used according to the manufacturer's instructions. Sorted hyperpolarized ΔΨ and depolarized ΔΨ cells were washed in RPMI 1640 Medium (no phenol red, Gibco, 11835030) and resuspended at a final concentration of 250,000 cells/mL. A total of 100 µL per well was seeded into a 96-well round-bottom plate. Then, 50 µL of XTT working solution were added to each well and mixed. Absorbance was measured every 15 minutes from 0 to 120 minutes using a Clariostar (BMG LABTECH) microplate reader.

Four technical replicates were performed per condition, and the average value was used for subsequent analysis. Both negative and positive controls were included to ensure assay validity. The negative control consisted of media without cells, while the positive control was generated using untreated Jurkat cells with known metabolic activity.

4.6 CellTiter-Glo Assay

To assess ATP production in sorted cells, the CellTiter-Glo® Luminescent Cell Viability Assay (Promega, G9241) was performed following the manufacturer's instructions. hyperpolarized ΔΨ and depolarized ΔΨ cells were washed in RPMI (no phenol red) and resuspended at 125,000 cells/mL. 50 µL of cell suspension were added to a 96-well flat-bottom plate, followed by 50 µL of CellTiter-Glo reagent. The plate was covered with aluminium foil to protect it from light and incubated for 10 minutes at room temperature. Luminescence was then measured using a Clariostar (BMG LABTECH).

Each condition was tested in four technical replicates, and mean values were used in the analysis. Values were corrected by subtracting background luminescence from medium-only wells (negative control). A positive control using metabolically active Jurkat cells was included to verify assay sensitivity.

4.7 RNA Isolation and Quantitative Real-Time PCR

Sorted cells were collected at 48 and 96 hours after FACS, and RNA was extracted using TRIzol reagent (Sigma-Aldrich, Saint Louis, MO, USA). For every 500,000 cells, 500 µL of TRIzol was added, followed by cell lysis. Subsequently, 100 µL of chloroform was added, and the samples were centrifuged at 11,600 × g for 15 minutes at 4°C. The aqueous phase was carefully collected. To precipitate RNA, a 1:1 mixture of isopropanol and 1:10 sodium acetate buffer (3 M; Sigma-

Aldrich) was added, and samples were incubated overnight at –20°C. The samples were then centrifuged at 11,600 × g for 30 minutes at 4°C. The RNA pellet was washed with 75% ethanol and reconstituted in RNase-free water.

To remove residual genomic DNA, RNA samples were treated with DNase I (Roche, Basel, Switzerland) according to the manufacturer's instructions. cDNA synthesis was performed using standard protocols. Quantitative real-time PCR (qPCR) was carried out using Power SYBR™ Green PCR Master Mix (Applied Biosystems, 4368708, Waltham, MA, USA) on an Applied Biosystems QuantStudio 1 Real-Time PCR System. Primer information used in the qPCR is listed in *Supplementary Table 4*. All primers were validated for amplification efficiency prior to use. The selection of reference genes is provided in *Supplementary Figure 5.*

Gene expression was calculated relative to the housekeeping genes *HSDNA*, *PL37A*, and *RPS27A*, and is presented as –ΔCt values. The –ΔCt values were calculated as follows:

–ΔCT = Average CT of 3 reference genes – CT value of the gene of interest

4.8 SCENITH

4.8.1 SCENITH Assay for Metabolic Profiling of Th17-Differentiated CD4⁺ T Cells

SCENITH was performed as described by Argüello et al. [178]. leveraging the close relationship between protein synthesis and ATP levels to assess cellular metabolic dependencies. This method evaluates the impact of metabolic inhibitors on puromycin incorporation during protein translation, providing insights into glycolytic and mitochondrial contributions via flow cytometry.

4.8.2 Cell Preparation and Culture Conditions

Naïve $CD4^+$ T cells were isolated and plated at a density of 1×10^6 cells/mL in 100 µL per well within 96-well round-bottom plates, under Th17-polarizing conditions. Cells were cultured in complete X-VIVO medium devoid of pyruvate to prevent interference with the SCENITH assay's metabolic readouts. For each condition, five wells were prepared for the 48-hour time point and three wells for the 96-hour time point. Cells from respective wells were pooled prior to flow cytometry analysis. Experiments encompassed samples from 11 individual donors, with data from each pooled condition utilized for subsequent analyses.

4.8.3 Metabolic Inhibitor Treatments

At designated time points, cells underwent treatment with the following metabolic inhibitors for 15 minutes:

- 2-Deoxy-D-glucose (2-DG) at a final concentration of 100 mM
- Oligomycin (O) at a final concentration of 1 µM
- A combination of 2-DG and Oligomycin (DGO)
- Control (medium only)

To serve as a negative control, 2 µg/mL of the translation initiation inhibitor Harringtonine was added 15 minutes prior to puromycin administration. Primary antibody information is listed in *Supplementary Table 5*

4.8.4 Puromycin Incorporation and Staining

Subsequent to inhibitor treatments, puromycin was introduced at a final concentration of 10 µg/mL for an additional 15 minutes. Cells were then washed with cold PBS and stained with a combination of Fc receptor blockade and ViaKrome 808 viability dye (Beckman Coulter, Pasadena, CA, USA) for 30 minutes. Following staining, cells were fixed and permeabilized using the FOXP3 Fixation/Permeabilization Buffer Set (Thermo Fisher eBioscience™), in accordance with the manufacturer's instructions.

Intracellular staining for puromycin was performed using Alexa Fluor® 488-conjugated anti-puromycin antibody (clone 2A4, BioLegend, 381506). Cells were incubated for 1 hour at 4°C in a 1:10 dilution of the permeabilization buffer. Data acquisition was executed on a CytoFlex LX flow cytometer (Beckman Coulter).

4.8.5 Data Analysis

SCENITH calculation were performed as described by Argüello et al., utilizing median fluorescence intensity (MFI) values of puromycin incorporation to determine metabolic dependencies and capacities.

(1) ***CONTROL*** = gMFI of anti – Puro – Fluorochrome upon Control treatment

(2) ***2DG*** = gMFI of anti – Puro – Fluorochrome upon 2DG treatment

(3) ***O*** = gMFI of anti – Puro – Fluorochrome upon Oligomycin treatment

(4) ***DGO*** = gMFI of anti – Puro – Fluorochrome upon (2 – DG + Oligomycin)treatment

(5) ***H*** = gMFI of anti – Puro Fluorochrome upon Harringtonine treatment

(6) **Glucose dependence** = $\frac{100 \times (control - 2 - DG)}{Control - DGO}$

(7) **Mitochondrial dependence** = $\frac{100 \times (control - O)}{Control - DGO}$

(8) ***Glycolytic Capacity*** **=** 100 – Mitochondrial dependence

(9) ***FAA and AAO*** **=** 100 – Glucose dependence

(10) ***ΔΨ depolarized cells*** = approximately the lowest 20% of anti – MitoTracker Deep Red – Fluorochrome

(11) ***ΔΨ hyperpolarized cells*** = approximately highest 20% of anti – MitoTracker Deep Red – Fluorochrome

4.9 Cytokine Measurements

Human cytokines in the culture supernatants were quantified using the Luminex platform. Cell culture supernatants were collected, centrifuged at 300g for 10 minutes, and then transferred to new 500 µL Eppendorf tubes, which were stored at -20°C. Cytokine levels were measured using the Human Luminex Discovery Assay (Bio-Techne, LXSAHM-06) according to the manufacturer's instructions. Sample analysis was performed using BioPlex Manager 4 software (Bio-Rad Laboratories, Hercules, CA, USA).

4.10 Co-Culture Reporters' Luciferase Assay

The activation of JAK-STAT (SIE), MAPK (AP-1), and NF-κB (NF-κB) signalling pathways was evaluated using reporter constructs cloned into primary dermal myofibroblasts, originally obtained from Neefjes et al.[193]. Reporter fibroblasts were seeded at a density of 150,000 cells per well. IL-6 was used as a positive control for the JAK-STAT (SIE) reporter, PMA + Ionomycin for the MAPK (AP-1) reporter, and TNF-α for the NF-κB reporter. After 24 hours of co-culture with a 1:1 ratio of hyperpolarized ΔΨ cells and depolarized ΔΨ cells**,** the cells were collected and centrifuged. The resulting pellet was resuspended in 150 µL of Assay Buffer containing a 50x substrate from the Nano-Glo Luciferase Assay Kit (Promega). Luciferase activity was measured using a ClarioStar plate reader (BMG Labtech), with emission recorded at 590 nm.

4.11 Statistical Analysis

Statistical analyses were performed using GraphPad Prism software. First, the normal distribution of the data was assessed. If the data followed a normal distribution, paired t-tests were used to compare two matched experimental groups from independent donors. If the data did not follow a normal distribution, Wilcoxon signed-rank tests were used for comparisons. Data for Figure 1G, H, I and Figure 2H show mean of multiple donors, and error bars represent mean ± SD.

For qPCR data, the expression levels of mitochondrial dynamic genes were analysed within hyperpolarized ΔΨ cells and depolarized ΔΨ cells from 6 independent donors. Paired analyses were performed for each donor, and Z-scores were calculated for each gene. The Z-scores were then plotted in a heatmap to visualize gene expression patterns across conditions. Z-scores were calculated using the following formula:

$$Z = \frac{(X - \mu)}{\sigma}$$

Where X is the gene expression value, μ is the mean gene expression across all conditions, and σ is the standard deviation of the gene expression values.

For flow cytometry analysis, gMFI values and percentages were determined using Kaluza software (Beckman Coulter) and were used for subsequent statistical analysis. Dimensionality reduction, tSNE analysis and plots were processed via Cytobank (Beckman Coulter). p values are indicated by *p < 0.05, **p < 0.01, ***p < 0.001, and ****p < 0.0001 where statistically significant differences were observed.

Declaration of Generative AI and AI-Assisted Technologies in the Writing Process

AI-assisted technologies (e.g., grammar and language editing tools) were used to correct grammar and spelling errors in the manuscript. No AI tools were used to generate scientific content, perform data interpretation, or draw conclusions.

Declaration of Competing Interests

The authors declare no competing interests.

Data Availability

Data will be made available on request.

SUPPLEMENTARY FIGURES

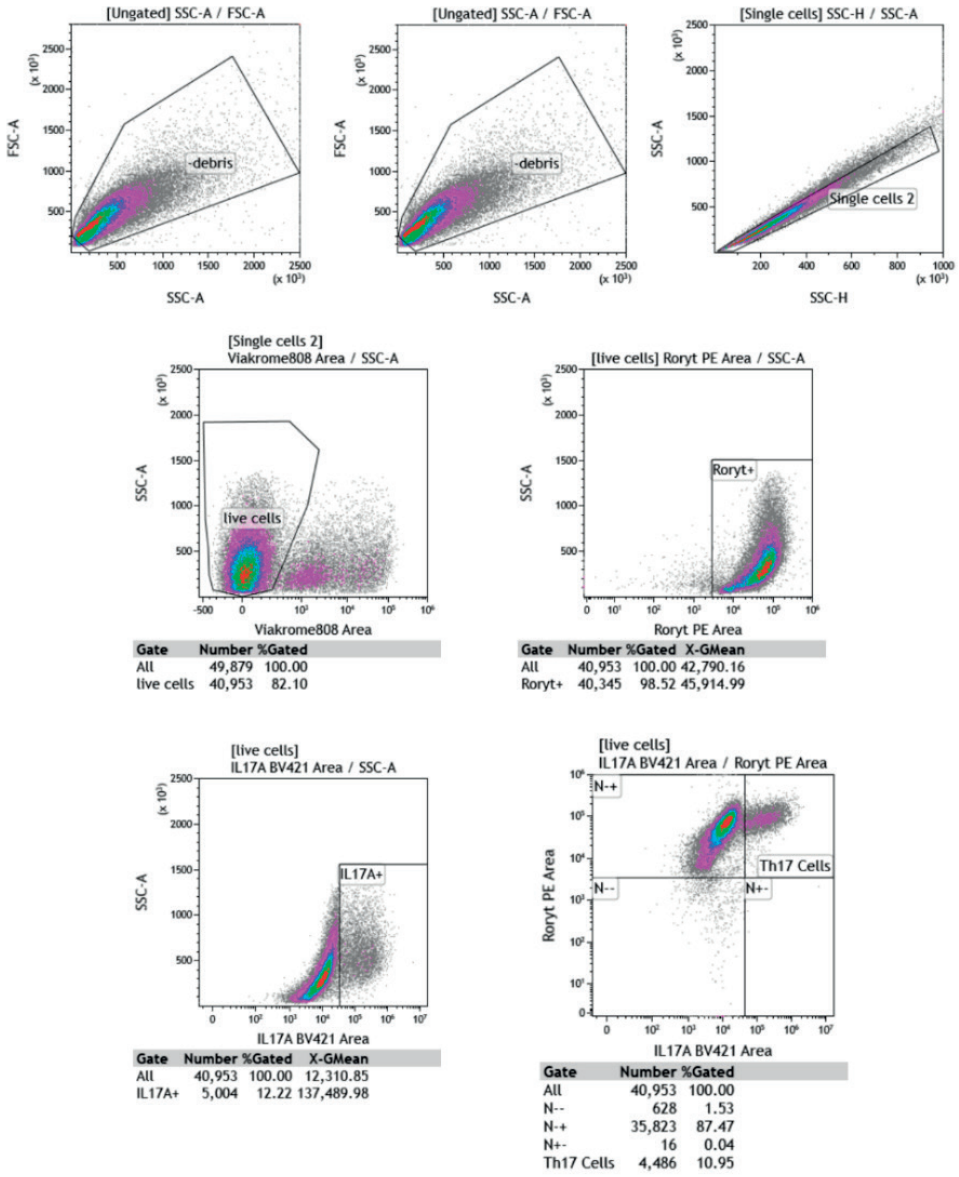

Supplementary Figure1: Flow Cytometry Gating Strategy for Th17 cells.
The gating strategy for identifying Th17 cells is as follows: First, debris and doublets are excluded using FSC vs. SSC and FSC-A vs. FSC-H gates. Live cells are then selected based on side scatter and Viakrom808 characteristics. RORγt+ cells are identified, followed by gating for IL-17A+ cells. The final population of RORγt+ IL-17A+ cells, defined as Th17 cells, is identified based on the appropriate isotype controls and fluorescence minus one (FMO) or non-staining controls for gating validation.

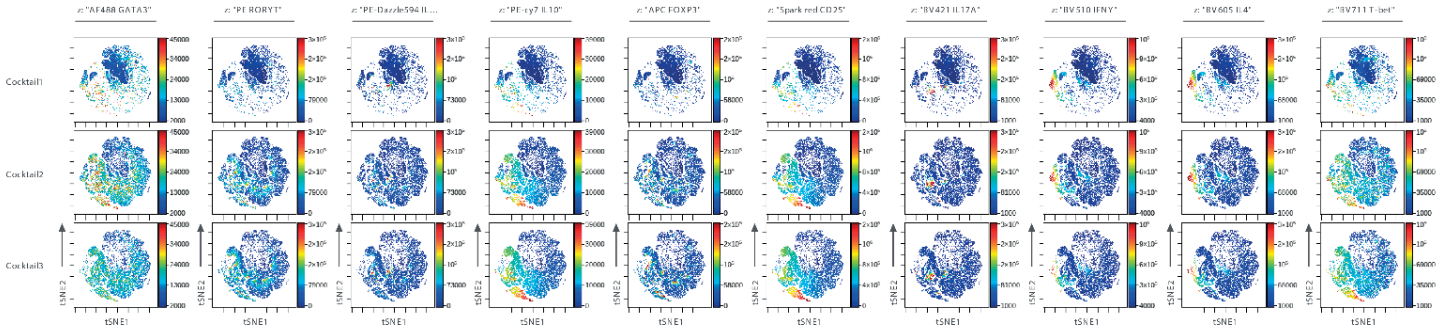

Supplementary Figure 2: Three Th17 differentiation cocktails result in different cytokine and transcription factor profiles.
To further investigate the differentiation profiles across the three Th17 cocktails, we applied semi-supervised flow cytometric analysis using vi-SNE software (Cytobank). The analysis was performed with an equal input of 8700 cells per cocktail sample. In addition to IL-17A and IFN-gamma, we measured the expression of other T helper subset-related transcription factors and cytokines, including IL-4, T-bet, FoxP3, IL10 and so on. The results highlight differences in cytokine and transcription factor expression across the cocktails, providing a more comprehensive view of the differentiation outcomes and confirming the specificity of the cocktails in driving distinct T helper subset profiles.

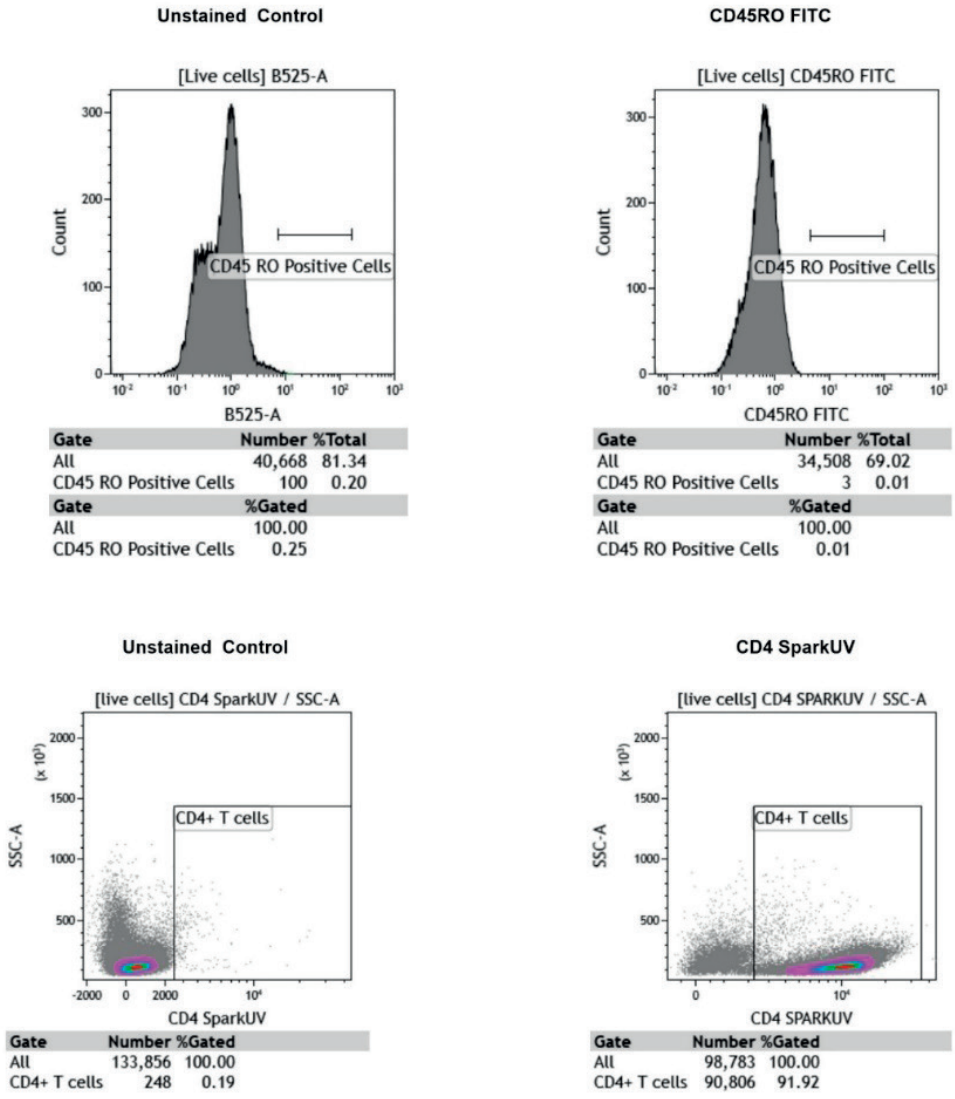

Supplementary Figure 3: Naïve CD4 T cell isolation kit purity check.
Flow cytometry analysis was performed to assess the purity of naïve CD4 T cells following isolation using the Miltenyi Biotec negative selection kit. Initially, CD45RO-FITC staining was used to confirm the absence of memory T cells, with almost all cells being CD45RO-negative. Subsequently, CD4 SPARK-UV staining was applied to confirm that over 90% of the isolated cells were CD4+ T cells, ensuring the high purity of the isolated naïve CD4 T cell population.

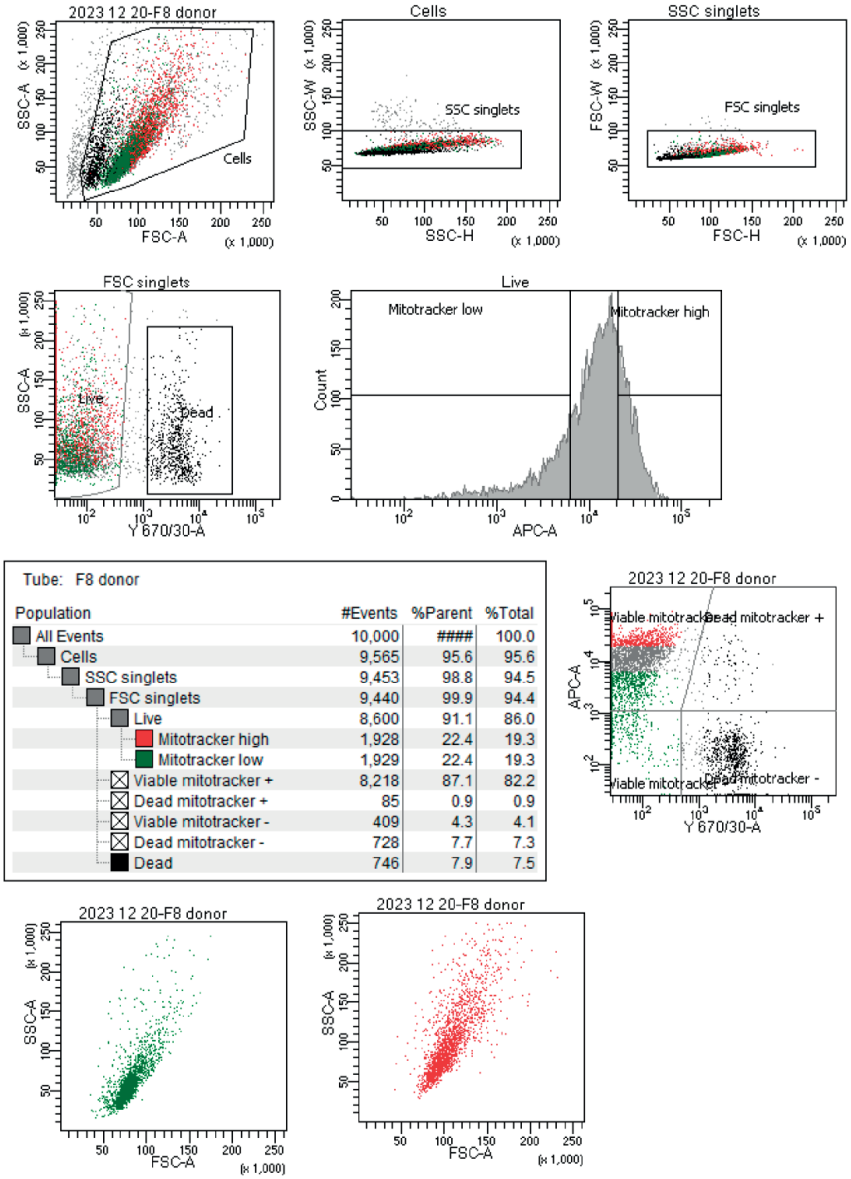

Supplementary Figure 4: Flow Cytometry Sorting Strategy for Isolation hyperpolarized ΔΨ cells and depolarized ΔΨ cells.

The flow cytometry sorting process involved sequential gating to ensure high purity of the sorted population. First, debris was excluded, followed by singlet selection to isolate individual cells. Viability was then assessed to ensure only live cells were included in subsequent analysis. Hyperpolarized ΔΨ and depolarized ΔΨ populations were sorted based on MitoTracker Deep Red staining, with approximately 20% of the cells classified hyperpolarized ΔΨ cells. After sorting, cell purity, viability, and cell number were reassessed to confirm the integrity and quality of the sorted population.

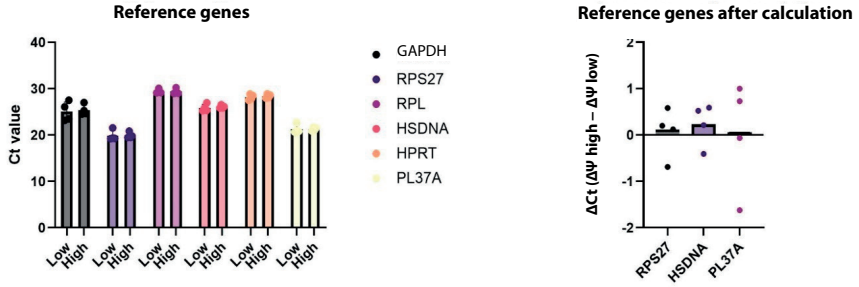

Supplementary Figure 5: Gene selection for mitochondrial gene expression analysis.

To ensure the reliability of gene expression normalization in mitochondrial morphology and activity-related gene measurements (Figure 2F), reference genes with stable expression across distinct mitochondrial populations were validated. Naïve CD4+ T cells cultured in our Th17 differentiation cocktail for 48 hours were sorted into ΔΨm high and low populations based on MitoTracker Deep Red staining. The Ct values for six commonly used reference genes (GAPDH, RPS27, RPL, HSDNA, HPRT, and PL37A) were assessed in three individual donors. As shown in the graph, no significant differences in Ct values were observed between ΔΨm high and low populations, confirming the stable expression of these reference genes. Based on these findings, RPS27, HSDNA, and PL37A were selected as the reference genes for subsequent qPCR analysis in Figure 2F, with the goal of achieving Ct values below 30 to ensure reliable normalization of mitochondrial-related gene expression.

SUPPLEMENTARY TABLES

Supplementary Table 1: Th17 polarization cocktails

Cytokines/ reagents	cocktail 3 our cocktail	Additional cocktail 1	Additional cocktail 2	Supplier	Identifier
CD3	5 µg/ml	5 µg/ml	5 µg/ml	BioLegend	*317326*
CD28	0.25 µg/ml	-	2.5 µg/ml	BioLegend	*302934*
IL-1β	10 ng/ml	50 ng/ml	10 ng/ml	*R&D*	*201-LB*
IL-2	10 U/ml	-	10 U/ml	BioLegend	*589104*
TGF-β	1 ng/ml	-	1 ng/ml	Pepro Tech	*100-21c*
IL-6	30 ng/ml	-	10 ng/ml	BioLegend	*570804*
IL-23	10 ng/ml	50 ng/ml	-	BioLegend	*574102*
IL-21	-	-	20 ng/ml	BioLegend	*571202*
Anti-IFN-γ	10 µg/ml	10 µg/ml	10 µg/ml	BioLegend	*506533*
Anti-IL-4	10 µg/ml	10 µg/ml	10 µg/ml	BioLegend	*500839*

Supplementary Table 2: List of antibodies used for cell surface flow cytometry staining

Antigen	Clone	Fluorochrome	Supplier	Identifier
CD4	SK3	SPARK UV	BioLegend	344685
CD45R0	UCHL1	FITC	BioLegend	983110
CD25	M-A251	PE/CYANINE7 or SPARK UV	BioLegend	356107/356157
CD69	FN50	PE/DAZZLE594	BioLegend	310941
PD-1	EH12.2H7	Brilliant Violet 421	BioLegend	329919
TIGIT	VSTM3	Brilliant Violet 785	BioLegend	372735

Supplementary Table 3: List of antibodies used for intracellular flow cytometry staining.

Antigen	Clone	Fluorochrome	Supplier	Identifier
RORyt	12-6988-82	PE	INVITROGEN	12-6988-82
IL-17A	BL168	Brilliant Violet 421	BioLegend	512322
IFN-y	4S.B3	Brilliant Violet 510	BioLegend	502544
Granzyme B	GB11	FITC	BioLegend	515403
Anti puromycin	2A4	ALEXA FLUOR 488	BioLegend	381505
Gata3	16E10A23	ALEXA FLUOR 488	BioLegend	653807
IL-22	2G12A41	PEDazzle594	BioLegend	366715
IL-10	JES3-9D7	PE-Cy7	BioLegend	501419
Foxp3	PCH101	APC	INVITROGEN	17-4776-42
IL-4	MP4-25D2	PE/Dazzle594	BioLegend	500831
T-bet	4B10	Brilliant Violet711	BioLegend	644819
IL-6	MQ2-13A5	Pacific Blue	BioLegend	501113
IL-21	eBIO3A3-N2	PE	eBioscience	12-7219-42
ViaKrome 808			Beckman Coulter	C36628

Supplementary Table 4: List of primers used for qPCR.

Gene	Forward primer sequence (5'-3')	Reverse primer sequence (3'-5')
HSDNA	TGGAGCTGCAGAACCTGATG	TGTAGTCTTCCCTGGCATGC
PL37A	ATTGAAATCAGCCAGCACG	AGGAACCACAGTGCCAGAT
RPS27a	TGGCTGTCCTGAAATATTATAAGGT	CCCCAGCACCACATTCATCA
OPA1	ACGTCTTTTGTCCAGCCTCT	GGTTAAAGCGCCCGTAACAT
MFN1	CCTGGCATCCAGGAGTTAGA	TGGTTCCAGCAATGCGATTT
MFN2	TGCAGGTGTAAGGGACGATT	GAGGCTCTGCAAATGGGATG
DRP1	CAAAGCAGTTTGCCTGTGGA	TCTTGGAGGACTATGGCAGC
FIS1	CCAAATCCTGAAGGAGACGC	GCTGAAGGCCACAGAGGATA
TEFM	TGAGAAAGCTCCTCAAACCAGAC	CAGTCCAGCACTGTCAACTTACG
POLRMT	GTCAACACCTCCAAGCTGCTC	GCTGCTTCTCAAAGAGGCACTG
TFB2M	GGGAAAACCAAGTAGACCTCCAC	TTTCGAGCGCAACCACTTTGGC
NRF1	GGCAACAGTAGCCACATTGGCT	GTCGTCTGGATGGTCATCTCAC
GOT1	CAACTGGGATTGACCCAACT	GGA ACA GAA ACC GGT GCT T
RORC	TGAGAAGGACAGGGAGCCAA	CCACAGATTTTGCAAGGGATCA
IL17A	TTGATTGGAAGAAACAACGATGA	CTCAGCAGCAGTAGCAGTGACA

Supplementary Table 5: List of SCENITH Reagents.

Chemicals	Supplier	Identifier
Oligomycin A	Merck	75351-5Mg
2-Deoxy-D-glucose	Sanbio	14325-1
Harringtonine	Sanbio	15361-1



Chapter 4

Activated but not exhausted: vigilant memory T cells in end-stage osteoarthritis synovium

Xinlai Chen[1], Theodoros Ioannis Papadimitriou[2], Nienke J.T. van Kooten[1], Lorena Wunderink[1], Birgitte Walgreen[1], Fons A.J. van de Loo[1], Peter M. van der Kraan[1], Martijn H.J. van den Bosch[1], Marije I. Koenders[1], Arjan P.M. van Caam[1]

1. Department of Rheumatology and Laboratory of Experimental Rheumatology, Radboudumc, Nijmegen, the Netherlands

2. Department of Rheumatology, Leiden University Medical Centre, Leiden, Netherlands

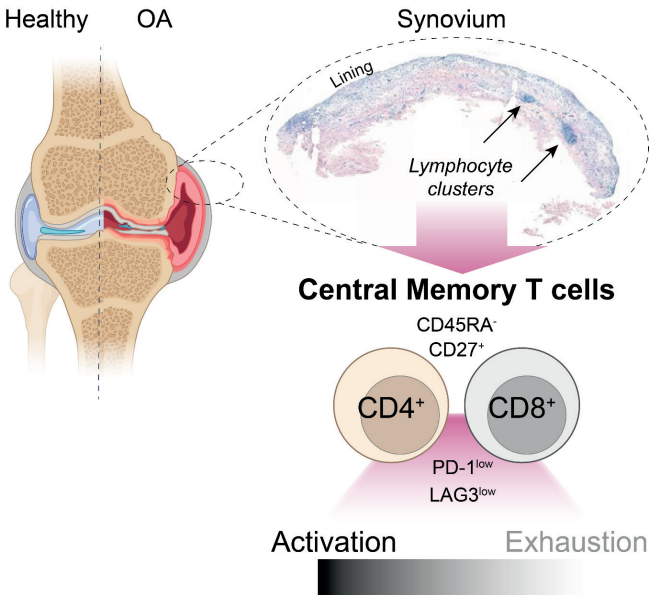

Created with BioRender.com

ABSTRACT

Objectives: In osteoarthritis (OA), chronic inflammation is present within the synovial microenvironment. This study aimed to characterize the activation, exhaustion, effector subsets and memory states of synovial T cells in end-stage OA to explore their possible contribution to disease pathophysiology.

Methods: Human OA synovial tissue obtained from total joint replacement was enzymatically digested for single cell analysis. Multiparameter flow cytometry was used to profile macrophage polarization and T cell helper and cytotoxic subsets ($CD4^+$, $CD8^+$), including markers of activation (CD69, ICOS), senescence (CD57, TIGIT), exhaustion (PD-1, LAG-3), and differentiation state (CD45RA, CD27). Intracellular staining for transcription factors (T-bet, GATA3, RORγt, FOXP3) and cytokines (IFN-γ, IL-4, IL-17A, IL-22) was used to assess T cell polarization. Complementary multicolor immunofluorescence staining was conducted to evaluate spatial distribution of T cells.

Results: $CD3^+$ T cell frequencies within the $CD45^+$ immune compartment ranged from 1% to 22% across donors, and clear lymphocyte clusters were observed in one-third of patients. Among the nine donors with sufficient T cell numbers for subset analysis (≥500 $CD3^+$ events), both $CD4^+$ and $CD8^+$ T cells showed an activated phenotype, with increased expression of CD69 and ICOS. In these donors, most synovial T cells displayed a $CD45RA^-CD27^+$ central memory-like phenotype. $CD8^+$ T cells contained a higher proportion of senescent $CD57^+TIGIT^-$ cells. Both $CD4^+$ and $CD8^+$ T cells retained cytokine-producing capacity, particularly IFN-γ, and included $ROR\gamma t^+IL\text{-}17^-IFN\text{-}\gamma^+$ non-classical Th17 cells. $PD\text{-}1^+LAG\text{-}3^+$ exhausted cells were rare (<2% of $CD4^+$ and <1% of $CD8^+$ T cells). Macrophages showed a mixed expression pattern of M1- and M2-associated markers, which was not associated with $CD3^+$ T cell abundance.

Conclusions: Synovial T cells in end-stage OA with sufficient infiltration for phenotypic characterization were predominantly central memory-like $CD4^+$ and $CD8^+$ cells with an activated, largely non-exhausted phenotype and preserved effector function. These findings indicate that synovial T cells in end-stage OA remain functionally competent rather than terminally exhausted.

INTRODUCTION

Synovial inflammation is a key characteristic of numerous OA patients and is associated with pain and radiographic progression [110]. Among the various immune cells present in the OA synovium, macrophages are the most abundant and well-characterized. Their roles in mediating inflammation, extracellular matrix remodeling, and osteophyte formation have been extensively described [114, 194]. Beyond macrophages, T cells are increasingly recognized in OA synovium and implicated in disease pathogenesis [116]. In OA synovium, both $CD4^+$ and $CD8^+$ T cells can be found. $CD4^+$ T cells are typically associated with helper and regulatory roles, and functionally distinct T helper subsets have been described in OA synovium. These include Th1 cells characterized by IFN-γ production, which are enriched in synovial fluid and tissue [195, 196] and regulatory T cells (Tregs) which have been inversely associated with pain and functional disability [197, 198]. In contrast, overall $CD4^+$ T cell abundance has also been positively associated with OA pain [268]. Less is known about the role of $CD8^+$ T cells in OA. Aging, an OA risk factor, and chronic inflammation may promote increased $CD8^+$ T cell infiltration, altering the $CD4^+/CD8^+$ ratio and the overall local T cell composition [199].

Moreover, T cell activation has been consistently observed in OA [200, 201]. Chronic activation can affect T cell function by inducing exhaustion, impairing memory formation, and limiting plasticity, but these processes are scarcely investigated and remain poorly understood in OA.

Therefore, this study aimed to define the phenotypic diversity of synovial T cells in OA, focusing on activation, exhaustion, memory, and effector profiles. Understanding these features may help explain synovial T cells persistence in residual tissue after joint replacement, which may sustain post-surgical inflammation [202, 203]. Those T cells also express immune checkpoint molecules targeted by cancer immunotherapy, linking OA synovial biology to immune-related arthritis after checkpoint inhibitor treatment [204].

RESULTS

Macrophages and T cells are the most abundant immune cell populations in end-stage OA synovium

Using flow cytometry, we examined the composition of $CD45^+$ immune cells in OA synovium **(Figure 1A).** Macrophages ($CD45^+CD68^+$) formed the dominant fraction (mean 61%, range 28.64% – 89.4% across donors), followed by the remainder comprising other $CD45^+$ cells not further characterized in this study. T cells ($CD45^+CD3^+$) represented a smaller but variable fraction (mean 8%, range 1.06%–22.49% of $CD45^+$ cells; **Figure 1B, D**). Immunofluorescence

confirmed this inter-donor variability, with CD3⁺ cells distributed in either diffuse or clustered patterns across synovial tissue **(Figure 1C).**

To assess whether macrophage polarization influenced T cell infiltration, we first characterized synovial macrophages using classical surface markers: M1-like cells (CD163⁻CD86⁺HLA-DR⁺) and M2-like cells (CD163⁺CD206⁺). M2-like CD163⁺ macrophages co-expressed M1-associated CD86 and HLA-DR markers, consistent with the mixed phenotype previously reported by our group [205] (**Figure 1E**). For comparison of T cell infiltration, donors were stratified into M1-predominant (CD163⁺ <50%, n=5) and M2-predominant (CD163⁺ >50%, n=7) groups using the 50% midpoint of CD163 expression as a pragmatic cutoff. CD3⁺ T cell frequencies varied across donors, but CD3⁺ T cell frequencies were similar between M1- and M2-predominant groups **(Figure 1F)**, indicating no obvious link between macrophage polarization and T cell infiltration.

Figure 1: Macrophage –T cell composition and heterogeneity in end-stage OA synovium.
(A) Flow cytometry gating strategy for CD45⁺ immune cells from live synovial single-cell suspensions, identifying macrophages (CD45⁺CD68⁺), T cells (CD45⁺CD3⁺), and other CD45⁺ cells (n=12). **(B)** Frequencies of CD45⁺ cells, CD68⁺ macrophages, and CD3⁺ T cells across 12 OA donors. **(C)** Representative immunofluorescence images of OA synovium showing CD3 (cyan) and CD68 (yellow) in donors with low and high immune-cell infiltration; DAPI (blue) marks nuclei. Scale bars: 200 µm (overview), 50 µm (magnification). **(D)** Per-donor composition of the CD45⁺ compartment: macrophages (CD68⁺, pink), T cells (CD3⁺, yellow), and remaining CD45⁺ cells (blue) for each donor (n=12). Pie chart shows mean proportions across all donors. **(E)** Co-expression of HLA-DR and CD86 on M2-like (CD163⁺CD206⁺) macrophages, demonstrating that M2-like cells also express M1-associated activation markers (n=12). **(F)** CD3⁺ T cell frequencies in donors stratified as M1-predominant (CD163⁺ <50%, n=5) or M2-predominant (CD163⁺ >50%, n=7); no significant difference was observed.

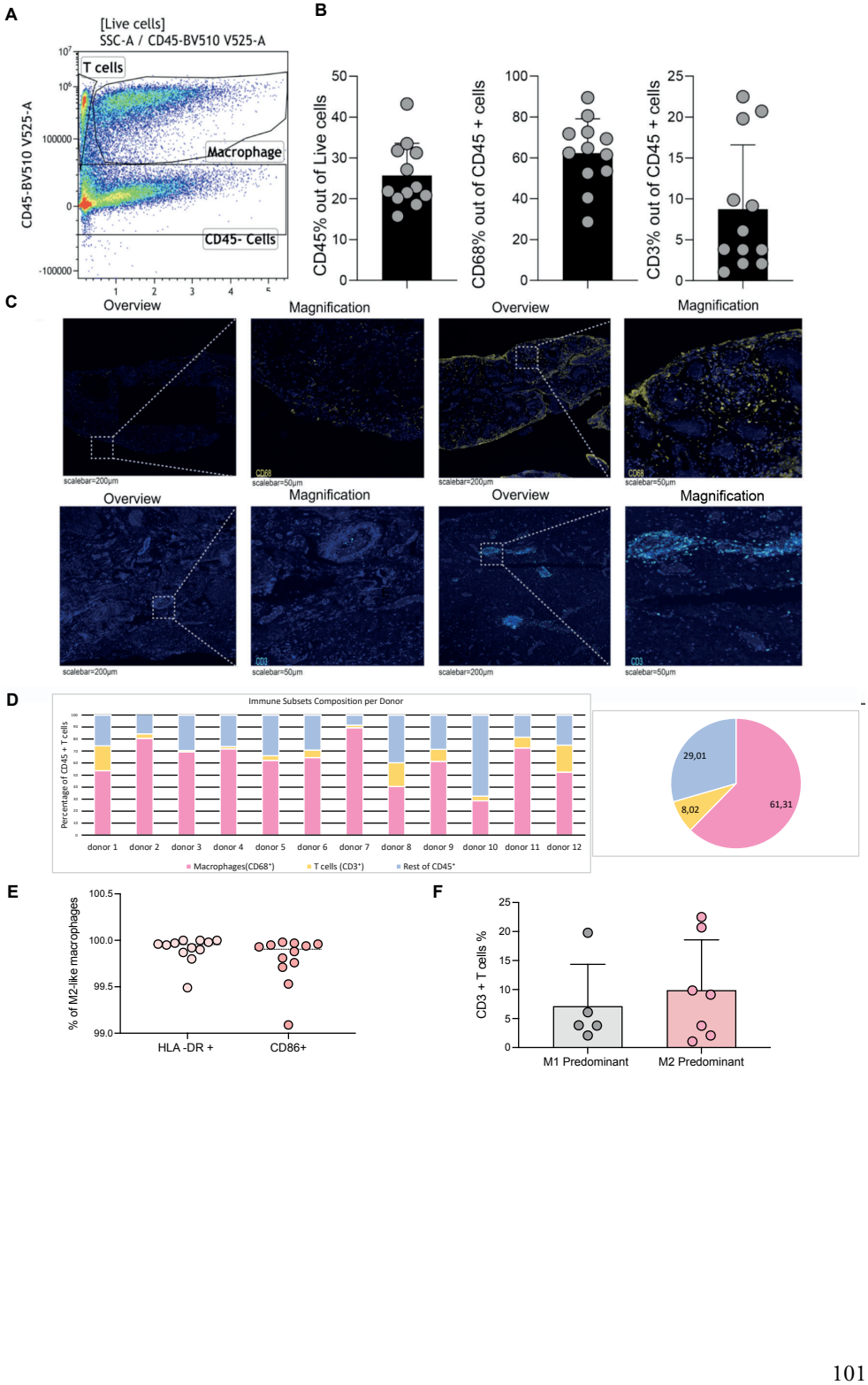
A
[Live cells]
SSC-A / CD45-BV510 V525-A
T cells
Macrophage
CD45- Cells
CD45-BV510 V525-A
B
CD45% out of Live cells
CD68% out of CD45 + cells
CD3% out of CD45 + cells
C
Overview
Magnification
Overview
Magnification
Overview
Magnification
Overview
Magnification
D
Immune Subsets Composition per Donor
Percentage of CD45 + T cells
donor 1
donor 2
donor 3
donor 4
donor 5
donor 6
donor 7
donor 8
donor 9
donor 10
donor 11
donor 12
Macrophages(CD68+)
T cells (CD3+)
Rest of CD45+
29,01
8,02
61,31
E
% of M2-like macrophages
HLA -DR +
CD86+
F
CD3 + T cells %
M1 Predominant
M2 Predominant

Synovial T cells comprise CD4⁺ and CD8⁺ subsets with central memory predominance

In further flow cytometry analysis, CD3⁺ T cells were subdivided into CD4⁺ helper T cell and CD8⁺ cytotoxic T cell subsets **(Figure 2A)**. Both subsets were consistently present across donors, though the CD4:CD8 ratio varied inter-individually. In over half of the samples, CD4⁺ T cells were more frequent than CD8⁺ T cells (**Figure 2A**), as we also observed in our immunostaining showing CD3⁺ (cyan) and CD8⁺ (red) T cell numbers and distribution **(Figure 2B)**. We next investigated whether CD4⁺ or CD8⁺ T cell frequencies differed between M1- and M2-predominant synovial environments (as previously stratified in **Figure 1E, F**). When grouped by macrophage profile, CD4⁺ as well as CD8⁺ frequencies remained broadly similar between groups **(Figure 2C)**.

Next, we assessed whether synovial T cells were naïve or antigen-experienced. Although the specific antigens driving potential OA immune responses remain unknown, antigen-experienced T cells can adopt memory or effector phenotypes, including bystander-activated cells that respond independently of TCR recognition [206]. To assess T cell differentiation status, we used CD27 and CD45RA as classical markers for immunophenotyping. CD27 is typically expressed on naïve and central memory T cells and is downregulated as cells become antigen experienced. CD45RA identifies naïve and terminally differentiated effector cells. Based on the combined expression of these two markers, we defined four T cell subsets: naïve (CD27⁺CD45RA⁺), central memory (TCM; CD27⁺CD45RA⁻), effector memory (TEM; CD27⁻CD45RA⁻), and terminal effector (TEMRA; CD27⁻CD45RA⁺) subsets. Subset analysis was restricted to nine donors with ≥500 CD3⁺ events, the minimum for reliable downstream gating. In these donors, TCM cells (CD27⁺CD45RA⁻) were the dominant differentiation state in both CD4⁺ (median 84.31%, range 77.24% – 92%) and CD8⁺ (median 57.88%, range 51.38% – 66.15%) compartments, followed by naïve cells (CD27⁺CD45RA⁺). TEM (CD27⁻CD45RA⁻) and TEMRA (CD27⁻CD45RA⁺) subsets together accounted for <5% of CD4⁺ and <20% of CD8⁺ T cells **(Figure 2D–E)**.

Figure 2: Synovial T cells comprise CD4⁺ and CD8⁺ subsets with central memory predominance.
(A) Flow cytometry gating strategy to identify CD4⁺ and CD8⁺ T cells among CD3⁺ lymphocytes. Percentages of CD4⁺ and CD8⁺ subsets out of CD3⁺ T cells, and CD4:CD8 ratio across 12 OA donors. **(B)** Representative immunofluorescence imaging of immune cells (CD3, cyan; CD8, red) in OA synovium; DAPI staining (blue) was used to visualize nuclei. **(C)** CD4⁺ and CD8⁺ T cell percentages in M1-predominant vs M2-predominant donors. CD4⁺ and CD8⁺ frequencies are comparable (n=12). **(D)** Gating strategy and subset distribution of CD4⁺ T cells based on CD27 and CD45RA expression (n=9; donors with events <500 CD3⁺ T cell events excluded). Naïve (CD27⁺CD45RA⁺), central memory (TCM; CD27⁺CD45RA⁻), effector memory (TEM; CD27⁻CD45RA⁻), and terminal effector (TEMRA; CD27⁻CD45RA⁺) subsets were identified. Central memory T cells predominated within the CD4⁺ T cell compartment, followed by naïve T cells. **(E)** Gating strategy and subset distribution of CD8⁺ T cells based on CD27 and CD45RA expression (n=9; donors with events <500 CD3⁺ T cell events excluded). CD8⁺ T cells also showed a predominance of central memory phenotype.

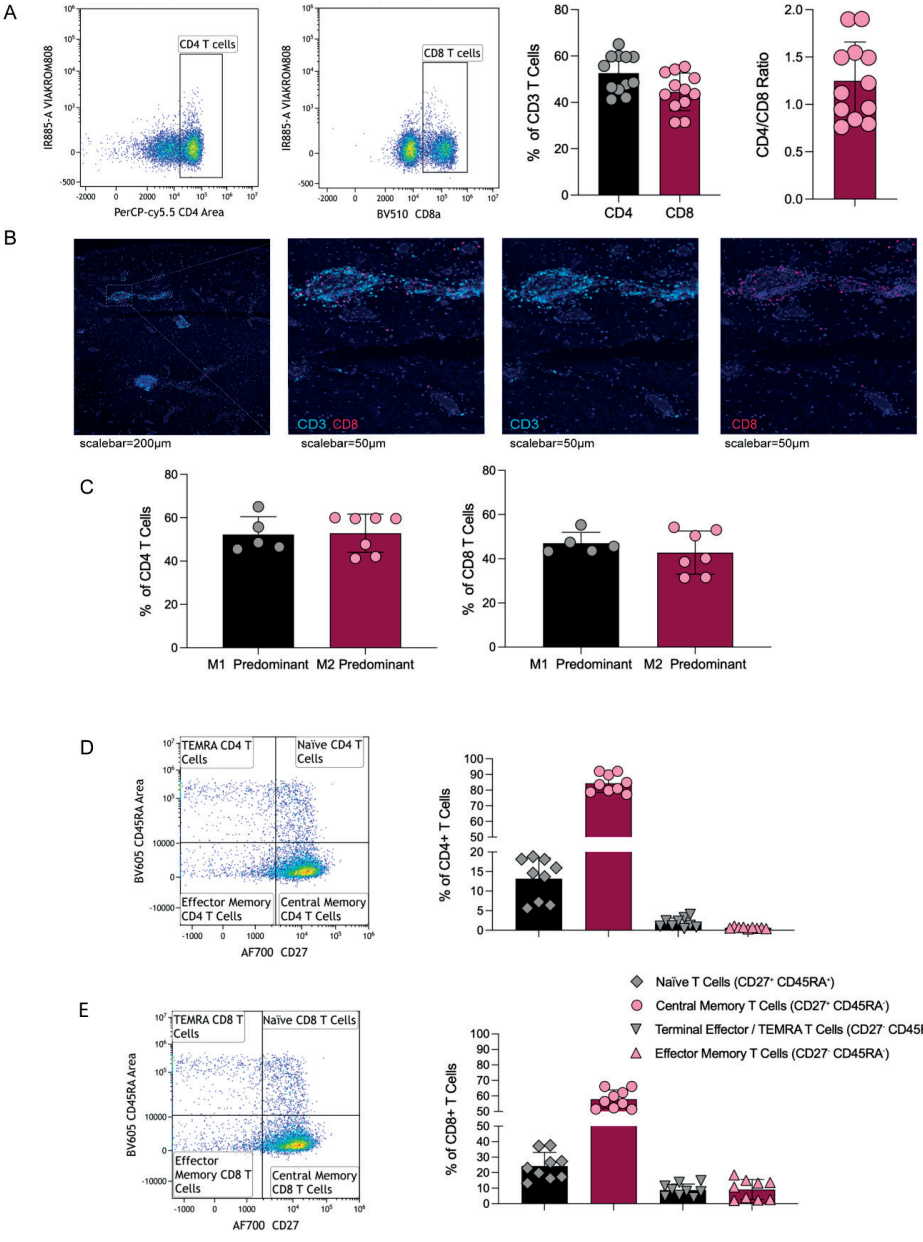
A
CD4 T cells
IR885-A VIAKROM808
PerCP-cy5.5 CD4 Area
CD8 T cells
BV510 CD8a
% of CD3 T Cells
CD4
CD8
CD4/CD8 Ratio
B
CD3 CD8
CD3
CD8
scalebar=200µm
scalebar=50µm
scalebar=50µm
scalebar=50µm
C
% of CD4 T Cells
M1 Predominant M2 Predominant
% of CD8 T Cells
M1 Predominant M2 Predominant
D
TEMRA CD4 T Cells
Naïve CD4 T Cells
Effector Memory CD4 T Cells
Central Memory CD4 T Cells
BV605 CD45RA Area
AF700 CD27
% of CD4+ T Cells
E
TEMRA CD8 T Cells
Naïve CD8 T Cells
Effector Memory CD8 T Cells
Central Memory CD8 T Cells
BV605 CD45RA Area
AF700 CD27
% of CD8+ T Cells
Naïve T Cells (CD27+ CD45RA+)
Central Memory T Cells (CD27+ CD45RA-)
Terminal Effector / TEMRA T Cells (CD27- CD45RA+)
Effector Memory T Cells (CD27- CD45RA-)

Synovial T cells exhibit cytokine production capacity with low classical polarization

To assess the $CD4^+$ and $CD8^+$ subsets in further detail based upon their lineage-specific cytokine expression, synovial cells were stimulated with PMA and ionomycin in the presence of GolgiPlug™ to enable intracellular cytokine staining. Flowcytometric analysis revealed robust IFN-γ protein expression in both $CD4^+$ and $CD8^+$ T cells, while IL-4, IL-17A, and IL-22 were detected at lower frequencies **(Figure 3A)**. $CD8^+$ T cells produced significantly more IL-4 than $CD4^+$ T cells (**p =0.0039, Wilcoxon matched-pairs test).

However, canonical $CD4^+$ T helper subsets (Th1, Th2, Th17, Th22, Treg) and $CD8^+$ cytotoxic (Tc1, Tc2, Tc17) T cell subsets are defined by co-expression of lineage-specific cytokines and transcription factors. Interestingly, when using these classical definitions for T cell type 1 ($Tbet^+IFN\text{-}\gamma^+$), type 2 ($GATA3^+IL\text{-}4^+$), type 17 ($ROR\gamma t^+IL\text{-}17^+$), and Treg cell ($CD25^+FOXP3^+$), all these subpopulations were detected at low frequencies (<2% of $CD4^+$ or $CD8^+$ T cells) **(Figure 3B)**.

By contrast, a non-classical Th17-like subset, defined as $ROR\gamma t^+IFN\text{-}\gamma^+$, was detected in both $CD4^+$ and $CD8^+$ T cells, with significantly higher frequencies in $CD4^+$ T cells (*p = 0.0419). $IFN\text{-}\gamma^+IL\text{-}17A^+$ dual producers were also more frequent among $CD4^+$ than $CD8^+$ T cells (**p = 0.0039), supporting the predominance of $ROR\gamma t^+IFN\text{-}\gamma^+$ cells over classical IL-17A-producing Th17-like cells **(Figure 3C)**. These IFN-γ producing $ROR\gamma t^+$ cells may represent a non-classical, memory-like subset with cytokine plasticity in chronically inflamed tissue.

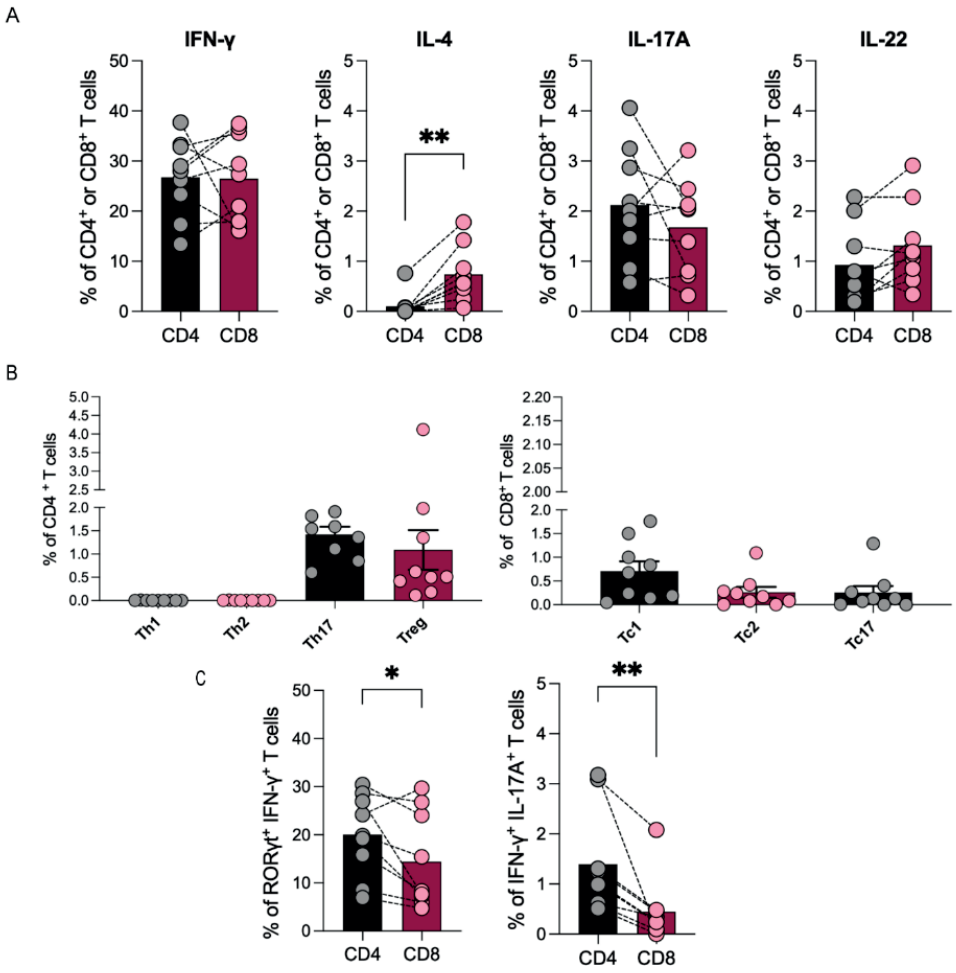

Figure 3: Effector subset composition and cytokine production capacity of OA synovial T cells. (A) Intracellular cytokine production in CD4⁺ and CD8⁺ T cells after PMA/ionomycin stimulation. Frequencies of IFN-γ⁺, IL-4⁺, IL-17A⁺ and IL-22⁺ cells are shown as a percentage of total CD3⁺ T cells. IFN-γ was the predominant cytokine produced in both CD4⁺ and CD8⁺ compartments. CD8⁺ T cells produced more IL-4 than CD4⁺ T cells (**p = 0.0039, Wilcoxon matched-pairs test). IL-17A and IL-22 expression levels were low in both subsets. **(B)** Frequencies of classical CD4⁺ helper subsets (Th1: T-bet⁺IFN-γ⁺; Th2: GATA3⁺IL-4⁺; Th17: RORγt⁺IL-17A⁺; Treg: CD25⁺ FOXP3⁺) and CD8⁺ cytotoxic subsets (Tc1, Tc2, Tc17) defined by transcription factor–cytokine co-expression. All subsets were detected at low frequencies (<2% of parent population). **(C)** Detection of abundant RORγt⁺IFN-γ⁺ in both CD4⁺ and CD8⁺ compartments, with significantly higher frequencies in CD4⁺. Paired t-test: *p = 0.0419. IL-17A⁺IFN-γ⁺ dual-producers were rare (<2% of T cells), but detected in both lineages (**p = 0.0039, Wilcoxon matched-pairs test).

Synovial T cells display activation-associated profiles with minimal features of exhaustion

T cell function is closely linked to activation and differentiation state. Repeated TCR stimulation during chronic inflammation can, for example, drive T cells towards an exhausted phenotype. To assess the functional state of synovial $CD4^+$ and $CD8^+$ T cells, we used a separate flow cytometry panel to evaluate markers of activation (CD69, ICOS), senescence (CD57, $TIGIT^-$), and exhaustion (PD-1, TIGIT, LAG-3). tSNE mapping showed prominent expression of CD69 and ICOS in both subsets, detectable expression of PD-1 and CD57, and comparatively lower expression of LAG-3 and TIGIT **(Figure 4A)**. Quantitative analysis confirmed higher frequencies of $CD69^+$, $PD\text{-}1^+$, $CD57^+$, and $TIGIT^+$ cells among $CD8^+$ than $CD4^+$ T cells (CD69: *p=0.0366; PD-1: ****p<0.0001; CD57: ***p=0.0003; TIGIT: **p=0.0016) **(Figure 4B)**. Multiplex immunofluorescence further confirmed co-localization of CD3 (cyan), CD8 (red), CD69 (orange), and PD-1 (green) in OA synovial tissue **(Figure 4C)**.

However, since it is particularly the combination of markers that defines the state of the T cells, we further analyzed co-expression of markers as mentioned above. Co-expression analysis revealed that the majority of $CD4^+$ and $CD8^+$ T cells were activated $CD69^+ICOS^+$ T cells, with this population significantly enriched among $CD8^+$ T cells (****p<0.0001). CD69 is an early activation marker on T cells, which also suppresses T cell migration and therefore promotes tissue retention, while ICOS (Inducible T cell CO-Stimulator) promotes cytokine production and survival. In contrast, PD-1, LAG-3, and TIGIT are upregulated under chronic antigen stimulation and are commonly associated with T cell exhaustion in persistent inflammatory settings. $PD\text{-}1^+LAG\text{-}3^+$ double-positive T cells were detected at low frequencies but were more prevalent in $CD4^+$ T cells (*p=0.0192). Finally, $CD57^+TIGIT^-$ T cells refer to a specific subset of T lymphocytes often associated with a terminally differentiated or senescent phenotype. $CD8^+$ T cells showed an increased proportion of $CD57^+TIGIT^-$ cells (***p=0.0003) **(Figure 4D)**.

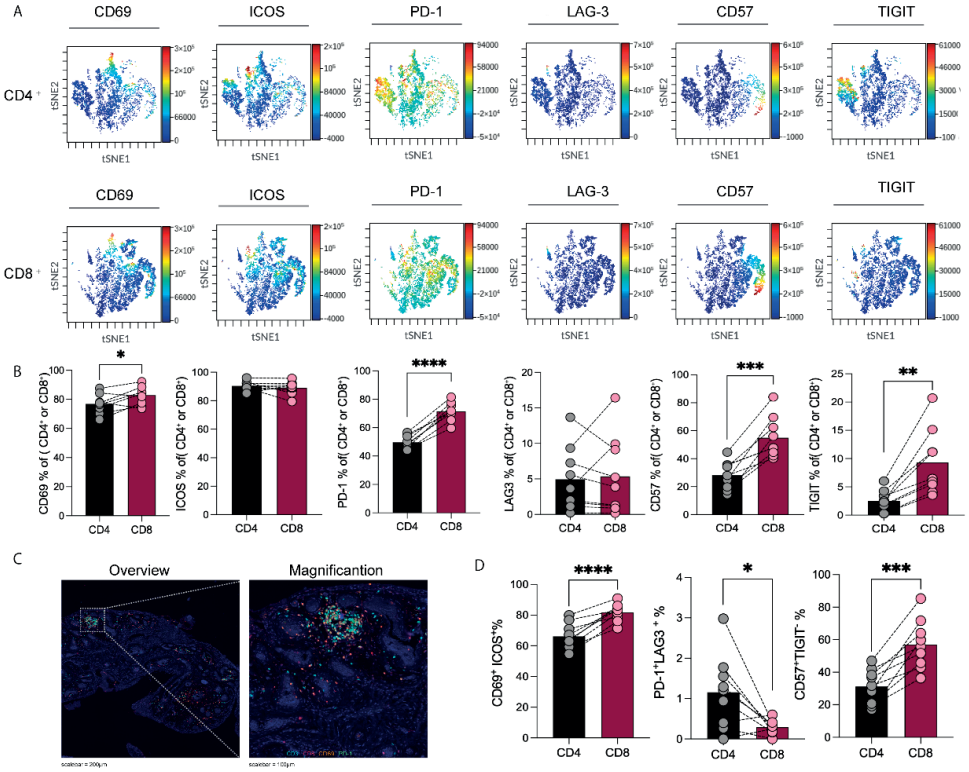

Figure 4: Synovial T cells exhibit a vigilant but non-exhausted phenotype in end-stage OA.
(A) tSNE maps visualize expression of activation markers (CD69, ICOS), exhaustion markers (PD-1, LAG-3, TIGIT), and the senescence marker CD57 in CD4⁺ and CD8⁺ T cells isolated from OA synovial tissue (n=9). **(B)** CD69 and ICOS were highly expressed in both CD4⁺ and CD8⁺ T cells, while PD-1 and CD57 showed intermediate levels. LAG-3 and TIGIT were detected at lower frequencies. Across markers, CD8⁺ T cells consistently showed higher expression of CD69 (p=0.0366), PD-1 (****p<0.0001), CD57 (***p=0.0003), and TIGIT (**p=0.0016), based on paired t testing. **(C)** Representative immunofluorescence imaging of immune cells (CD3, cyan), (CD8, red), (CD69, orange) and (PD-1 green) in OA synovium; DAPI staining (blue) was used to visualize nuclei. **(D)** Marker co-expression profiles. A majority of CD4⁺ and CD8⁺ T cells were CD69⁺ICOS⁺, consistent with a tissue-resident, activated phenotype. This population was significantly larger among CD8⁺ T cells (****p<0.0001). Double-positive PD-1⁺LAG-3⁺ cells were rare but more common in CD4⁺ (*p=0.0192). CD8⁺ T cells had more CD57⁺TIGIT⁻ cells (***p=0.0003).

Activation and exhaustion profiles within central memory T cells

Given the predominance of central memory ($CD27^+CD45RA^-$) T cells in OA synovial tissue **(Figure 2D,E)**, we further analyzed their activation, exhaustion, and senescence profiles **(Figure 5)**. Both $CD4^+$ and $CD8^+$ TCM cells frequently co-expressed CD69 and ICOS. $PD\text{-}1^+LAG\text{-}3^+$ cells were infrequent overall, but were more common in $CD4^+$ than $CD8^+$ TCM cells ($p=0.0117$). Over 50% of $CD8^+$ TCM cells were $CD57^+TIGIT^-$ ($^{***}p=0.0001$), indicating that this phenotype was common within the $CD8^+$ central memory compartment. Together, these data indicate that synovial TCM cells are activated and not predominantly exhausted. At the same time, the presence of PD-1, TIGIT, and LAG-3 indicates expression of immune checkpoint molecules within this compartment, while retained activation suggests preserved effector potential in end stage inflamed OA tissue.

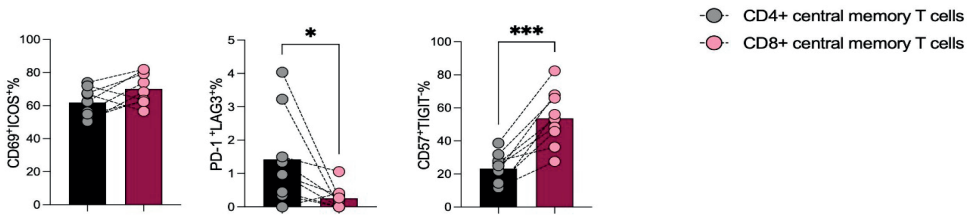

Figure 5. Central memory T cells in OA synovium show an activated, non-exhausted phenotype. Marker co-expression analysis within $CD4^+$ and $CD8^+$ central memory T cells ($CD27^+CD45RA^-$) revealed frequent $CD69^+ICOS^+$ cells and a rare exhaustion profile ($PD\text{-}1^+LAG\text{-}3^+$), which was more common in $CD4^+$ than $CD8^+$ ($^*p=0.0117$). $CD8^+$ TCM cells showed abundant $CD57^+TIGIT^-$ expression, consistent with a senescent-like state ($^{***}p=0.0001$). n=9; each data point represents an independent donor. Paired t-test.

DISCUSSION

Synovitis contributes to OA pathology [109, 207, 208], with macrophages as the most studied immune cells, while T cells remain less well explored [109, 209]. This study provides a flow cytometric characterization of synovial T cells from end-stage OA patients, focusing on subset composition, memory states, and activation versus exhaustion signatures.

Our data show that synovial macrophages frequently co-expressed markers traditionally associated with only M1-like ($CD163^-CD86^+HLA\text{-}DR^+$) or M2-like ($CD163^+CD206^+$) phenotypes. This is consistent with our previous report that OA synovial macrophages display a mixed phenotype and express both M1-like and M2-like macrophage markers [205]. This overlap in M1 and M2 markers suggests that, in the chronically inflamed OA synovium, macrophages adopt mixed or context-dependent activation states rather than mutually exclusive polarization states. Such plasticity mirrors observations in rheumatoid arthritis and tumor-

associated macrophages [210, 211], where sustained inflammatory signals drive non-classical activation patterns. These hybrid phenotypes may reflect chronic stimulation within the OA joint microenvironment, in contrast to the discrete M1/M2 profiles generated under controlled *in vitro* conditions. We had hypothesized that $CD3^+$ T cell numbers would be higher in M2-predominant samples, with the possibility that M2-like macrophages can support T cell activation, proliferation, or differentiation via IL-10 and BAFF secretion [212, 213]. However, no clear difference was observed between the stratified groups. This may reflect limited sample size or indicate that macrophage polarization, as defined here, is not a major determinant of synovial T cell abundance in end stage OA.

CD4:CD8 ratios varied between donors without consistent dominance of either subset, contrasting with earlier reports of a slight $CD4^+$ predominance in OA synovial fluid and tissue [214, 215]. Tissue specific $CD8^+$ enrichment has also been reported: in synovial tissue and infrapatellar fat pad, $CD8^+$ T cell proportions exceed those in matched circulating peripheral blood [216]. Local synovial $CD8^+$ T cell enrichment in both studies [199, 216] stressed the importance of tissue-specific immune profiling. Together, these observations demonstrate that systemic and tissue T cell compartments differ in OA, and that synovial $CD8^+$ frequencies cannot be inferred from blood.

An important finding of our study is that $CD4^+$ and $CD8^+$ T cells in OA synovium predominantly exhibited a central memory (TCM; $CD27^+CD45RA^-$) phenotype. TCM cells are long-lived, lymphoid-homing, and rapidly expand upon antigen re-stimulation [217]. By contrast, rheumatoid and psoriatic arthritis synovium is dominated by effector memory (TEM) or terminally differentiated effector cells (TEMRA) [218, 219], indicating that OA synovium presents a distinct immune environment in which T cells are less skewed toward terminal differentiation.

The predominance of memory T cells in OA synovium may be influenced by local factors such as TGF-β . TGF-β is elevated in OA joints compared to healthy controls [220] and is involved in OA pathogenesis [221]. Although TGF-β has been reported to promote memory T cells differentiation [222] and promote tissue-resident memory (TRM) phenotypes via CD103 induction [223], its role in shaping TCM cells in OA remains unclear. In this study, TCM were defined as $CD27^+CD45RA^-$ cells; however, markers of tissue residency such as CD103 were not included due to panel limitations. Future work is needed to clarify the relationship and potential overlap between TCM and TRM subsets in OA tissue, and how local TGF-β signaling may influence their development in this chronically inflamed environment.

The predominance of central memory T cells was accompanied by the low frequencies of classical effector $CD4^+$ T helper and $CD8^+$ cytotoxic T cell subsets. Nonetheless, both $CD4^+$

and CD8⁺ T cells retained the capacity to produce cytokines upon stimulation. Classical Th1, Th2, Th17, and Treg subsets were present at low frequencies within the CD4⁺ compartment, while Tc1, Tc2, and Tc17 subsets were barely detectable in the CD8⁺ compartment. We also identified polyfunctional IFN-γ⁺IL-17A⁺ T cells, referred to as Th1/17 cells, which are considered Th17 cells with a Th1-like phenotype. In addition, a subset of RORγt⁺IFN-γ⁺IL-17A⁻ T cells was detected in both CD4⁺ and CD8⁺ lineages. These so-called "ex-Th17" cells have been described in chronic mucosal inflammation, reflecting lineage plasticity rather than fixed polarization[156]. Their presence in osteoarthritis, a non-autoimmune context, suggests that chronic tissue stress and inflammation may induce T cell functional plasticity [224].

Both total T cells and TCM cells showed prominent CD69 and ICOS co-expression, with CD8⁺ TCM cells consistently exhibiting the highest co-expression across donors. This pattern indicates ongoing local stimulation without terminal exhaustion, and aligns with reports linking CD69⁺ICOS⁺ co-expression to tissue retention and effector readiness[225-227]. Because arthroplasty removes cartilage but not synovial tissue, given the role of memory T cells in long-term immune responses, this activated memory compartment may persist after surgery and contribute to post-surgical immune activity.

Despite frequent PD-1 expression, consistent LAG-3 and TIGIT co-expression was absent, indicating adaptation to chronic activation rather than terminal exhaustion [228]. This checkpoint-positive but non-exhausted state matters for immune checkpoint inhibitor (ICI) therapy: ICI-activated OA (ICI-aOA) and increased ICI-induced inflammatory arthritis risk in OA patients have both been reported recently, with PD-1⁺ synovial T cells proposed as a likely cellular target [229, 230]. In our cohort, PD-1 and other immune checkpoint molecules were also expressed in OA synovial T cells, suggesting that chronic local inflammation may establish a checkpoint-positive T cell state that could become relevant during ICI treatment. Furthermore, in both CD4⁺ and CD8⁺ TCM cells, PD-1⁺LAG-3⁺ cells were rare, supporting the conclusion that these cells are not predominantly terminally exhausted. Collectively, our data indicate that synovial T cells in end-stage OA, particularly the abundant central memory subsets, are activated and remain functionally competent, forming a vigilant rather than broadly exhausted immunological state.

In parallel, we examined T cell senescence, focusing on CD57 and the absence of TIGIT. CD57⁺ T cells were common in OA synovium, particularly among CD8⁺ T cells, consistent with a highly differentiated or senescence-like phenotype associated with repeated stimulation, reflecting long-lived, repeatedly stimulated effectors that may contribute to chronic inflammation [231, 232]. These cells largely lacked TIGIT co-expression, suggesting a senescent-like phenotype. CD57⁺ TIGIT⁻ cells were also observed within both CD4⁺ and CD8⁺ TCM cells, potentially

reflecting chronic inflammatory imprinting or features of immunological ageing[233]. The contribution of these cells to OA inflammation remains to be tested.

Several limitations of this study should be acknowledged. The dataset is observational and cross-sectional, limiting insights into temporal dynamics. PMA/ionomycin stimulation, while widely used to assess cytokine potential, does not reflect antigen-specific activation and may overestimate physiological responses. The relatively small cohort and lack of detailed clinical data restrict our ability to correlate T cell states with individual symptom profiles or radiographic severity. Although all samples were processed in parallel to minimize technical variability, this approach limited our capacity to adapt stimuli or examine functional kinetics across donors. Additionally, TCM cells were defined by CD27 and CD45RA, which identifies central memory-like T cells but does not capture canonical tissue-resident memory markers such as CD103, and signals shaping local memory programming, such as TGF-β, were also not assessed. Future studies employing antigen-specific assays and clinically-linked sampling will be critical to refine our understanding of memory T cell subsets and their functional roles in OA.

In summary, our findings identify OA synovial T cells as a memory-enriched, activation-competent, and not predominantly exhausted population. These vigilant memory T cells retain functional capacity and express immune checkpoint molecules, with potential relevance for ICI-associated joint pathology and persistent symptoms after joint replacement. Although OA is not classically autoimmune, immune memory shapes the inflammatory milieu of late-stage disease, and synovial immune activity is not resolved by addressing structural damage alone.

MATERIAL AND METHODS

Study cohorts

OA synovial tissue was obtained during joint replacement surgery from end-stage knee OA patients at the Sint Maartenskliniek or Radboudumc in Nijmegen (n=20). Patients from the Sint Maartenskliniek (METC 2018-4319) gave written informed consent. Patients from the Radboudumc had the opportunity to object to the use of their waste tissue for research purposes.

Tissue Cryopreservation

Synovial tissue specimens were sectioned into approximately 3 mm^2 pieces and either processed immediately for multiplex immunohistochemistry (n = 8), or preserved for flow cytometric analysis (n = 12). For preservation, tissues were immersed in a cryoprotective medium consisting of 60% RPMI 1640 (72400021, Thermo Fisher Scientific, Waltham, MA, USA), 10% human pooled serum (HPS), and 20% dimethyl sulfoxide (DMSO), and subsequently stored in liquid nitrogen.

Enzymatic digestion for single cell isolation.

To reduce inter-donor technical variation, all cryopreserved synovial samples were thawed and processed on the same day. To identify various cell subsets in patient synovium, synovial tissue was minced with a scalpel and digested by enzymatic digestion using 500 µl digestion mix with 0.1 mg/mL DNase (DN-25, Merck, Darmstadt, Germany) and 200 U/ml collagenase D (45-11088882001, Roche, Vienna, Austria) and plain RPMI 1640 medium for one hour on a roller bench at 37°C. Digestion enzymes were inactivated by adding 50 µl FCS. The resulting suspension was brought through a 70 µm cell strainer to obtain a single-cell solution, then mechanically disrupted by careful pipetting up and down and subsequently spun down for 5 minutes at 300 g. The supernatant was removed and the cells used for further processing.

Flow cytometry staining

Synovium cells were divided into 3 portions, approximately 1×10^6 cells per condition, in a polystyrene FACS (5 mL round-bottom) tube and incubated for 15 minutes in staining buffer (PBS + 1% BSA + 2 mM EDTA) containing Fc-block (564220, BD Biosciences, Franklin Lakes, NJ, USA). After washing, cells were incubated with (1.5:1000 PBS) Viakrome808 (Beckman Coulter) viability dye for 30 minutes at 4°C in the dark. Thereafter cells were washed twice with PBS and then the extracellular staining was performed by adding 50 µl staining buffer with extracellular antibodies and incubating for 25 minutes at room temperature protected from light. In case of intracellular staining, cells were fixed with 50 µl eBioscience™ Fix/Perm solution (00-5523-00, Invitrogen, Waltham, MA, USA), followed by 20 minutes incubation at room temperature. Then, cells were washed twice with permeabilization buffer from the same eBioscience™ kit before staining with intracellular antibodies for 25 minutes at room temperature protected from light. Cells were washed with permeabilization buffer, resuspended in FACS buffer and stored at 4°C until measurement. To enable detection of cytokine production, cells were pre-stimulated with 50 ng/mL phorbol 12-myristate 13-acetate (PMA, Merck, P1585-1MG) and 1 µg/mL ionomycin (Merck, I0634-1MG) in the presence of 1 µg/mL Golgi Plug (BD Biosciences, 555029) for 4 hours at 37°C prior to the staining process above. Samples were acquired in a Beckman Coulter Cytoflex LX 21-color flow cytometer. Flow cytometry data were analyzed using Kaluza software version 2.1.3 and Cytobank (Beckman Coulter, Brea, CA, USA).

Immunohistochemistry

Synovial tissue pieces were collected, formalin-fixed, and paraffin-embedded (FFPE). FFPE tissue sections were deparaffinized in xylene and rehydrated through graded ethanol. Antigen retrieval was performed in 10 mM sodium citrate buffer (pH 6.0) by heating the slides at 97°C for 10 minutes. Endogenous peroxidase activity was blocked with 3% H_2O_2 in PBS. Primary antibodies (detailed in Supplementary Table 1) and the corresponding secondary antibodies (BrightVision Poly-HRP, Immunologic, DPVO55HRP) were applied, followed by visualization

with 3,3′-diaminobenzidine (Bright DAB, Immunologic). Sections were then counterstained with hematoxylin.

Statistical analyses

Statistical analyses were performed with GraphPad Prism version 10.0.3. Pairwise comparisons were analysed with paired t-tests, or with Wilcoxon matched-pairs signed-rank tests when the data were not normally distributed. P values below 0.05 were considered statistically significant.

SUPPLEMENTARY MATERIALS

Supplementary Table 1: List of antibodies used for multiplex immunofluorescent staining.

Antigen	Clone	Dilution	Fluorophore	Supplier	Cat. no.
CD69	Polyclonal	1:800	Opal 520	Proteintech	10803-1-AP
CD25	RM418	1:100	Opal 480	Invitrogen	MA5-36078
CD8	C8/144B	1:200	Opal 690	Dako	M710301-2
CD3	SP7	1:400	Opal 620	Invitrogen	MA1-90582
FoxP3	236A/E7	1:100	Opal 570	eBioscience	14-4777-82
PD-1	D4W2J	1:200	Opal 780	Cell Signaling	86163

Supplementary Table 2: List of antibodies used for flow cytometry.

Antigen	Fluorochrome	Cat. no.	Supplier
Surface staining			
Viability	ViaKrome 808	C36628	Beckman Coulter
CD3	APC	344811	BioLegend
CD3	BUV737	612751	BD Horizon
CD3	PE	300307	BioLegend
CD4	FITC	300506	BioLegend
CD4	Spark UV 387	300579	BioLegend
CD4	PerCP/Cy5.5	300529	BioLegend
CD8a	BV510	301047	BioLegend
CD15	BV605	323031	BioLegend
CD19	FITC	302205	BioLegend
CD25	Spark Red 718	356157	BioLegend
CD25	APC	302610	BioLegend
CD25	PE/Cy7	356107	BioLegend
CD25	BV605	302631	BioLegend
CD27	Alexa Fluor 700	356415	BioLegend
CD45	BV510	304035	BioLegend
CD45RA	BV605	304133	BioLegend
CD56	FITC	318303	BioLegend
CD57	PE	359611	BioLegend
CD69	PE/Dazzle 594	310941	BioLegend
CD86	PE	371205	BioLegend
CD86	APC	374207	BioLegend

CD134	FITC	350006	BioLegend
CD163	BV421	333611	BioLegend
CD206	PE/Cy5	321108	BioLegend
HLA-DR	BV785	307641	BioLegend
PD-1	BUV737	612792	BD Horizon
PD-1	BV421	329919	BioLegend
TIGIT	BV785	372735	BioLegend
LAG-3	BV510	369317	BioLegend
ICOS	BV711	313547	BioLegend
Intracellular staining			
T-bet	Alexa Fluor 647	644803	BioLegend
GATA3	Alexa Fluor 488	653807	BioLegend
RORγt	PE	12-6988-82	Invitrogen
FOXP3	BV421	320123	BioLegend
FOXP3	PE	12-4776-42	Invitrogen
FOXP3	APC	17-4776-42	Invitrogen
IFN-γ	BV510	502544	BioLegend
IFN-γ	BV785	502541	BioLegend
IL-4	BV605	500827	BioLegend
IL-17A	BV711	512328	BioLegend
IL-17A	BV421	512322	BioLegend
IL-17A	PE/Cy7	512315	BioLegend
IL-22	APC	17-7222-82	Invitrogen
IL-22	PerCP/Cy5.5	366709	BioLegend
CD68	PE/Cy7	333815	BioLegend



Chapter 5

Summary

GENERAL SUMMARY

CD4⁺ naive T cells can differentiate into functionally distinct helper T cell subsets Th1, Th2, Th9, Th17, T follicular helper, and regulatory T cells (Treg), which together form a major effector part of adaptive immunity. Each subset is conventionally defined by a characteristic transcription factor and cytokine output, and each performs a specific role in host defence, immune tolerance, or inflammatory pathology. Th17 cells, defined by RORγt expression and IL-17A and IL-17F production, are essential for protection against extracellular bacteria and fungi at mucosal surfaces but are also involved in the pathogenesis of autoimmune and chronic inflammatory diseases including rheumatoid arthritis, inflammatory bowel disease, and multiple sclerosis. Th17 cells are considered highly plastic and can shift between pathogenic and regulatory states depending on environmental signals. Findings from murine models often fail to translate directly to human systems, and this gap motivated the development of a defined human *in vitro* Th17 differentiation system as the foundation for the work in this thesis.

In **Chapter 2**, we established a human *in vitro* Th17 differentiation model from naive CD4⁺ T cells of healthy donors using defined, serum-free and xeno-free conditions, and combined it with single-cell RNA sequencing to examine how TGF-β concentration, extracellular lactate, and hypoxia shape Th17 transcriptional identity. TGF-β acted as a graded regulator: low concentrations supported Th17 differentiation, while high concentrations suppressed it, likely through SMAD-pathway feedback genes including *PMEPA1* and *SKIL*, accompanied by reduced expression of inflammatory transcripts such as CSF2. Extracellular lactate at concentrations mimicking the inflamed tissue environment reduced Th17 frequency without affecting proliferation and induced coordinated metabolic changes including upregulation of *MCT1*, *LDHA*, *LDHB* and JAK-STAT changes, including upregulation of, *SOCS3*, *STAT3*, and *CD36*. Hypoxia stabilized HIF-1α and induced a canonical glycolytic gene program but, surprisingly, did not significantly alter Th17 frequency. VEGFA was induced only when TGF-β and hypoxia were present together, with neither signal sufficient alone. STAT3 transcript increased under lactate and, independently, under combined TGF-β and hypoxia, marking it as a transcriptional convergence point for cytokine, metabolic, and oxygen-sensing signals. Th17 differentiation efficiency varied between donors and conditions, reflecting the limited mechanistic understanding of human Th17 induction *in vitro* and consistent with the absence of a standardized protocol in the field. Together, TGF-β concentrations, lactate, and hypoxia shape the human Th17 transcriptional landscape, with potential relevance to chronically inflamed and tumor-associated tissue where these signals co-occur and STAT3 sustains pathogenic Th17 activity.

Chapter 3 examined the role of mitochondrial activity in human Th17 differentiation. Using single-cell metabolic profiling and functional assays, we found that Th17 cells held a

hyperpolarized mitochondrial membrane potential (ΔΨ) relative to non-Th17 cells, and that hyperpolarized cells showed greater metabolic activity. Sorting cells by ΔΨ confirmed a link to differentiation: ΔΨ-high cells gave higher Th17 frequencies after culture than ΔΨ-low cells, showing that cells with high mitochondrial membrane potential are more likely to become Th17. Metabolic profiling at 48 hours revealed early reliance on glycolysis followed by a shift toward oxidative phosphorylation by 96 hours, with early upregulation of the mitochondrial transcription regulator TEFM and later downregulation of the fission and fusion regulators DRP1 and MFN2. Functionally, ΔΨ-high cells expressed elevated activation markers (CD69, CD25) alongside increased exhaustion markers (TIGIT, PD-1), and produced lower levels of effector molecules including IFN-γ and granzyme B than ΔΨ-low (less polarized) cells. Mitochondrial activity therefore tracks Th17 differentiation, and a high metabolic state is coupled to a greater tendency toward exhaustion and reduced effector output, identifying mitochondrial regulation as a potential therapeutic target in Th17-driven autoimmune disease.

Chapter 4 brought T cell phenotype analysis into a clinical context of osteoarthritis (OA), which has traditionally been considered a mechanical, wear-and-tear disease of cartilage with the adaptive immune compartment considered a marginal contributor. Synovial tissue obtained at total knee arthroplasty from aging patients with end-stage osteoarthritis was analysed using multiparameter flow cytometry and immunofluorescence imaging and showed clear presence of T cells. Rather than the exhausted phenotype expected after years of chronic disease, synovial T cells retained an activated, non-exhausted state, with preserved cytokine production, central memory T cell-like differentiation, and non-classical IFN-γ^+ Th17 populations, consistent with cells that remain responsive to restimulation. These findings challenge the assumption that adaptive immune cells in OA are functionally inert and raise the possibility that synovial T cells continue to contribute to inflammation and to clinical symptoms, including post-surgical pain and persistent low-grade inflammation after total knee arthroplasty.

Taken together, the three chapters describe a Th17 differentiation that is dynamically shaped by cytokines, oxygen, extracellular metabolic cues, mitochondrial activity, and the local tissue environment. T cell differentiation is flexible and plastic rather than strictly fixed. Targeting these signals in combination rather than individually may offer more effective therapeutic strategies for chronically inflamed tissue, where multiple stresses drive continuous pathogenic T cell formation and activity.



Chapter 6

General Discussion

GENERAL DISCUSSION

Th17 cell identity is shaped by the integration of cytokine, metabolic, and tissue signals

The classical framework of $CD4^+$ T helper differentiation treated lineages as stable and irreversible, each defined by a master transcription factor and signature cytokine. Accumulating evidence suggests otherwise, particularly for Th17 and Treg cells, whose transcriptional programs overlap and whose function shifts with context[234]. Th17 cells are functionally and metabolically heterogeneous, and shift toward IFN-γ-producing pathogenic or IL-10-producing regulatory states depending on cytokine, metabolic, and tissue signals[235]. The work in this thesis examines how environmental signals shape Th17 differentiation across three contexts: the cytokine and microenvironmental inputs that govern human Th17 differentiation *in vitro* **(Chapter 2)**, the mitochondrial mechanisms that sustain Th17 formation and function **(Chapter 3),** and the behavior of T cells within inflamed synovial tissue **(Chapter 4)**. Across these studies, human Th17 biology is shaped by the integration of multiple signals rather than by any single cue.

STAT3 integrates microenvironmental signals and converges on angiogenic output

The main insight from Chapter 2 is that human Th17 differentiation integrates multiple microenvironmental inputs, with STAT3 emerging as an intersection point. STAT3 transcript was upregulated under both lactate exposure and combined hypoxia plus TGF-β, indicating that metabolic and oxygen-sensing inputs add to the cytokine signal that drives STAT3 instead of IL-6 alone. At protein level, TCR engagement drives STAT3 phosphorylation and acts synergistically with IL-6/IL-23 to reach maximal STAT3 activity, while neither signal alone is sufficient [236]. Our data suggest the same logic extends across metabolic and oxygen-sensing inputs, at the transcript level.

In other cell types, STAT3 binds the VEGFA promoter, interacts with HIF-1α at hypoxia response elements, stabilizes HIF-1α protein[237, 238], and cooperates with SMAD3 at TGF-β -responsive promoters. These properties make STAT3 a strong candidate integrator of the metabolic, oxygen, and cytokine inputs that converge on VEGFA, which would explain why VEGFA induction requires both TGF-β and hypoxia together. Because the present evidence is at the transcript level, the direct test would begin with confirming STAT3 activation at the protein level (pSTAT3) under each condition, and then asking whether reducing STAT3 removes the combined-condition VEGFA induction without simply blocking Th17 formation.

STAT3 is already targeted indirectly through IL-6/IL-6R blockade with tocilizumab and through JAK inhibitors including tofacitinib, baricitinib, and upadacitinib [239, 240], but responses in rheumatoid arthritis and IBD remain partial, with American College of Rheumatology 50%

response (ACR50) rates for tofacitinib monotherapy of about 30–40% [241]. Two recent observations are relevant. First, a transcriptomic re-analysis showed that tofacitinib acts more strongly on Th1 cells than on IL-17-producing Th17 cells, and ulcerative colitis patients with more IL-17A$^+$ mononuclear cells in their colonic biopsies responded less well [242]. Second, in refractory myasthenia gravis tofacitinib did engage the JAK–STAT3–Th17 axis, lowering pSTAT3, IL-6, and IL-23 and suppressing pathogenic Th17.1 cells [243]. Our Chapter 2 data suggest one reason for this context-dependence: STAT3 was induced transcriptionally not only by cytokine signaling but, independently, by lactate and by combined TGF-β and hypoxia, conditions that occur together in inflamed mucosa and rheumatoid synovium. If these microenvironmental inputs activate STAT3 in parallel with IL-6, JAK blockade alone may not reach them. A direct test would be to measure pSTAT3 in our Th17 cultures under combined TGF-β, hypoxia, and / or lactate, with and without tofacitinib, and ask whether tofacitinib blocks STAT3 phosphorylation under microenvironmental input as efficiently as under IL-6 alone.

The TGF-β–hypoxia–STAT3–VEGFA axis offers a mechanism for the persistence of inflammation. HIF-1α and SMAD3 cooperate at the VEGFA promoter to drive angiogenesis, and the resulting neovasculature sustains tissue oxygenation, nutrient delivery, and immune cell recruitment that maintain the inflammatory environment. This loop may contribute to the persistent inflammation and partial therapeutic response seen in the rheumatoid synovium and the inflammatory bowel mucosa, where vascular remodeling and immune activation reinforce each other. Across the three chapters, Th17 and Treg programs respond as a tunable axis rather than as fixed lineages, integrating cytokine signaling, oxygen tension, metabolite availability, mitochondrial state, and tissue context. The same axis is skewed toward Th17 in autoimmune tissue and toward Treg in the tumor microenvironment[244], with distinct downstream effects on local inflammation and angiogenesis.

Mitochondrial structure and dynamics in Th17 differentiation

Chapter 3 linked mitochondrial activity to Th17 differentiation and effector function. Mitochondrial structure, however, was not directly examined. Th17 cells maintain fused mitochondria with tight cristae, and the OPA1–LKB1 axis couples membrane dynamics to IL-17 output: fused networks favor oxidative metabolism and memory programs while fragmented networks favor glycolysis and effector specialization[68, 180]. This frames our early DRP1 and MFN2 changes as part of a structural transition rather than as incidental gene-expression shifts. Electron microscopy and high-resolution live cell fluorescence imaging would allow direct quantification of mitochondrial mass, network architecture, and respiratory capacity in differentiating Th17 cells. Such measurements would clarify whether specific structural configurations underlie Th17 effector function, whether these configurations can be manipulated to bias differentiation outcome, and whether mitochondrial mass differs systematically

between Th17 and Treg lineages. The dependence we observed on a glycolysis-to-oxidative-phosphorylation shift by 96 hours parallels the finding that ATP-linked respiration is required for Th17 specification and that its inhibition diverts cells toward Foxp3$^+$ Treg fate[84]. Our data fit the Th17-promoting side of this, with the shift toward OXPHOS-tracking differentiation, and raise the question of what sets that mitochondrial state.

One possibility relates Chapter 3 back to the STAT3 framework of Chapter 2 through a non-canonical function of STAT3. STAT3 controls mitochondrial membrane potential in Th17 cells, the same parameter measured in Chapter 3: deletion of STAT3 in effector Th17 cells lowers $\Delta\Psi$ and impairs antigen-driven cytokine production through a non-transcriptional route [245]. Beyond its canonical nuclear role, a fraction of STAT3 phosphorylated at Ser727 localizes to mitochondria, where it directly enhances electron transport chain complex I and complex II activity and supports oxidative phosphorylation [246, 247]. Mitochondrial STAT3 has also been reported to restrain inflammation in the rheumatoid joint by regulating autophagy and inflammatory cell death in Th17 cells and synovial fibroblasts [248], linking the STAT3, mitochondrial, and synovial themes of this thesis in a single (disease) context.

If STAT3 operates simultaneously in the nucleus, driving the transcriptional convergence described in Chapter 2, and in the mitochondria, regulating the bioenergetic state described in Chapter 3, pharmacological STAT3 inhibition would target both axes at once. A more direct next step follows from Chapter 2: measuring pSTAT3 in our cultures under combined TGF-β, hypoxia, and/or lactate, with and without tofacitinib, would show whether tofacitinib blocks STAT3 activation by these microenvironmental signals as well as by IL-6.

Vigilant T cells in end-stage osteoarthritis and post-surgical inflammation

Limited clinical metadata constrained the interpretation of Chapter 4. Variables such as body mass index, abdominal circumference, muscle composition, fasting glucose, and lifestyle factors were not consistently captured, which makes it impossible to determine whether the vigilant T cell phenotype reflects local microenvironmental conditions, systemic metabolic dysregulation, or both. Obesity is strongly associated with OA, and obesity in particular has been linked to enhanced Th17 responses to maintain a basal inflammatory state[249], and integrating detailed clinical and metabolic phenotyping with single-cell immune profiling in future cohorts would test whether systemic metabolic state predicts synovial T cell activation. In our cohort, T cell abundance varied substantially across donors, and the cells appeared either as scattered single cells or as small clustered aggregates within the synovial tissue. Correlating these patterns with patient characteristics such as age, sex, body mass index, disease duration, pre-surgical medication, and comorbid metabolic conditions could identify the clinical factors that drive synovial T cell organization in OA.

Lymphocyte clusters indicate sites of active antigen recognition in chronically inflamed tissue. Lymphocyte clusters are a recognized hallmark of local antigen presentation and clonal expansion in chronic inflammation, and in some disease contexts they organize into tertiary lymphoid structures that support sustained immune activation within the tissue[250]. T cell receptor sequencing combined with single-cell transcriptional analysis would establish whether the clusters in OA synovium represent antigen-driven expansions and whether specific clones preferentially adopt inflammatory or regulatory phenotypes. The microenvironmental conditions that drive STAT3 convergence in our *in vitro* Th17 model are also present in the OA synovium. Synovial fluid in osteoarthritic joints is hypoxic, with measured oxygen tensions well below systemic levels [251], and elevated TGF-β has been documented in OA synovial fluid and cartilage and contributes to subchondral bone remodeling and synovial fibrosis [221]. Continuous STAT3 activation has been reported in OA synovial tissue and in chondrocytes, where it has been linked to cartilage degradation and inflammatory cytokine production[252]. The inflammatory and hypoxic OA synovial environment, together with local TGF-β and STAT3 activity, supports examining whether OA synovium derived T cells acquire the molecular phenotype observed *in vitro*.

Chapter 4 established that synovial T cells in osteoarthritis are vigilant: activated but not exhausted. Whether they retain effector responsiveness would determine whether they actively contribute to continued inflammation in the joint after surgery or remain phenotypically poised without engaging. Testing whether these cells can be functionally reactivated, and what cytokines they produce with stimulation, would address this directly. Before that we need to confirm whether the central memory-like T cells in OA synovium are tissue-resident memory T cells (TRM), defined by $CD69^{+}CD103^{+}$ co-expression, or circulating central memory T cells temporarily passing through the tissue[253, 254]. TRM cells can be reactivated locally without further T cell influx from circulation, and are well-positioned to respond rapidly to local triggers, a property that determines whether the cells we observed could plausibly drive post-surgical inflammation. Magnetic isolation of synovial $CD3^{+}$ T cells followed by anti-CD3/CD28 stimulation would directly test their reactivation potential and the cytokines they produce, with particular interest in GM-CSF and IL-1β, both of which drive macrophage activation and could initiate a feed-forward inflammatory loop within the post-surgical joint.

Most osteoarthritis research focuses on the mechanisms of early disease, while the drivers of inflammation, pain, and stiffness that persist after total knee arthroplasty remain poorly understood. Surgical trauma releases damage associated molecular patterns that activate innate immunity, altered biomechanics following implant placement create new mechanical stress on the residual synovium, and wear debris from prosthesis materials can sustain chronic immune activation [255, 256]. How vigilant synovial T cells respond to these post-surgical signals has not been studied. The term "end-stage" osteoarthritis describes the moment at which tissue

becomes accessible through joint replacement surgery, not the end of the patient's disease experience: patients live with their prosthetic joint for 15 to 25 years on average[257], and persistent symptoms, especially pain, during this period substantially affect quality of life [258]. If vigilant synovium T cells contribute to post-surgical inflammation through cytokines such as GM-CSF and IL-1β, identifying and modulating their reactivation could become a relevant therapeutic target for the subset of patients with persistent post-TKA symptoms [259].

Donor variability and the limits of human *in vitro* models

Th17 differentiation efficiency varied substantially across donors. This variation appeared with all three differentiation cocktails tested, consistent with the well-recognized donor-to-donor variability that has prevented a single standardized human Th17 protocol from being established in the field. The Single-cell sequencing dataset in Chapter 2 was generated from donor-pooled libraries. Pooling has clear advantages: it stabilizes the averaged transcriptional signal, increases cell numbers for detecting rare transcriptional states such as the Treg-like cluster, and reduces the cost of individual library preparation. A limitation of this approach is the lack of donor-specific resolution, the patterns observed in our pooled data may reflect a dominant response from one donor rather than a generalizable feature of human Th17 biology. However, computational tools now assign pooled cells back to individual donors using the natural single-nucleotide polymorphisms (SNPs) that differ between people, recovering donor identity from a pooled library without separate sample barcoding [260]. Of note we have used such an approach to evaluate the data in Chapter 2 and no sample was dominated by a single donor. Notably, donor-specific single-cell sequencing in larger cohorts may identify donor characteristics, including baseline metabolic status, prior immune activation history, and the ratio of naive to memory $CD4^+$ T cells at the start of culture, that predict responsiveness to TGF-β, lactate, or hypoxia. This is particularly relevant *in vitro*: donors with substantial prior immune exposure have a smaller and less diverse naive $CD4^+$ T cell pool with reduced proliferative and differentiation capacity [96, 261], which could itself account for part of the donor variability observed in this thesis.

Isolating viable differentiated human Th17 cells remains technically difficult. *In vivo* Th17 numbers are low, requiring large blood volumes for adequate cell numbers, which makes *in vitro* culture an attractive source, but reliable isolation with preserved viability is the bottleneck. Surface marker combinations and cytokine capture assays each carry methodological limitations: prolonged *in vitro* activation alters the expression of canonical surface markers and reduces their specificity for Th17 cells; IL-17A cytokine capture assays require additional PMA/ionomycin stimulation to induce detectable cytokine secretion, which itself perturbs cell state; and intracellular staining for lineage-defining transcription factors such as RORγt requires

fixation and permeabilization, preventing recovery of viable cells for downstream functional or transcriptional analysis.

In blood, $CCR4^+CCR6^+CXCR3^-$ identifies functional Th17 cells but when we applied this combination to in-vitro-cultured cells [262], this did not result in a relatively pure Th17 cell population, and alternatively, a commercial IL-17 secretion-capture kit also did not yield a usable population. These attempts are not part of this thesis, but they show that markers validated *ex vivo* do not transfer *to in vitro* culture, and that a method integrating surface, transcriptional, and functional readouts in viable cells is needed to define and isolate functional Th17 subsets reliably. One direct application would be to isolate naive $CD4^+$ T cells from healthy donors and from patients with chronic inflammatory disease, differentiate both under our standardized polarizing conditions, and compare the resulting Th17 frequency, marker profile, transcriptional signature, and effector cytokine output. This design will clarify whether discrepancies between healthy and diseased populations originate in the naive starting material or emerge during differentiation under identical conditions, directly testing whether the microenvironmental integration described in Chapter 2 operates differently in disease.

This experimental framework also addresses an interesting question relevant to the Th17/Treg balance: whether the imbalance observed in chronic inflammatory disease arises primarily from microenvironmental cues that bias naive $CD4^+$ T cell fate toward Th17 over Treg, or from intrinsic alterations in the naive T cell pool itself that pre-dispose differentiation outcomes [263]. The two possibilities are not mutually exclusive, and the experimental design proposed here would directly distinguish their relative contribution. Furthermore, we did not measure metabolic parameters at day 0, before activation, and including this in future work would clarify whether intrinsic metabolic priming of the naive pool predicts subsequent Th17 differentiation. Naive T cells are maintained in a quiescent state with low glycolysis and predominant oxidative phosphorylation, and exit from this state upon activation is a regulated transition that shapes downstream effector identity [264, 265]. Donor variation in baseline naive T cell metabolic state may therefore contribute to the variation in Th17 differentiation efficiency observed in this thesis.

This thesis shows that human Th17 differentiation depends on several microenvironmental signals acting at the same time, including cytokines, oxygen, and metabolic cues. $\Delta\Psi$-high cells became Th17 more readily than $\Delta\Psi$-low cells, which suggests that the metabolic state of a cell predicts its fate rather than only reflecting its activation.

This thesis also draws attention to the dynamic balance between Th17 and Treg cells. The two fates are closely linked: they share a requirement for TGF-β, and in our cultures RORγt and Foxp3 were co-expressed in some single cells. High TGF-β together with IL-2 favors Foxp3 and

Treg over Th17[29], which may contribute to the lower Th17 and higher Treg obtained *in vitro*. *In vitro* induced Treg, however, differ substantially from natural human Treg in their stability and gene expression[266], so fates assigned in culture do not fully match Treg isolated from blood, and the Th17/Treg balance is better studied under chronic inflammatory conditions where it matters most: in autoimmune disease and cancer. Because high yield Th17 differentiation is difficult to achieve *in vitro*, the system in which both fates appear together is more useful as a model of this balance than as a route to pure Th17 cells. Single-cell level methods make this practical: in a mixed cultured population, the inputs, cell–cell interactions, and outputs can be measured at the level of individual cells, so the balance can be studied and viewed as a dynamic whole rather than reconstructed from isolated populations.

In our cultures, combined TGF-β and hypoxia induced VEGFA in human Th17 cells. VEGFA promotes angiogenesis, which is prominent in both tumors and the rheumatoid synovium and is driven there by the same hypoxia, lactate, and TGF-β [267]. If Th17 cells are a source of VEGFA in these tissues, the same signals that shift the Th17/Treg balance would also act on the local vasculature, with STAT3 as the likely link to VEGFA. Whether targeting this node affects both the inflammatory balance and angiogenesis remains to be tested, but it would be relevant to chronic inflammatory disease and cancer.

REFERENCES

1. Janeway, C.A., Jr., *How the immune system works to protect the host from infection: a personal view.* Proc Natl Acad Sci U S A, 2001. **98**(13): p. 7461–8.
2. Kawai, T. and S. Akira, *The role of pattern-recognition receptors in innate immunity: update on Toll-like receptors.* Nat Immunol, 2010. **11**(5): p. 373–84.
3. Janeway, C.A., Jr. and R. Medzhitov, *Innate immune recognition.* Annu Rev Immunol, 2002. **20**: p. 197–216.
4. Taylor, P.R., et al., *Macrophage receptors and immune recognition.* Annu Rev Immunol, 2005. **23**: p. 901–44.
5. Netea, M.G., et al., *Trained immunity: A program of innate immune memory in health and disease.* Science, 2016. **352**(6284): p. aaf1098.
6. Wang, R., et al., *The interaction of innate immune and adaptive immune system.* MedComm (2020), 2024. **5**(10): p. e714.
7. Chi, H., M. Pepper, and P.G. Thomas, *Principles and therapeutic applications of adaptive immunity.* Cell, 2024. **187**(9): p. 2052–2078.
8. Dempsey, P.W., S.A. Vaidya, and G. Cheng, *The art of war: Innate and adaptive immune responses.* Cell Mol Life Sci, 2003. **60**(12): p. 2604–21.
9. Sallusto, F. and A. Lanzavecchia, *The instructive role of dendritic cells on T-cell responses.* Arthritis Res, 2002. **4 Suppl 3**(Suppl 3): p. S127–32.
10. Sun, L., et al., *T cells in health and disease.* Signal Transduct Target Ther, 2023. **8**(1): p. 235.
11. Eisenbarth, S.C., *Dendritic cell subsets in T cell programming: location dictates function.* Nat Rev Immunol, 2019. **19**(2): p. 89–103.
12. Carroll, S.L., C. Pasare, and G.M. Barton, *Control of adaptive immunity by pattern recognition receptors.* Immunity, 2024. **57**(4): p. 632–648.
13. Maloy, K.J. and F. Powrie, *Intestinal homeostasis and its breakdown in inflammatory bowel disease.* Nature, 2011. **474**(7351): p. 298–306.
14. Zhu, J., H. Yamane, and W.E. Paul, *Differentiation of effector CD4 T cell populations (*).* Annu Rev Immunol, 2010. **28**: p. 445–89.
15. Davidson, A. and B. Diamond, *Autoimmune diseases.* N Engl J Med, 2001. **345**(5): p. 340–50.
16. O'Shea, J.J. and W.E. Paul, *Mechanisms underlying lineage commitment and plasticity of helper CD4+ T cells.* Science, 2010. **327**(5969): p. 1098–102.
17. Luckheeram, R.V., et al., *CD4+T cells: differentiation and functions.* Clin Dev Immunol, 2012. **2012**: p. 925135.
18. Lee, G.R., *The Balance of Th17 versus Treg Cells in Autoimmunity.* International Journal of Molecular Sciences, 2018. **19**(3).
19. Eisenstein, E.M. and C.B. Williams, *The T(reg)/Th17 cell balance: a new paradigm for autoimmunity.* Pediatr Res, 2009. **65**(5 Pt 2): p. 26r–31r.
20. Josefowicz, S.Z., L.F. Lu, and A.Y. Rudensky, *Regulatory T cells: mechanisms of differentiation and function.* Annu Rev Immunol, 2012. **30**: p. 531–64.
21. Sakaguchi, S., et al., *Regulatory T cells and immune tolerance.* Cell, 2008. **133**(5): p. 775–87.
22. Korn, T., et al., *IL-17 and Th17 Cells.* Annu Rev Immunol, 2009. **27**: p. 485–517.
23. Gaffen, S.L., et al., *The IL-23-IL-17 immune axis: from mechanisms to therapeutic testing.* Nat Rev Immunol, 2014. **14**(9): p. 585–600.
24. Janeway, C.A., Jr., *How the immune system protects the host from infection.* Microbes Infect, 2001. **3**(13): p. 1167–71.
25. Alunno, A., et al., *Altered immunoregulation in rheumatoid arthritis: the role of regulatory T cells and proinflammatory Th17 cells and therapeutic implications.* Mediators Inflamm, 2015. **2015**: p. 751793.
26. Mease, P.J., et al., *Secukinumab Inhibition of Interleukin-17A in Patients with Psoriatic Arthritis.* N Engl J Med, 2015. **373**(14): p. 1329–39.
27. Baeten, D., et al., *Secukinumab, an Interleukin-17A Inhibitor, in Ankylosing Spondylitis.* N Engl J Med, 2015. **373**(26): p. 2534–48.
28. Bettelli, E., et al., *Reciprocal developmental pathways for the generation of pathogenic effector TH17 and regulatory T cells.* Nature, 2006. **441**(7090): p. 235–8.

29. Zhou, L., et al., *TGF-beta-induced Foxp3 inhibits T(H)17 cell differentiation by antagonizing RORgammat function.* Nature, 2008. **453**(7192): p. 236–40.
30. Ueno, A., et al., *Th17 plasticity and its changes associated with inflammatory bowel disease.* World J Gastroenterol, 2015. **21**(43): p. 12283–95.
31. Muranski, P. and N.P. Restifo, *Essentials of Th17 cell commitment and plasticity.* Blood, 2013. **121**(13): p. 2402–14.
32. Ivanov, II, et al., *The orphan nuclear receptor RORgammat directs the differentiation program of proinflammatory IL-17+ T helper cells.* Cell, 2006. **126**(6): p. 1121–33.
33. Manel, N., D. Unutmaz, and D.R. Littman, *The differentiation of human T(H)-17 cells requires transforming growth factor-beta and induction of the nuclear receptor RORgammat.* Nat Immunol, 2008. **9**(6): p. 641–9.
34. Dong, C., *TH17 cells in development: an updated view of their molecular identity and genetic programming.* Nat Rev Immunol, 2008. **8**(5): p. 337–48.
35. Zielinski, C.E., et al., *Pathogen-induced human TH17 cells produce IFN-γ or IL-10 and are regulated by IL-1β.* Nature, 2012. **484**(7395): p. 514–8.
36. Stadhouders, R., E. Lubberts, and R.W. Hendriks, *A cellular and molecular view of T helper 17 cell plasticity in autoimmunity.* Journal of Autoimmunity, 2018. **87**: p. 1–15.
37. Ye, J., R.S. Livergood, and G. Peng, *The role and regulation of human Th17 cells in tumor immunity.* Am J Pathol, 2013. **182**(1): p. 10–20.
38. Huber, S., et al., *Th17 cells express interleukin-10 receptor and are controlled by Foxp3⁻ and Foxp3+ regulatory CD4+ T cells in an interleukin-10-dependent manner.* Immunity, 2011. **34**(4): p. 554–65.
39. Cui, H., et al., *The dynamic shifts of IL-10-producing Th17 and IL-17-producing Treg in health and disease: a crosstalk between ancient "Yin-Yang" theory and modern immunology.* Cell Commun Signal, 2024. **22**(1): p. 99.
40. Tartar, D.M., et al., *FoxP3+RORgammat+ T helper intermediates display suppressive function against autoimmune diabetes.* J Immunol, 2010. **184**(7): p. 3377–85.
41. Fu, S.H., et al., *Interplay between Cytokine Circuitry and Transcriptional Regulation Shaping Helper T Cell Pathogenicity and Plasticity in Inflammatory Bowel Disease.* Int J Mol Sci, 2020. **21**(9).
42. Guéry, L. and S. Hugues, *Th17 Cell Plasticity and Functions in Cancer Immunity.* Biomed Res Int, 2015. **2015**: p. 314620.
43. Weaver, C.T., et al., *Th17: an effector CD4 T cell lineage with regulatory T cell ties.* Immunity, 2006. **24**(6): p. 677–688.
44. Smith-Garvin, J.E., G.A. Koretzky, and M.S. Jordan, *T cell activation.* Annu Rev Immunol, 2009. **27**: p. 591–619.
45. Lenschow, D.J., T.L. Walunas, and J.A. Bluestone, *CD28/B7 system of T cell costimulation.* Annu Rev Immunol, 1996. **14**: p. 233–58.
46. Sharpe, A.H. and G.J. Freeman, *The B7-CD28 superfamily.* Nat Rev Immunol, 2002. **2**(2): p. 116–26.
47. Veldhoen, M., et al., *TGFbeta in the context of an inflammatory cytokine milieu supports de novo differentiation of IL-17-producing T cells.* Immunity, 2006. **24**(2): p. 179–89.
48. Harbour, S.N., et al., *T(H)17 cells require ongoing classic IL-6 receptor signaling to retain transcriptional and functional identity.* Sci Immunol, 2020. **5**(49).
49. Nishihara, M., et al., *IL-6-gp130-STAT3 in T cells directs the development of IL-17+ Th with a minimum effect on that of Treg in the steady state.* Int Immunol, 2007. **19**(6): p. 695–702.
50. Langrish, C.L., et al., *IL-23 drives a pathogenic T cell population that induces autoimmune inflammation.* J Exp Med, 2005. **201**(2): p. 233–40.
51. Chung, Y., et al., *Critical regulation of early Th17 cell differentiation by interleukin-1 signaling.* Immunity, 2009. **30**(4): p. 576–87.
52. McGeachy, M.J., et al., *The interleukin 23 receptor is essential for the terminal differentiation of interleukin 17-producing effector T helper cells in vivo.* Nat Immunol, 2009. **10**(3): p. 314–24.
53. Mus, A.M., et al., *Interleukin-23 promotes Th17 differentiation by inhibiting T-bet and FoxP3 and is required for elevation of interleukin-22, but not interleukin-21, in autoimmune experimental arthritis.* Arthritis Rheum, 2010. **62**(4): p. 1043–50.
54. Laurence, A., et al., *Interleukin-2 signaling via STAT5 constrains T helper 17 cell generation.* Immunity, 2007. **26**(3): p. 371–81.
55. Zhu, J. and W.E. Paul, *Heterogeneity and plasticity of T helper cells.* Cell Res, 2010. **20**(1): p. 4–12.
56. Wang, Z., et al., *Metabolic regulation of Th17 and Treg cell balance by the mTOR signaling.* Metabol Open, 2025. **26**: p. 100369.

57. Shi, L.Z., et al., *HIF1alpha-dependent glycolytic pathway orchestrates a metabolic checkpoint for the differentiation of TH17 and Treg cells.* J Exp Med, 2011. **208**(7): p. 1367–76.
58. Zhang, D., et al., *High Glucose Intake Exacerbates Autoimmunity through Reactive-Oxygen-Species-Mediated TGF-β Cytokine Activation.* Immunity, 2019. **51**(4): p. 671–681.e5.
59. Hochrein, S.M., et al., *The glucose transporter GLUT3 controls T helper 17 cell responses through glycolytic-epigenetic reprogramming.* Cell Metab, 2022. **34**(4): p. 516–532.e11.
60. Lopez Krol, A., et al., *Lactate induces metabolic and epigenetic reprogramming of pro-inflammatory Th17 cells.* EMBO Rep, 2022. **23**(12): p. e54685.
61. Fan, W., et al., *Global lactylome reveals lactylation-dependent mechanisms underlying T(H)17 differentiation in experimental autoimmune uveitis.* Sci Adv, 2023. **9**(42): p. eadh4655.
62. Wu, L., et al., *Niche-Selective Inhibition of Pathogenic Th17 Cells by Targeting Metabolic Redundancy.* Cell, 2020. **182**(3): p. 641–654.e20.
63. McNamee, E.N., et al., *Hypoxia and hypoxia-inducible factors as regulators of T cell development, differentiation, and function.* Immunol Res, 2013. **55**(1-3): p. 58–70.
64. Ikejiri, A., et al., *Dynamic regulation of Th17 differentiation by oxygen concentrations.* Int Immunol, 2012. **24**(3): p. 137–46.
65. Wilfahrt, D. and G.M. Delgoffe, *Metabolic waypoints during T cell differentiation.* Nat Immunol, 2024. **25**(2): p. 206–217.
66. Macintyre, A.N., et al., *The glucose transporter Glut1 is selectively essential for CD4 T cell activation and effector function.* Cell Metab, 2014. **20**(1): p. 61–72.
67. Yang, Z., et al., *T-cell metabolism in autoimmune disease.* Arthritis Res Ther, 2015. **17**(1): p. 29.
68. Baixauli, F., et al., *An LKB1-mitochondria axis controls T(H)17 effector function.* Nature, 2022. **610**(7932): p. 555–561.
69. Cluxton, D., et al., *Differential Regulation of Human Treg and Th17 Cells by Fatty Acid Synthesis and Glycolysis.* Front Immunol, 2019. **10**: p. 115.
70. Qin, Y., C. Gao, and J. Luo, *Metabolism Characteristics of Th17 and Regulatory T Cells in Autoimmune Diseases.* Front Immunol, 2022. **13**: p. 828191.
71. Zhou, X., X. Zhu, and H. Zeng, *Fatty acid metabolism in adaptive immunity.* Febs j, 2023. **290**(3): p. 584–599.
72. Ma, S., et al., *Cellular metabolism regulates the differentiation and function of T-cell subsets.* Cell Mol Immunol, 2024. **21**(5): p. 419–435.
73. Johnson, M.O., et al., *Distinct Regulation of Th17 and Th1 Cell Differentiation by Glutaminase-Dependent Metabolism.* Cell, 2018. **175**(7): p. 1780–1795.e19.
74. Nakaya, M., et al., *Inflammatory T cell responses rely on amino acid transporter ASCT2 facilitation of glutamine uptake and mTORC1 kinase activation.* Immunity, 2014. **40**(5): p. 692–705.
75. Wang, P., et al., *The Regulatory Effects of mTOR Complexes in the Differentiation and Function of CD4(+) T Cell Subsets.* J Immunol Res, 2020. **2020**: p. 3406032.
76. Delgoffe, G.M., et al., *The kinase mTOR regulates the differentiation of helper T cells through the selective activation of signaling by mTORC1 and mTORC2.* Nat Immunol, 2011. **12**(4): p. 295–303.
77. Wei, J., et al., *Nutrient and Metabolic Sensing in T Cell Responses.* Front Immunol, 2017. **8**: p. 247.
78. Luo, Y., et al., *Mesenchymal Stem Cell Protects Injured Renal Tubular Epithelial Cells by Regulating mTOR-Mediated Th17/Treg Axis.* Front Immunol, 2021. **12**: p. 684197.
79. Dang, E.V., et al., *Control of T(H)17/T(reg) balance by hypoxia-inducible factor 1.* Cell, 2011. **146**(5): p. 772–84.
80. Chen, H. and D.C. Chan, *Mitochondrial dynamics--fusion, fission, movement, and mitophagy--in neurodegenerative diseases.* Hum Mol Genet, 2009. **18**(R2): p. R169–76.
81. Sena, L.A., et al., *Mitochondria are required for antigen-specific T cell activation through reactive oxygen species signaling.* Immunity, 2013. **38**(2): p. 225–36.
82. Martínez-Reyes, I. and N.S. Chandel, *Mitochondrial TCA cycle metabolites control physiology and disease.* Nat Commun, 2020. **11**(1): p. 102.
83. Xie, J.H., Y.Y. Li, and J. Jin, *The essential functions of mitochondrial dynamics in immune cells.* Cell Mol Immunol, 2020. **17**(7): p. 712–721.
84. Shin, B., et al., *Mitochondrial Oxidative Phosphorylation Regulates the Fate Decision between Pathogenic Th17 and Regulatory T Cells.* Cell Rep, 2020. **30**(6): p. 1898–1909.e4.

85. Phan, A.T. and A.W. Goldrath, *Hypoxia-inducible factors regulate T cell metabolism and function.* Mol Immunol, 2015. **68**(2 Pt C): p. 527–35.
86. Clambey, E.T., et al., *Hypoxia-inducible factor-1 alpha-dependent induction of FoxP3 drives regulatory T-cell abundance and function during inflammatory hypoxia of the mucosa.* Proc Natl Acad Sci U S A, 2012. **109**(41): p. E2784–93.
87. Kanno, T., K. Nakano, and Y. Endo, *Cellular metabolism in Th9, Th17, and Treg cell differentiation.* Int Immunol, 2025. **37**(11): p. 673–682.
88. MacIver, N.J., et al., *The liver kinase B1 is a central regulator of T cell development, activation, and metabolism.* J Immunol, 2011. **187**(8): p. 4187–98.
89. Xin, Y., et al., *AIM2 deficiency in CD4(+) T cells promotes psoriasis-like inflammation by regulating Th17-Treg axis via AIM2-IKZF2 pathway.* J Autoimmun, 2025. **150**: p. 103351.
90. van der Zande, H.J., et al., *Dendritic cell-intrinsic LKB1-AMPK/SIK signaling controls metabolic homeostasis by limiting the hepatic Th17 response during obesity.* JCI Insight, 2023. **8**(11).
91. Liu, W., et al., *Lactate and lactylation: emerging roles in autoimmune diseases and metabolic reprogramming.* Front Immunol, 2025. **16**: p. 1589853.
92. Pucino, V., et al., *Lactate Buildup at the Site of Chronic Inflammation Promotes Disease by Inducing CD4(+) T Cell Metabolic Rewiring.* Cell Metab, 2019. **30**(6): p. 1055–1074.e8.
93. Damasceno, L.E.A., et al., *PKM2 promotes Th17 cell differentiation and autoimmune inflammation by fine-tuning STAT3 activation.* J Exp Med, 2020. **217**(10).
94. Wherry, E.J. and M. Kurachi, *Molecular and cellular insights into T cell exhaustion.* Nat Rev Immunol, 2015. **15**(8): p. 486–99.
95. Blank, C.U., et al., *Defining 'T cell exhaustion'.* Nat Rev Immunol, 2019. **19**(11): p. 665–674.
96. Kumar, B.V., T.J. Connors, and D.L. Farber, *Human T Cell Development, Localization, and Function throughout Life.* Immunity, 2018. **48**(2): p. 202–213.
97. Sukumar, M., et al., *Inhibiting glycolytic metabolism enhances CD8+ T cell memory and antitumor function.* J Clin Invest, 2013. **123**(10): p. 4479–88.
98. Doedens, A.L., et al., *Hypoxia-inducible factors enhance the effector responses of CD8(+) T cells to persistent antigen.* Nat Immunol, 2013. **14**(11): p. 1173–82.
99. Scharping, N.E., et al., *Mitochondrial stress induced by continuous stimulation under hypoxia rapidly drives T cell exhaustion.* Nat Immunol, 2021. **22**(2): p. 205–215.
100. Collier, J.L., et al., *Not-so-opposite ends of the spectrum: CD8(+) T cell dysfunction across chronic infection, cancer and autoimmunity.* Nat Immunol, 2021. **22**(7): p. 809–819.
101. Khan, O., et al., *TOX transcriptionally and epigenetically programs CD8(+) T cell exhaustion.* Nature, 2019. **571**(7764): p. 211–218.
102. Li, F., et al., *Metabolic plasticity and regulation of T cell exhaustion.* Immunology, 2022. **167**(4): p. 482–494.
103. Bengsch, B., et al., *Epigenomic-Guided Mass Cytometry Profiling Reveals Disease-Specific Features of Exhausted CD8 T Cells.* Immunity, 2018. **48**(5): p. 1029–1045.e5.
104. Belk, J.A., B. Daniel, and A.T. Satpathy, *Epigenetic regulation of T cell exhaustion.* Nat Immunol, 2022. **23**(6): p. 848–860.
105. Felson, D.T., et al., *Osteoarthritis: new insights. Part 1: the disease and its risk factors.* Ann Intern Med, 2000. **133**(8): p. 635–46.
106. *Global, regional, and national burden of osteoarthritis, 1990-2020 and projections to 2050: a systematic analysis for the Global Burden of Disease Study 2021.* Lancet Rheumatol, 2023. **5**(9): p. e508–e522.
107. de Lange-Brokaar, B.J., et al., *Synovial inflammation, immune cells and their cytokines in osteoarthritis: a review.* Osteoarthritis Cartilage, 2012. **20**(12): p. 1484–99.
108. Loeser, R.F., et al., *Osteoarthritis: a disease of the joint as an organ.* Arthritis Rheum, 2012. **64**(6): p. 1697–707.
109. Mathiessen, A. and P.G. Conaghan, *Synovitis in osteoarthritis: current understanding with therapeutic implications.* Arthritis Res Ther, 2017. **19**(1): p. 18.
110. Sanchez-Lopez, E., et al., *Synovial inflammation in osteoarthritis progression.* Nat Rev Rheumatol, 2022. **18**(5): p. 258–275.
111. Philpott, H.T., et al., *Synovitis Is Associated With Constant Pain in Knee Osteoarthritis: A Cross-sectional Study of OMERACT Knee Ultrasound Scores.* J Rheumatol, 2022. **49**(1): p. 89–97.

112. Xu, M. and Y. Ji, *Immunoregulation of synovial macrophages for the treatment of osteoarthritis.* Open Life Sci, 2023. **18**(1): p. 20220567.
113. Thomson, A. and C.M.U. Hilkens, *Synovial Macrophages in Osteoarthritis: The Key to Understanding Pathogenesis?* Front Immunol, 2021. **12**: p. 678757.
114. Zhang, H., D. Cai, and X. Bai, *Macrophages regulate the progression of osteoarthritis.* Osteoarthritis Cartilage, 2020. **28**(5): p. 555–561.
115. Orlowsky, E.W. and V.B. Kraus, *The role of innate immunity in osteoarthritis: when our first line of defense goes on the offensive.* J Rheumatol, 2015. **42**(3): p. 363–71.
116. Li, Y.S., et al., *T Cells in Osteoarthritis: Alterations and Beyond.* Front Immunol, 2017. **8**: p. 356.
117. Ishii, H., et al., *Characterization of infiltrating T cells and Th1/Th2-type cytokines in the synovium of patients with osteoarthritis.* Osteoarthritis Cartilage, 2002. **10**(4): p. 277–81.
118. Luo, P., et al., *Effects of Immune Cells and Cytokines on Different Cells in OA.* J Inflamm Res, 2023. **16**: p. 2329–2343.
119. Stockinger, B. and S. Omenetti, *The dichotomous nature of T helper 17 cells.* Nat Rev Immunol, 2017. **17**(9): p. 535–544.
120. Knochelmann, H.M., et al., *When worlds collide: Th17 and Treg cells in cancer and autoimmunity.* Cell Mol Immunol, 2018. **15**(5): p. 458–469.
121. Mangan, P.R., et al., *Transforming growth factor-beta induces development of the T(H)17 lineage.* Nature, 2006. **441**(7090): p. 231–4.
122. Korn, T., et al., *IL-21 initiates an alternative pathway to induce proinflammatory T(H)17 cells.* Nature, 2007. **448**(7152): p. 484–487.
123. Yang, X.O., et al., *STAT3 regulates cytokine-mediated generation of inflammatory helper T cells.* J Biol Chem, 2007. **282**(13): p. 9358–9363.
124. Saijo, S., et al., *Dectin-2 recognition of alpha-mannans and induction of Th17 cell differentiation is essential for host defense against Candida albicans.* Immunity, 2010. **32**(5): p. 681–91.
125. Acosta-Rodriguez, E.V., et al., *Interleukins 1beta and 6 but not transforming growth factor-beta are essential for the differentiation of interleukin 17-producing human T helper cells.* Nat Immunol, 2007. **8**(9): p. 942–9.
126. Wilson, N.J., et al., *Development, cytokine profile and function of human interleukin 17-producing helper T cells.* Nat Immunol, 2007. **8**(9): p. 950–7.
127. Volpe, E., et al., *A critical function for transforming growth factor-beta, interleukin 23 and proinflammatory cytokines in driving and modulating human T(H)-17 responses.* Nat Immunol, 2008. **9**(6): p. 650–7.
128. Palazon, A., et al., *HIF transcription factors, inflammation, and immunity.* Immunity, 2014. **41**(4): p. 518–28.
129. Semenza, G.L., *Targeting HIF-1 for cancer therapy.* Nat Rev Cancer, 2003. **3**(10): p. 721–32.
130. Ullah, M.S., A.J. Davies, and A.P. Halestrap, *The plasma membrane lactate transporter MCT4, but not MCT1, is up-regulated by hypoxia through a HIF-1alpha-dependent mechanism.* J Biol Chem, 2006. **281**(14): p. 9030–7.
131. Semenza, G.L., et al., *Transcriptional regulation of genes encoding glycolytic enzymes by hypoxia-inducible factor 1.* J Biol Chem, 1994. **269**(38): p. 23757–63.
132. Forsythe, J.A., et al., *Activation of vascular endothelial growth factor gene transcription by hypoxia-inducible factor 1.* Mol Cell Biol, 1996. **16**(9): p. 4604–13.
133. Mor, F., F.J. Quintana, and I.R. Cohen, *Angiogenesis-inflammation cross-talk: vascular endothelial growth factor is secreted by activated T cells and induces Th1 polarization.* J Immunol, 2004. **172**(7): p. 4618–23.
134. Pickup, M., S. Novitskiy, and H.L. Moses, *The roles of TGFβ in the tumour microenvironment.* Nat Rev Cancer, 2013. **13**(11): p. 788–99.
135. Batlle, E. and J. Massagué, *Transforming Growth Factor-β Signaling in Immunity and Cancer.* Immunity, 2019. **50**(4): p. 924–940.
136. Acuto, O. and F. Michel, *CD28-mediated co-stimulation: a quantitative support for TCR signalling.* Nat Rev Immunol, 2003. **3**(12): p. 939–51.
137. Chen, X.W. and S.F. Zhou, *Inflammation, cytokines, the IL-17/IL-6/STAT3/NF-κB axis, and tumorigenesis.* Drug Des Devel Ther, 2015. **9**: p. 2941–6.
138. Gutcher, I., et al., *Autocrine transforming growth factor-β1 promotes in vivo Th17 cell differentiation.* Immunity, 2011. **34**(3): p. 396–408.
139. Veldhoen, M., et al., *The aryl hydrocarbon receptor links TH17-cell-mediated autoimmunity to environmental toxins.* Nature, 2008. **453**(7191): p. 106–9.

140. Watanabe, Y., et al., *TMEPAI, a transmembrane TGF-beta-inducible protein, sequesters Smad proteins from active participation in TGF-beta signaling.* Mol Cell, 2010. **37**(1): p. 123–34.
141. Tecalco-Cruz, A.C., et al., *Transcriptional cofactors Ski and SnoN are major regulators of the TGF-β/Smad signaling pathway in health and disease.* Signal Transduct Target Ther, 2018. **3**: p. 15.
142. Codarri, L., et al., *RORγt drives production of the cytokine GM-CSF in helper T cells, which is essential for the effector phase of autoimmune neuroinflammation.* Nat Immunol, 2011. **12**(6): p. 560–7.
143. El-Behi, M., et al., *The encephalitogenicity of T(H)17 cells is dependent on IL-1- and IL-23-induced production of the cytokine GM-CSF.* Nat Immunol, 2011. **12**(6): p. 568–75.
144. Xu, K., et al., *Glycolytic ATP fuels phosphoinositide 3-kinase signaling to support effector T helper 17 cell responses.* Immunity, 2021. **54**(5): p. 976–987.e7.
145. Buck, M.D., et al., *Metabolic Instruction of Immunity.* Cell, 2017. **169**(4): p. 570–586.
146. Quinn, W.J., 3rd, et al., *Lactate Limits T Cell Proliferation via the NAD(H) Redox State.* Cell Rep, 2020. **33**(11): p. 108500.
147. Zhang, Y.T., et al., *Effects of lactate on metabolism and differentiation of CD4(+)T cells.* Mol Immunol, 2023. **154**: p. 96–107.
148. Yoshimura, A., T. Naka, and M. Kubo, *SOCS proteins, cytokine signalling and immune regulation.* Nat Rev Immunol, 2007. **7**(6): p. 454–65.
149. Brand, A., et al., *LDHA-Associated Lactic Acid Production Blunts Tumor Immunosurveillance by T and NK Cells.* Cell Metab, 2016. **24**(5): p. 657–671.
150. Shen, H., et al., *HIF1α-regulated glycolysis promotes activation-induced cell death and IFN-γ induction in hypoxic T cells.* Nat Commun, 2024. **15**(1): p. 9394.
151. Kasembeli, M.M., et al., *Contribution of STAT3 to Inflammatory and Fibrotic Diseases and Prospects for its Targeting for Treatment.* Int J Mol Sci, 2018. **19**(8).
152. Hillmer, E.J., et al., *STAT3 signaling in immunity.* Cytokine Growth Factor Rev, 2016. **31**: p. 1–15.
153. Sánchez-Elsner, T., et al., *Synergistic cooperation between hypoxia and transforming growth factor-beta pathways on human vascular endothelial growth factor gene expression.* J Biol Chem, 2001. **276**(42): p. 38527–35.
154. Jarad, M., et al., *Release of endothelial cell associated VEGFR2 during TGF-β modulated angiogenesis in vitro.* BMC Cell Biol, 2017. **18**(1): p. 10.
155. Hayatsu, N., et al., *Analyses of a Mutant Foxp3 Allele Reveal BATF as a Critical Transcription Factor in the Differentiation and Accumulation of Tissue Regulatory T Cells.* Immunity, 2017. **47**(2): p. 268–283.e9.
156. Basdeo, S.A., et al., *Ex-Th17 (Nonclassical Th1) Cells Are Functionally Distinct from Classical Th1 and Th17 Cells and Are Not Constrained by Regulatory T Cells.* J Immunol, 2017. **198**(6): p. 2249–2259.
157. Hirota, K., et al., *Fate mapping of IL-17-producing T cells in inflammatory responses.* Nat Immunol, 2011. **12**(3): p. 255–63.
158. Bending, D., et al., *Highly purified Th17 cells from BDC2.5NOD mice convert into Th1-like cells in NOD/SCID recipient mice.* J Clin Invest, 2009. **119**(3): p. 565–72.
159. Burashed, K.K. and F.A. AlAbbasi, *Janus Kinase (JAK) Inhibitors in Rheumatoid Arthritis.* Cureus, 2026. **18**(1): p. e102634.
160. Yasuda, K., Y. Takeuchi, and K. Hirota, *The pathogenicity of Th17 cells in autoimmune diseases.* Semin Immunopathol, 2019. **41**(3): p. 283–297.
161. Khader, S.A., S.L. Gaffen, and J.K. Kolls, *Th17 cells at the crossroads of innate and adaptive immunity against infectious diseases at the mucosa.* Mucosal Immunol, 2009. **2**(5): p. 403–11.
162. Harrington, L.E., et al., *Interleukin 17-producing CD4+ effector T cells develop via a lineage distinct from the T helper type 1 and 2 lineages.* Nat Immunol, 2005. **6**(11): p. 1123–32.
163. Burgler, S., et al., *Differentiation and functional analysis of human T(H)17 cells.* J Allergy Clin Immunol, 2009. **123**(3): p. 588–95, 595.e1–7.
164. Monteleone, I., et al., *Th17-related cytokines in inflammatory bowel diseases: friends or foes?* Curr Mol Med, 2012. **12**(5): p. 592–7.
165. Gálvez, J., *Role of Th17 Cells in the Pathogenesis of Human IBD.* ISRN Inflamm, 2014. **2014**: p. 928461.
166. Smith, J.A. and R.A. Colbert, *Review: The interleukin-23/interleukin-17 axis in spondyloarthritis pathogenesis: Th17 and beyond.* Arthritis Rheumatol, 2014. **66**(2): p. 231–41.
167. Batalla, A., et al., *Association between single nucleotide polymorphisms IL17RA rs4819554 and IL17E rs79877597 and Psoriasis in a Spanish cohort.* J Dermatol Sci, 2015. **80**(2): p. 111–5.

168. Yang, P., et al., *Th17 cell pathogenicity and plasticity in rheumatoid arthritis.* J Leukoc Biol, 2019. **106**(6): p. 1233–1240.

169. Vidal-Castiñeira, J.R., et al., *A Single Nucleotide Polymorphism in the Il17ra Promoter Is Associated with Functional Severity of Ankylosing Spondylitis.* PLoS One, 2016. **11**(7): p. e0158905.

170. Qian, Y., et al., *The adaptor Act1 is required for interleukin 17-dependent signaling associated with autoimmune and inflammatory disease.* Nat Immunol, 2007. **8**(3): p. 247–56.

171. Wellen, K.E. and C.B. Thompson, *A two-way street: reciprocal regulation of metabolism and signalling.* Nat Rev Mol Cell Biol, 2012. **13**(4): p. 270–6.

172. Wagner, A., et al., *Metabolic modeling of single Th17 cells reveals regulators of autoimmunity.* Cell, 2021. **184**(16): p. 4168–4185.e21.

173. Kaufmann, U., et al., *Calcium Signaling Controls Pathogenic Th17 Cell-Mediated Inflammation by Regulating Mitochondrial Function.* Cell Metab, 2019. **29**(5): p. 1104–1118.e6.

174. Hong, H.S., et al., *OXPHOS promotes apoptotic resistance and cellular persistence in T(H)17 cells in the periphery and tumor microenvironment.* Sci Immunol, 2022. **7**(77): p. eabm8182.

175. Yang, L., et al., *IL-21 and TGF-beta are required for differentiation of human T(H)17 cells.* Nature, 2008. **454**(7202): p. 350–2.

176. Revu, S., et al., *IL-23 and IL-1β Drive Human Th17 Cell Differentiation and Metabolic Reprogramming in Absence of CD28 Costimulation.* Cell Rep, 2018. **22**(10): p. 2642–2653.

177. Xu, W., et al., *GOT1 constrains T(H)17 cell differentiation, while promoting iT(reg) cell differentiation.* Nature, 2023. **614**(7946): p. E1–e11.

178. Argüello, R.J., et al., *SCENITH: A Flow Cytometry-Based Method to Functionally Profile Energy Metabolism with Single-Cell Resolution.* Cell Metab, 2020. **32**(6): p. 1063–1075.e7.

179. Weinberg, S.E., L.A. Sena, and N.S. Chandel, *Mitochondria in the regulation of innate and adaptive immunity.* Immunity, 2015. **42**(3): p. 406–17.

180. Buck, M.D., et al., *Mitochondrial Dynamics Controls T Cell Fate through Metabolic Programming.* Cell, 2016. **166**(1): p. 63–76.

181. Zhao, Z., et al., *The PRAK-NRF2 axis promotes the differentiation of Th17 cells by mediating the redox homeostasis and glycolysis.* Proc Natl Acad Sci U S A, 2023. **120**(19): p. e2212613120.

182. Posse, V., et al., *TEFM is a potent stimulator of mitochondrial transcription elongation in vitro.* Nucleic Acids Res, 2015. **43**(5): p. 2615–24.

183. Li, Y.H., et al., *Mdivi-1, a mitochondrial fission inhibitor, modulates T helper cells and suppresses the development of experimental autoimmune encephalomyelitis.* J Neuroinflammation, 2019. **16**(1): p. 149.

184. Chandhok, G., M. Lazarou, and B. Neumann, *Structure, function, and regulation of mitofusin-2 in health and disease.* Biol Rev Camb Philos Soc, 2018. **93**(2): p. 933–949.

185. Gerriets, V.A. and J.C. Rathmell, *Metabolic pathways in T cell fate and function.* Trends Immunol, 2012. **33**(4): p. 168–73.

186. Anvar, M.T., et al., *Th17 cell function in cancers: immunosuppressive agents or anti-tumor allies?* Cancer Cell Int, 2024. **24**(1): p. 355.

187. Chapman, N.M., M.R. Boothby, and H. Chi, *Metabolic coordination of T cell quiescence and activation.* Nat Rev Immunol, 2020. **20**(1): p. 55–70.

188. Cibrián, D. and F. Sánchez-Madrid, *CD69: from activation marker to metabolic gatekeeper.* Eur J Immunol, 2017. **47**(6): p. 946–953.

189. Pauken, K.E., et al., *Epigenetic stability of exhausted T cells limits durability of reinvigoration by PD-1 blockade.* Science, 2016. **354**(6316): p. 1160–1165.

190. Yi, J.S., M.A. Cox, and A.J. Zajac, *T-cell exhaustion: characteristics, causes and conversion.* Immunology, 2010. **129**(4): p. 474–81.

191. Scharping, N.E., et al., *The Tumor Microenvironment Represses T Cell Mitochondrial Biogenesis to Drive Intratumoral T Cell Metabolic Insufficiency and Dysfunction.* Immunity, 2016. **45**(2): p. 374–88.

192. Patsoukis, N., et al., *PD-1 alters T-cell metabolic reprogramming by inhibiting glycolysis and promoting lipolysis and fatty acid oxidation.* Nat Commun, 2015. **6**: p. 6692.

193. Neefjes, M., et al., *Reporter gene comparison demonstrates interference of complex body fluids with secreted luciferase activity.* Sci Rep, 2021. **11**(1): p. 1359.

194. Hsueh, M.F., et al., *Synergistic Roles of Macrophages and Neutrophils in Osteoarthritis Progression.* Arthritis Rheumatol, 2021. **73**(1): p. 89–99.

195. Rosshirt, N., et al., *A predominant Th1 polarization is present in synovial fluid of end-stage osteoarthritic knee joints: analysis of peripheral blood, synovial fluid and synovial membrane.* Clin Exp Immunol, 2019. **195**(3): p. 395–406.

196. Yamada, H., et al., *Preferential accumulation of activated Th1 cells not only in rheumatoid arthritis but also in osteoarthritis joints.* J Rheumatol, 2011. **38**(8): p. 1569–75.

197. Nees, T.A., et al., *Infiltration Profile of Regulatory T Cells in Osteoarthritis-Related Pain and Disability.* Biomedicines, 2022. **10**(9).

198. Moradi, B., et al., *CD4$^+$CD25$^+$/highCD127low/$^-$ regulatory T cells are enriched in rheumatoid arthritis and osteoarthritis joints--analysis of frequency and phenotype in synovial membrane, synovial fluid and peripheral blood.* Arthritis Res Ther, 2014. **16**(2): p. R97.

199. Pawłowska, J., et al., *Different distribution of CD4 and CD8 T cells in synovial membrane and peripheral blood of rheumatoid arthritis and osteoarthritis patients.* Folia Histochem Cytobiol, 2009. **47**(4): p. 627–32.

200. Klein-Wieringa, I.R., et al., *Inflammatory Cells in Patients with Endstage Knee Osteoarthritis: A Comparison between the Synovium and the Infrapatellar Fat Pad.* J Rheumatol, 2016. **43**(4): p. 771–8.

201. Wang, C., et al., *Unraveling the spatial and signaling dynamics and splicing kinetics of immune infiltration in osteoarthritis synovium.* Front Immunol, 2025. **16**: p. 1521038.

202. Berenbaum, F., *Osteoarthritis as an inflammatory disease (osteoarthritis is not osteoarthrosis!).* Osteoarthritis Cartilage, 2013. **21**(1): p. 16–21.

203. Wood, M.J., et al., *Macrophage proliferation distinguishes 2 subgroups of knee osteoarthritis patients.* JCI Insight, 2019. **4**(2).

204. Cappelli, L.C., et al., *Inflammatory arthritis and sicca syndrome induced by nivolumab and ipilimumab.* Ann Rheum Dis, 2017. **76**(1): p. 43–50.

205. van Kooten, N.J.T., et al., *S100A8/A9 drives monocytes towards M2-like macrophage differentiation and associates with M2-like macrophages in osteoarthritic synovium.* Rheumatology (Oxford), 2024.

206. Lee, H.G., M.J. Cho, and J.M. Choi, *Bystander CD4(+) T cells: crossroads between innate and adaptive immunity.* Exp Mol Med, 2020. **52**(8): p. 1255–1263.

207. Menarim, B.C., et al., *Transcriptional and Histochemical Signatures of Bone Marrow Mononuclear Cell-Mediated Resolution of Synovitis.* Front Immunol, 2021. **12**: p. 734322.

208. Scanzello, C.R., et al., *Synovial inflammation in patients undergoing arthroscopic meniscectomy: molecular characterization and relationship to symptoms.* Arthritis Rheum, 2011. **63**(2): p. 391–400.

209. Wen, Z., et al., *The role of Th/Treg immune cells in osteoarthritis.* Front Immunol, 2024. **15**: p. 1393418.

210. Murray, P.J., et al., *Macrophage activation and polarization: nomenclature and experimental guidelines.* Immunity, 2014. **41**(1): p. 14–20.

211. Cutolo, M., et al., *The Role of M1/M2 Macrophage Polarization in Rheumatoid Arthritis Synovitis.* Front Immunol, 2022. **13**: p. 867260.

212. Chen, M., et al., *The function of BAFF on T helper cells in autoimmunity.* Cytokine Growth Factor Rev, 2014. **25**(3): p. 301–5.

213. Duong, L., et al., *Macrophage function in the elderly and impact on injury repair and cancer.* Immun Ageing, 2021. **18**(1): p. 4.

214. Penatti, A., et al., *Differences in serum and synovial CD4+ T cells and cytokine profiles to stratify patients with inflammatory osteoarthritis and rheumatoid arthritis.* Arthritis Res Ther, 2017. **19**(1): p. 103.

215. Kriegova, E., et al., *Gender-related differences observed among immune cells in synovial fluid in knee osteoarthritis.* Osteoarthritis Cartilage, 2018. **26**(9): p. 1247–1256.

216. Apinun, J., et al., *Immune Mediators in Osteoarthritis: Infrapatellar Fat Pad-Infiltrating CD8+ T Cells Are Increased in Osteoarthritic Patients with Higher Clinical Radiographic Grading.* Int J Rheumatol, 2016. **2016**: p. 9525724.

217. Sallusto, F., J. Geginat, and A. Lanzavecchia, *Central memory and effector memory T cell subsets: function, generation, and maintenance.* Annu Rev Immunol, 2004. **22**: p. 745–63.

218. Leijten, E.F., et al., *Tissue-Resident Memory CD8+ T Cells From Skin Differentiate Psoriatic Arthritis From Psoriasis.* Arthritis Rheumatol, 2021. **73**(7): p. 1220–1232.

219. Zhang, F., et al., *Defining inflammatory cell states in rheumatoid arthritis joint synovial tissues by integrating single-cell transcriptomics and mass cytometry.* Nature Immunology, 2019. **20**(7): p. 928–+.

220. van der Kraan, P.M., *Inhibition of transforming growth factor-β in osteoarthritis. Discrepancy with reduced TGFβ signaling in normal joints.* Osteoarthr Cartil Open, 2022. **4**(1): p. 100238.
221. van der Kraan, P.M., *The changing role of TGFβ in healthy, ageing and osteoarthritic joints.* Nat Rev Rheumatol, 2017. **13**(3): p. 155–163.
222. Dahmani, A., et al., *TGFβ Programs Central Memory Differentiation in Ex Vivo-Stimulated Human T Cells.* Cancer Immunol Res, 2019. **7**(9): p. 1426–1439.
223. Mackay, L.K., et al., *T-box Transcription Factors Combine with the Cytokines TGF-β and IL-15 to Control Tissue-Resident Memory T Cell Fate.* Immunity, 2015. **43**(6): p. 1101–11.
224. Cosmi, L., et al., *T helper cells plasticity in inflammation.* Cytometry A, 2014. **85**(1): p. 36–42.
225. Milner, J.J., et al., *Runx3 programs CD8(+) T cell residency in non-lymphoid tissues and tumours.* Nature, 2017. **552**(7684): p. 253–257.
226. Sallusto, F., et al., *Two subsets of memory T lymphocytes with distinct homing potentials and effector functions.* Nature, 1999. **401**(6754): p. 708–12.
227. Tanel, A., et al., *Cellular and molecular mechanisms of memory T-cell survival.* Expert Rev Vaccines, 2009. **8**(3): p. 299–312.
228. Hofmann, M., R. Thimme, and W.W. Schamel, *PD-1 and LAG-3: synergistic fostering of T cell exhaustion.* Signal Transduct Target Ther, 2024. **9**(1): p. 291.
229. Paiola, M., et al., *Osteoarthritis increases the risk of inflammatory arthritis due to immune checkpoint inhibitors associated with tissue-resident memory T cells.* J Immunother Cancer, 2025. **13**(3).
230. Reid, P., et al., *Activated osteoarthritis following immune checkpoint inhibitor treatment: an observational study.* J Immunother Cancer, 2021. **9**(9).
231. Akbar, A.N. and S.M. Henson, *Are senescence and exhaustion intertwined or unrelated processes that compromise immunity?* Nat Rev Immunol, 2011. **11**(4): p. 289–95.
232. Shive, C.L., et al., *Markers of T Cell Exhaustion and Senescence and Their Relationship to Plasma TGF-β Levels in Treated HIV+ Immune Non-responders.* Front Immunol, 2021. **12**: p. 638010.
233. Slaets, H., et al., *Are immunosenescent T cells really senescent?* Aging Cell, 2024. **23**(10): p. e14300.
234. Zhou, L., M.M. Chong, and D.R. Littman, *Plasticity of CD4+ T cell lineage differentiation.* Immunity, 2009. **30**(5): p. 646–55.
235. Karmaus, P.W.F., et al., *Metabolic heterogeneity underlies reciprocal fates of T(H)17 cell stemness and plasticity.* Nature, 2019. **565**(7737): p. 101–105.
236. Qin, Z., et al., *TCR signaling induces STAT3 phosphorylation to promote TH17 cell differentiation.* J Exp Med, 2024. **221**(3).
237. Zhang, F., et al., *Metabolic effects of quercetin on inflammatory and autoimmune responses in rheumatoid arthritis are mediated through the inhibition of JAK1/STAT3/HIF-1α signaling.* Mol Med, 2024. **30**(1): p. 170.
238. Wei, D., et al., *Stat3 activation regulates the expression of vascular endothelial growth factor and human pancreatic cancer angiogenesis and metastasis.* Oncogene, 2003. **22**(3): p. 319–29.
239. Schwartz, D.M., et al., *JAK inhibition as a therapeutic strategy for immune and inflammatory diseases.* Nat Rev Drug Discov, 2017. **16**(12): p. 843–862.
240. Dudek, P., et al., *Efficacy, Safety and Future Perspectives of JAK Inhibitors in the IBD Treatment.* J Clin Med, 2021. **10**(23).
241. Fleischmann, R., et al., *Efficacy and safety of tofacitinib monotherapy, tofacitinib with methotrexate, and adalimumab with methotrexate in patients with rheumatoid arthritis (ORAL Strategy): a phase 3b/4, double-blind, head-to-head, randomised controlled trial.* Lancet, 2017. **390**(10093): p. 457–468.
242. Ito, Y., et al., *Activated type 17 helper T cells affect tofacitinib treatment outcomes.* Sci Rep, 2025. **15**(1): p. 6112.
243. Zhao, R., et al., *Targeting pathogenic Th17.1 cells via JAK-STAT3 pathway: A novel approach with tofacitinib for refractory myasthenia gravis.* Neurotherapeutics, 2026. **23**(1): p. e00831.
244. Imani, S., et al., *Reprogramming the breast tumor immune microenvironment: cold-to-hot transition for enhanced immunotherapy.* J Exp Clin Cancer Res, 2025. **44**(1): p. 131.
245. Poholek, C.H., et al., *Noncanonical STAT3 activity sustains pathogenic Th17 proliferation and cytokine response to antigen.* J Exp Med, 2020. **217**(10).
246. Wegrzyn, J., et al., *Function of mitochondrial Stat3 in cellular respiration.* Science, 2009. **323**(5915): p. 793–7.
247. Gough, D.J., et al., *Mitochondrial STAT3 supports Ras-dependent oncogenic transformation.* Science, 2009. **324**(5935): p. 1713–6.

248. Lee, S.Y., et al., *mtSTAT3 suppresses rheumatoid arthritis by regulating Th17 and synovial fibroblast inflammatory cell death with IL-17-mediated autophagy dysfunction.* Exp Mol Med, 2025. **57**(1): p. 221–234.
249. Endo, Y., K. Yokote, and T. Nakayama, *The obesity-related pathology and Th17 cells.* Cell Mol Life Sci, 2017. **74**(7): p. 1231–1245.
250. Pitzalis, C., et al., *Ectopic lymphoid-like structures in infection, cancer and autoimmunity.* Nat Rev Immunol, 2014. **14**(7): p. 447–62.
251. Lund-Olesen, K., *Oxygen tension in synovial fluids.* Arthritis Rheum, 1970. **13**(6): p. 769–76.
252. Latourte, A., et al., *Systemic inhibition of IL-6/Stat3 signalling protects against experimental osteoarthritis.* Ann Rheum Dis, 2017. **76**(4): p. 748–755.
253. Mueller, S.N. and L.K. Mackay, *Tissue-resident memory T cells: local specialists in immune defence.* Nat Rev Immunol, 2016. **16**(2): p. 79–89.
254. Jalili, S., et al., *Leveraging tissue-resident memory T cells for non-invasive immune monitoring via microneedle skin patches.* Nat Biomed Eng, 2026.
255. Lambert, C., et al., *The Damage-Associated Molecular Patterns (DAMPs) as Potential Targets to Treat Osteoarthritis: Perspectives From a Review of the Literature.* Front Med (Lausanne), 2020. **7**: p. 607186.
256. Goodman, S.B., Y.T. Konttinen, and M. Takagi, *Joint replacement surgery and the innate immune system.* J Long Term Eff Med Implants, 2014. **24**(4): p. 253–7.
257. Evans, J.T., et al., *How long does a knee replacement last? A systematic review and meta-analysis of case series and national registry reports with more than 15 years of follow-up.* Lancet, 2019. **393**(10172): p. 655–663.
258. Beswick, A.D., et al., *What proportion of patients report long-term pain after total hip or knee replacement for osteoarthritis? A systematic review of prospective studies in unselected patients.* BMJ Open, 2012. **2**(1): p. e000435.
259. Connors, J.P., et al., *The Role of the Innate Immune System in Wear Debris-Induced Inflammatory Peri-Implant Osteolysis in Total Joint Arthroplasty.* Bioengineering (Basel), 2022. **9**(12).
260. Kang, H.M., et al., *Multiplexed droplet single-cell RNA-sequencing using natural genetic variation.* Nat Biotechnol, 2018. **36**(1): p. 89–94.
261. Weyand, C.M. and J.J. Goronzy, *Immune mechanisms in medium and large-vessel vasculitis.* Nat Rev Rheumatol, 2013. **9**(12): p. 731–40.
262. Zhao, F., et al., *Human CCR4+ CCR6+ Th17 cells suppress autologous CD8+ T cell responses.* J Immunol, 2012. **188**(12): p. 6055–62.
263. Sajani, A., et al., *Heterogeneity and plasticity of the naive CD4(+) T cell compartment.* Cell Rep, 2026. **45**(3): p. 116980.
264. Gustafson, C.E., *Naïve T Cell Quiescence in Immune Aging.* Adv Geriatr Med Res, 2021. **3**(3).
265. Cano-Gamez, K., et al., *Single-cell transcriptomics identifies an effectorness gradient shaping the response of CD4(+) T cells to cytokines.* Nat Commun, 2020. **11**(1): p. 1801.
266. Floess, S., et al., *Epigenetic control of the foxp3 locus in regulatory T cells.* PLoS Biol, 2007. **5**(2): p. e38.
267. Maruotti, N., et al., *Angiogenesis in rheumatoid arthritis.* Histol Histopathol, 2006. **21**(5): p. 557–66.
268. Nees, T.A., et al., *T Helper Cell Infiltration in Osteoarthritis-Related Knee Pain and Disability*. J Clin Med, 2020. **9**(8): p. 2423.



Appendix

Appendix
Nederlandse Samenvatting
Research Data Management
Curriculum Vitae
List of Publications
Portfolio
Acknowledgements

NEDERLANDSE SAMENVATTING

Hoe afweercellen hun koers bepalen — en waarom dat ertoe doet

Ons immuunsysteem is geen strak geprogrammeerd systeem, maar een flexibel netwerk dat voortdurend reageert op zijn omgeving. Centrale spelers daarin zijn zogeheten $CD4^+$ T-cellen: witte bloedcellen die zich kunnen ontwikkelen tot verschillende typen "helpercellen", elk met een eigen taak.

Een van die typen, de Th17-cel, speelt een dubbelrol. Aan de ene kant beschermt deze cel ons tegen bacteriën en schimmels, vooral aan slijmvliezen. Aan de andere kant kan dezelfde cel betrokken zijn bij chronische ontstekingsziekten zoals reuma, de ziekte van Crohn en multiple sclerose. Opvallend is dat Th17-cellen niet vastliggen in hun gedrag: afhankelijk van hun omgeving kunnen ze zich aanpassen — van agressief naar juist remmend.

Dat vermogen tot aanpassing staat centraal in dit onderzoek.

De omgeving bepaalt de cel

In een nagebootste, gecontroleerde laboratoriumomgeving werd onderzocht hoe menselijke Th17-cellen ontstaan. Daarbij blijkt dat de omstandigheden waarin een cel zich bevindt — zoals de hoeveelheid en type signaalstoffen, zuurstof en afvalproducten — grote invloed hebben op de uiteindelijke functie.

Zo werkt het eiwit TGF-β als een soort dimmer: een beetje stimuleert de vorming van Th17-cellen, maar veel ervan remt dat juist af. Ook lactaat, een stof die vrijkomt in ontstoken weefsel, blijkt een rol te spelen: het vermindert het aantal Th17-cellen, maar verandert tegelijk hun stofwisseling.

Zuurstoftekort (hypoxie), een situatie die vaak voorkomt in ontstoken weefsel of tumoren, zet cellen aan tot een ander energiegebruik, maar verandert hun aantal nauwelijks. Pas wanneer zuurstoftekort en TGF-β samen optreden, komt een belangrijk groeimolecuul (VEGFA) op gang. Dit molecuul is betrokken bij de aanleg van nieuwe bloedvaten.

In dit web van signalen komt één eiwit steeds terug: STAT3. Het fungeert als een soort knooppunt waar verschillende prikkels samenkomen. Normaal gesproken wordt STAT3 vooral geactiveerd door cytokinen zoals IL-6, een bekende signaalstof en aanjager van ontsteking. Maar uit dit proefschrift blijkt dat ook andere factoren, zoals een zuurstofarme omgeving of een ophoping van lactaat, dezelfde route beïnvloeden.

Met andere woorden: STAT3 luistert niet alleen naar “klassieke” signaalstoffen, maar ook naar de toestand van het weefsel zelf.

De energiecentrale van de cel stuurt mee

Niet alleen de omgeving, maar ook de “energiecentrale” van de cel — de mitochondriën — blijkt bepalend bij het maken van Th17-cellen. Cellen met veel mitochondriële activiteit ontwikkelen zich vaker tot Th17-cellen. Maar daar hangt een prijskaartje aan: deze cellen raken sneller uitgeput en produceren uiteindelijk minder ontsteking-gevende signaalstoffen. Dit wijst op een basis mechanisme: hoe een cel energie gebruikt, beïnvloedt wat voor cel het wordt.

Ook bij artrose blijken T-cellen actief

Opvallend is dat T-cellen ook werden aangetroffen in gewrichtsweefsel van patiënten met vergevorderde artrose, een aandoening die meestal niet wordt gezien als een ziekte met een rol voor T cellen. In tegenstelling tot wat je zou verwachten bij een langdurige ziekte, waren deze T cellen niet “opgebrand”. Ze bleken juist actief en in staat opnieuw te reageren op prikkels. Dat roept de vraag op of ze bijdragen aan aanhoudende pijn en ontsteking, bijvoorbeeld na een knieoperatie.

Geen vaste identiteiten, maar een glijdende schaal

De klassieke indeling van T-cellen in vaste categorieën blijkt te simpel. In werkelijkheid bewegen cellen zich op een schaal — bijvoorbeeld tussen ontstekingsbevorderende Th17-cellen en remmende Treg-cellen. Dat evenwicht wordt continu beïnvloed door de omgeving: zuurstofgehalte, energiehuishouding, signaalstoffen en zelfs de fysieke eigenschappen van het weefsel.

Waarom dit ertoe doet

Behandelingen gericht op één enkel signaal werken vaak maar beperkt. Dit onderzoek suggereert waarom: T-cellen reageren niet op één prikkel, maar op een combinatie van factoren tegelijk. Een eiwit als STAT3, dat meerdere signalen samenbrengt, zou daarom een interessanter aangrijpingspunt kunnen zijn voor therapie — bijvoorbeeld bij chronische ontstekingen of zelfs kanker.

Kort samengevat

- Th17-cellen zijn flexibel en reageren sterk op hun omgeving
- Niet één factor, maar een combinatie van signalen bepaalt hun gedrag
- De energiehuishouding van de cel speelt een sleutelrol
- Ook bij artrose kunnen actieve T-cellen een rol spelen
- Toekomstige therapieën moeten waarschijnlijk meerdere routes tegelijk aanpakken of gebruik maken van signaal-knooppunten

RESEARCH DATA MANAGEMENT

The research presented in this thesis was carried out and stored in accordance with the rules and regulations of the Radboud university medical center for FAIR (Findable, Accessible, Interoperable, Reusable) research data management.

Ethics and privacy

This thesis is based on research involving primary human cells and human tissue, obtained from healthy blood donors and from patients undergoing joint replacement surgery. No experiments involving animals were performed.

For chapters 2 and 3, peripheral blood mononuclear cells were isolated from buffy coats of healthy donors obtained through Sanquin Blood Bank (the Netherlands; project number NVT 0397-02). As this material derives from healthy volunteers who provided consent at Sanquin, and not from patients, these studies were not subject to the Dutch Medical Research Involving Human Subjects Act (WMO). The material was anonymized and donors were not identifiable to the researchers. All procedures were conducted in accordance with the Declaration of Helsinki.

For chapter 4, osteoarthritic synovial tissue was obtained during joint replacement surgery from patients with end-stage knee osteoarthritis at the Sint Maartenskliniek and the Radboud university medical center (Nijmegen, the Netherlands). Patients at the Sint Maartenskliniek provided written informed consent (METC 2018-4319). At the Radboudumc, tissue was obtained as residual material under an opt-out procedure, in which patients were given the opportunity to object to donation. This coded residual tissue was used in accordance with the Declaration of Helsinki and the Dutch FEDERA Code of Conduct for Responsible Use of human tissue in medical research.

Data collection and storage

Data presented in this thesis were generated through laboratory experiments on primary human cells and tissue. For chapter 2, single-cell RNA sequencing was performed on the 10x Genomics platform; raw reads were processed with Cell Ranger and analyzed in R, and gene expression was additionally quantified by quantitative PCR. For chapter 3, data were generated by flow cytometry and fluorescence-activated cell sorting, quantitative PCR, metabolic assays (XTT, CellTiter-Glo, and SCENITH), multiplex cytokine profiling (Luminex), and luciferase reporter assays. For chapter 4, data were generated by enzymatic digestion of synovial tissue followed by flow cytometry and immunohistochemistry.

All data and analyses generated during this PhD were stored on the departmental server, which is backed up daily and is accessible only to project members working at the Radboudumc.

Raw unaltered data were stored alongside processed files, organized per chapter and per figure. Experimental procedures and results were documented in a physical lab journal and in Labguru, the department's electronic lab journal, which is accessible to all members of the research group. These storage options safeguard the availability, integrity, and confidentiality of the data.

Data sharing according to the FAIR principles

Chapter 3 has been published with open access (DOI: 10.1111/imm.70037). Chapters 2 and 4 manuscripts are still in preparation at the time of writing.

All raw single-cell RNA sequencing data used in chapter 2 are stored on the departmental server to be released upon manuscript publication. Raw sequencing files, together with the analyzed result files, are also stored in the Radboud Data Repository (Radboud Collection identifier: https://doi.org/10.34973/w1g5-8x29) with restricted access; these data are available upon request from the principal investigator or upon manuscript publication, which we strive to achieve as soon as possible.

The data underlying chapter 3 are stored on the departmental server and archived in the Radboud Data Repository (Radboud Collection identifier: https://doi.org/10.34973/f2nm-wt33) with open access; these data are available upon reasonable request from the principal investigator, and the collection is linked to the corresponding article (DOI: 10.1111/imm.70037).

The data underlying chapter 4 are stored on the departmental server and archived in the Radboud Data Repository (Radboud Collection identifier: https://doi.org/10.34973/wh1w-6v59) with restricted access, and will be made available upon publication of the corresponding manuscript.

The Radboud Data Repository is a certified trusted repository that assigns a persistent identifier (DOI) to each dataset and indexes its descriptive metadata. Datasets therefore remain findable and citable even when access to the underlying data is restricted, following the principle of being as open as possible and as restricted as needed. Data were stored in widely used, non-proprietary file formats where possible, and were made reusable by including documentation of the research protocols, methods, and analysis scripts used to generate the results. Standard identifiers were used where applicable, including official gene symbols and sequence database accessions. The Radboud university medical center is the legal owner of the data. The datasets are shared under the Radboudumc standard data use agreement (RUMC-RA-DUA), which sets the conditions under which others may request access.

Analyses were performed using generally available software, including Cell Ranger, R, and GraphPad Prism. All data can be opened with commonly available software tools.

Overview of archived datasets

The table below indicates where the data for each data chapter are archived in the Radboud Data Repository (RDR). All archived data remain available for at least 10 years after termination of the studies.

Chapter	Radboud Data Repository (collection / access)	External repository	License / DUA
2	https://doi.org/10.34973/w1g5-8x29, restricted access,DAC	-	RUMC-RA-DUA
3	https://doi.org/10.34973/f2nm-wt33, open access,DSC	Article DOI: 10.1111/imm.70037	RUMC-RA-DSA 2.1
4	https://doi.org/10.34973/wh1w-6v59, Restricted access,DAC	—	RUMC-RA-DUA

CURRICULUM VITAE

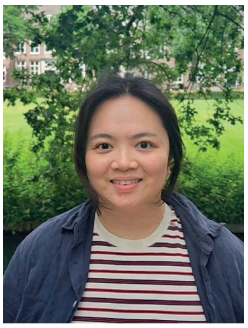

Xinlai Chen was born on August 20th, 1991, in Sichuan, China. She studied medicine for five years, including a one-year internship at Sichuan Provincial Hospital and West China Hospital, Sichuan University, and passed the medical licensing examination in 2015. That same year, she started a master's degree in sports medicine at Chengdu Sport University, under the supervision of Dr. Shen Hai and Prof. Hu Yushi, with research on hyperuricemia models. She then completed three years of residency training in orthopedics at Sichuan Provincial Orthopedics Hospital. In 2020, she started her PhD at the Department of Experimental Rheumatology, Radboud University Medical Center, in the Netherlands, under the supervision of Dr. Marije Koenders, Dr. Arjan van Caam, and Prof. Dr. Peter M. van der Kraan, focusing on human Th17 cells, the results of which are presented in this thesis. After completing her PhD, she intends to continue a career combining clinical practice and research, contributing to advances in health care.

LIST OF PUBLICATIONS

Aarts J, van Caam A, **Chen X**, et al. Local inhibition of TGF-β1 signaling improves Th17/Treg balance but not joint pathology during experimental arthritis. Sci Rep. 2022;12(1):3182. doi:10.1038/s41598-022-07075-w

Chen X, Papadimitriou TI, van Essen AHG, et al. Mitochondrial activity regulates human T helper 17 differentiation and function. Immunology. 2026;177(1):185-198. doi:10.1111/imm.70037

PhD PORTFOLIO OF XINLAI CHEN

Department: Reumatologie
PhD period: 2020-09-14 – 2025-11-24

PhD Supervisor(s):
prof. dr. P.M. van der Kraan

PhD Co-supervisor(s):
dr. M.I. Koenders
dr. A.P.M. van Caam

Training activities	Hours
Courses	
RIMLS - Introduction course “In the lead of my PhD” (2020)	15.00
RU - Language Development for Academic Writing (2021)	50.00
RU - Writing Scientific Articles (2021)	96.00
RU - Mindfulness Based Stress Reduction (2022)	45.00
Scientific Visual Design (2022)	26.00
Designing a PhD Research Project (2022)	125.00
Project Management for PhD Candidates (2022)	50.00
Radboudumc - Scientific integrity (2023)	20.00
RU - Effective Writing Strategies (2023)	75.00
Statistics for PhD candidates using SPSS (2024)	60.00
RU - Design and Illustration (2024)	26.00
Radboudumc - Career development for PhD candidates & postdocs “The next step in my career” (2024)	20.00
The Art of Finishing Up (2024)	10.00
Conferences	
Phd retreat 2021 (2021)	21.00
Phd Retreat 2022 (2022)	16.00
European workshop for Rheumatology 2023 (2023)	28.00
RIMLs PhD Retreat 2023 (2023)	16.00
NVVI Annual Meeting 2023 (2023)	16.00
European workshop for Rheumatology 2024 (2024)	28.00
NVVI Annual Meeting 2024 (2024)	16.00
Supervision	
Master student internship supervision 2023 (2023)	56.00
Master student internship supervision 2024 (2024)	56.00
Master student internship supervision 2025 (2025)	10.00
Total hours	**881.00**

ACKNOWLEDGEMENTS

I came to Nijmegen from China with the idea of becoming a clinician-scientist. This thesis is where that journey led, and along the way I met many people who taught me, helped me, and walked part of the road with me. Looking back now, I realise a PhD is not the end of learning how to do research. It is where it starts.

First of all, I would like to thank all the tissue and blood donors. Every experiment in this thesis rests on your contribution, and none of this work would exist without it.

Marije, you are the reason I came here, and you gave me the opportunity to work on Th17 cells, which I am fairly sure are your favourite cells. Thank you for being my supervisor. In the first year almost every differentiation experiment failed, and you stayed patient and optimistic through all of it, until it finally worked. I still remember our first Luminex, when there was no IL-6 in the condition and you said they would make it themselves, and the result showed exactly that. That was amazing. Chapter 4 began as a coffee break conversation about T cells in OA. The subject we chose was not an easy one for me, but neither of us gave up, and in the end we got there.

Arjan, I still remember the first time we met, when you explained something to me by drawing it on a piece of paper and told me you like to draw. The last time, we sat together working on the graphical abstract, and you were still drawing with me. Without your help none of these chapters would have been finished. Working with you changed how I think about science and about writing: that certain standards have to be met, and that there is always more to consider. Even the small things, like never putting green next to red in a figure. Thank you for the support during the final stretch of my PhD, when finishing and writing everything up was hard, and for the lunches and conversations along the way. Thank you for being my supervisor.

Peter, thank you for always being there, for your help with the publications and for your support in the difficult moments. I still remember your last line discussion, when you talked about your career, about OA, and about how you think about signalling and TGF-β. It was insightful, and it sounded like a beautiful story. I wish you all the best in your retirement.

I would like to thank the members of my manuscript committee, **prof. dr. Annemiek van Spriel**, **dr. ir. Merel Adjobo-Hermans** and **prof. dr. Erik Lubberts**, for the time you invested in reading my thesis and for your valuable comments.

Werner, my mentor and my guide in everything mitochondrial. Thank you for teaching me, for your care and practical advice, and for all the mitochondria discussions. Your precision and your sense of responsibility were inspiring.

I would like to thank all my colleagues at the Rheumatology lab, and especially those who were there for my whole PhD. **Fons**, you always thought along with me. You have far more experience and knowledge than I do, yet you were always humble and willing to sit down and work a problem through together. The word "vigilant" in the title of this thesis came from you. Thank you for your support, and enjoy your retirement. **Martijn**, thank you for your input on the OA chapter. Because of it we expanded the panel, and that is where the most interesting finding came from. Beyond your knowledge of OA and your efficiency, I remain impressed by how much spicy food you can handle. **Esmeralda**, thank you for your comments and advice during my presentations, and for the creativity and good energy you bring to the lab. **Rogier**, the ideas and papers you shared at the fibrosis and immunity meetings were always innovative, and seeing your path showed me that a career as a clinician-scientist is something I could aim for too.

Dear **WG1**, the name may be old by now, but I still like to write it this way. **Monique**, your calm and your elegance are something I really admire. You ran many of the Luminex measurements for me, and we did the Th17 differentiations together in the hood, as well as the CTG and XTT experiments. You are always gentle and always well prepared, and I learned from you how to be an early bird. **Birgitte**, I still remember all the little mice on your desk and your warm smile. Thank you for teaching me how to isolate synovial tissue and for all the immunostaining. You, Marije and I designed the panel together, and you did an amazing job. I am still impressed by how quickly you pick up new techniques and how fast you answer every email. **Daphne**, always smiling and always well prepared, the weekly meetings would not have been the same without you. **Joyce**, thank you for always being there, for helping me with so many things around the Th17 work, and for the honest conversations and encouragement.

Elly, you are energetic and precise, and I am grateful for your help with the co-culture experiments and the mitochondrial dye trials. You are a genuine work hard, play hard person. **Annet**, you are always kind, always willing to help, and always with a sense of humour. Thank you for all the qPCR experiments you did with me. Optimising the reference genes for the mitochondrial work was far from easy, and you tried again and again with me. **Onno**, thank you for your essential assistance and for always being available when I needed it. You are often in very early and you work extremely hard. **Henk**, thank you for sharing the OA synovium tissue with me, also on the days when the material was not suitable and we had to wait. I wish you all the best in your retirement.

Nienke, I still remember the first time we met, talking about flow cytometry and about your time studying in Japan. Time flies, and we have known each other for years now. We share a love of cats and some overlap in our OA projects, and you helped me with the macrophage panel. You were always there, helpful, kind and gentle, through the ups and the downs. I wish you all the best in this new chapter of your life and career at Limba.

Peng, it was a great stroke of fate that we met in this lab, the only two Chinese people here. Your presence made me feel less alone. Sometimes we could speak Chinese together and share news or TV shows from home, which gave me a lot of support. I admire how hard you work and how clear you are about what you want. This journey abroad brought both of us challenges and struggles, and it also taught us how much family and health matter. I am very happy that you finished and went back to your family. All the best with your career, Dr. Wang.

Last but not least, **Theo**. There is too much to say and I do not know where to start. You are brilliant and genuinely gifted in science, and you combine that with real interpersonal skill and a lot of energy. I value our friendship and the time we spent together. I know you will go far, and I hope you become a great researcher and supervisor. Take good care of yourself.

I would also like to thank the people I met in the later stage of my PhD. **Anne**, your eye for detail and your clever ideas still impress me, and your organisational skills are something I need to learn from. I enjoyed the time we spent together in the hood doing SCENITH, and in the Aesculaaf. **Donna**, you are always kind and gentle and it is always nice to talk with you. We both work on Th17, and I wish you all the best finishing your PhD. **Angela**, **Pedro**, **Sharona** and **Isabel**, you are all bright and talented, and it was a pleasure to share some cheerful moments with you. I hope you enjoy your own PhD journeys. **Djúlio**, welcome back to the Netherlands. You are a wonderful person, and I wish you all the best with work and life here.

Special thanks to **Thea** and **Linda**, who always helped with logistics and orders and made sure the reagents arrived in time for my experiments.

To those who have already moved on to the next step in their careers, many of you hold a special place in my heart and I am glad we are still in touch: **Yvonne Bartels**, **Yvonne van Gemert**, **Nathalie**, **Natalia**, **Iris**, **Bob**, **Ritchie**, **Juliana**, **Irene** and **Margot**.

Arjen and **Wessel**, sharing an office with you was wonderful. Thank you for the countless support and help, for the sincere conversations and the good times. I always felt welcome and looked after, and you gave me a place and an atmosphere where I could actually finish this thesis. Many, many thanks. **Arjen**, 身体健康, and enjoy your work and your artistic life as always. I hope I get to hear your handpan again. **Wessel**, you balance everything so well, work

and life, sport and hobbies, and you are always relaxed, calm, and clear about what matters. I am happy for you and for this new chapter of your life. Becoming a father must feel like a different world. 步步高升, and all the best to your beautiful new family. Thank you also for being willing to support me as my paranymph, even with everything you have going on.

I would also like to thank the people I worked with more briefly, who contributed to this thesis or inspired me along the way. **Laura** and **dr. Mulder** for the single-cell sequencing, **Tessa**, **Rob** and **Diede** for the flow cytometry, and **Emma**, **Rens**, **Jaime**, **Sonia**, **Felicitas** and **dr. Mocholi**.

I would also like to express my sincere thanks to the brilliant students I have guided, although it often felt less like guiding and more like learning from each other. **Britt**, **Lorena** and **Anh**, by coincidence or by fate, each of you contributed to one of the research chapters of this thesis. Without you, none of it would be complete.

Britt, you hold a special place in my heart. You were my first student here, and I wanted to do my best for you and hoped you would enjoy your time in our lab. I loved the experiments we did together and our brainstorming about mitochondria, and you often inspired me to look at things differently. You are exceptionally bright and hard-working. I could see how well you and Arjan work together, and I am genuinely happy that you are back in the lab working with him. I am sure wonderful results will come out of your PhD. Enjoy the journey, and thank you so much for being my paranymph.

Lorena, I still remember how uncertain you were at the start about what to do. Over six months I watched you run difficult experiments on your own, organise and analyse data from a large flow panel, and help me prepare everything for the big OA tissue experiment. You were a different person by the end, and you are capable of far more than you thought. Thank you also for inviting me to speak at your master's graduation ceremony.

Anh, I have to apologise that I did not have as much time for you during your internship as I would have liked, because I was finishing this thesis. Thank you for all the single-cell analysis and for the discussions about the data in my office. I wish you all the best with finishing your master's and finding a PhD position.

To my dear friends. Surprisingly, I met all of you after I came to the Netherlands. That is something I gained along the way during this PhD, and looking back it still amazes me that it is possible to make this many new friendships, with this much trust, at this stage of life. Each of you gave me support and inspiration when I needed it, and each of you has been there to share both the sorrow and the happiness. You shaped who I am now and helped me with everything here. I could write pages about each of you, so I would rather tell you in person: **Chunying**,

Michelle, **Natalia S.**, **Qiu**, **Xin**, **Xinyuan**, **Olivia**, **Xigua**, **Richard**, **Yangyang**, **Gina**, **Mark**, **Li**, **Jessica**, **Philip**, **Jingyi**, **Lu**, **Fiona**, **Vera**, **Loes** and **Martin**. **Baobao**, my little fur friend, thank you for the company. **Guido**, without your support I would not have been able to finish this, or to come this far.

To my family in China, thank you for your love and your patience across the distance, and for supporting me in going so far from home to do this. 感谢我的父母、爷爷奶奶以及家人，感谢你们始终如一、无条件的支持与爱。你们始终是我最坚强的后盾，也是我一路前行的力量。这些年，我远在异国求学，虽与家人相隔千里，不能时时相伴，但无论身在何处，亲情始终如月光一般相随，山高水远从未隔断牵挂与思念。愿此后岁月，仍有灯火可亲，家人安康，彼此相伴。

感谢国家给予我的培养与支持，也感谢硕士导师胡毓诗教授和沈海院长的教导与培养。感谢你们在求学道路上给予我的指导与信任，让我有机会走出熟悉的土地，来到异国继续深造，开启这段珍贵而难忘的博士旅程。

And finally, a word to myself. Thank you for having the courage to go abroad to do a PhD, for meeting so many challenges along the way, and for getting through them. 你辛苦了。Keep learning, stay grateful and stay humble, and use what you have learned to do something good for the people around you and for society.





Radboudumc
university medical center

Radboud University